Improving Model Constraints for Vertical Deformation Across the Northern Cascadia Margin

by

Lisa Wolynec

M.Sc. Thesis
School of Earth and Ocean Sciences

University of Victoria
2004

Improving Model Constraints for Vertical Deformation Across the Northern Cascadia Margin

by

Lisa Wolynec
B.Sc., University of Manitoba, 2000

A Thesis Submitted in Partial Fulfillment of the
Requirements for the Degree of

MASTER OF SCIENCE

In the School of Earth and Ocean Sciences

Co-Supervisors: Dr. Herb Dragert and Dr. George Spence

ABSTRACT

Over the past decade, patterns of horizontal crustal motion observed along the Cascadia subduction zone (CSZ) from Global Positioning System (GPS) measurements have been used to derive locked subduction zone models with varying geometry and coupling factors. Although vertical crustal deformation estimates have been less abundant and less accurate than horizontal component observations, they provide key constraints to the models for estimating the extent of rupture for the next subduction thrust earthquake. In order to provide updated model constraint estimates, the contemporary vertical deformation pattern across the northern Cascadia margin was investigated through the combined application of GPS, repeated leveling, precise gravity, and monthly mean sea level measurements across southern Vancouver Island and repeated leveling on the mainland. To the first order, these estimates are consistent with across-margin tilt predictions from current dislocation models for the region. In their details, however, they reflect a more complex system than suggested by the simple models. Minor landward tilt across the margin at Tofino determined from the re-analyses of ~8 years of continuous vertical GPS positions, ~40 years of monthly mean sea levels and long-term time (decadal) intervals of repeat leveling surveys is distinctly different than the ~3 mm yr^{-1} of landward tilt observed at Neah Bay. While this difference may be minimized by allowing for a small amount of tilt induced at the southern stations from northward migration of the Cascadia forearc, differences in tilting of 3-4 mm yr^{-1} between short- and long-term estimates of repeat leveling at Bamfield are attributed to transients. To a lesser degree, elevation changes across the margin at Tofino may also illustrate transients. As well, distinct differences in the magnitude of vertical deformation for stations to the north and south of Barkley Sound suggest that differential deformation may be occurring along the margin. Similarly, while repeat relative gravity measurements across the margin at Tofino indicate 3-7 mm yr^{-1} of seaward tilt (at odds with results from all other methods),

a temporal dependence of vertical deformation might also be evident from the long-term versus short-term tilt rates. However, although repeat absolute gravity estimates between 1995 and 2002 indicate little across-margin tilt, consistent with continuous GPS results, differences between the time series at the Ucluelet absolute gravity and GPS stations indicate that gravity observations could be influenced by episodic mass redistribution beneath western Vancouver Island. This suggests that gravity results might not be directly comparable to estimates from other geodetic methods in determining uplift rates.

Extension of the vertical deformation profile eastward into the backarc using repeat leveling surveys indicates a broad region of uplift in the Pemberton area with respect to the coast, which is consistent with the vertical component at the continuous GPS station WSLR. Current dislocation models cannot account for the observed deformation. Therefore, modification of one model was attempted in which a weaker crustal zone, coincident with high heat flow near the Garibaldi Volcanic Arc, was included. A poor fit to the observed deformation rates indicates that further refinements must be made to such a model. Nonetheless, these results suggest a complex system of strain accumulation in the northern CSZ, which may result from a greater 3-dimensionality of the tectonic controls than current dislocation models of the region employ.

TABLE OF CONTENTS

LIST OF TABLES

LIST OF FIGURES

ACKNOWLEDGEMENTS

I wish to thank my entire graduate committee for their encouragement, guidance, and continuous support. I truly appreciate your recent efforts in reviewing my thesis so that I could meet the convocation deadline. I wish to extend special thanks to my supervisors **Drs. Herb Dragert** and **George Spence**, for your countless ideas, your patience, and your guidance.

I extend my appreciation to everyone at the Pacific Geoscience Centre. To **Dr. Jianjheng He** for developing the "soft zone" model. To **Dr. Stephane Mazzotti** for invaluable discussions and providing 3-D dislocation model curves for this study. To **Taimi Mulder** for seismicity support. To **Dr. John Ristau** for providing earthquake data from the GSC database, for invaluable discussions, and most of all for being a great friend! To **Dr. Tom James** for insightful discussions. To **Dr. Garry Rogers** for help with tide gauge data both through discussions and allowing me to view unpublished work. To **Nicholas Courtier** for collecting and providing absolute gravity data. To **Yuan Lu**, **Michael Schmidt**, and **Brian Schofield** for keeping the WCDA network alive! Special thanks to Brian, who has been a wonderful officemate and friend. Thank you for making the last 3 years an exceptional time for me. I will always remember the Enda-lite! Thank you also to **Karen Simon** for being an extraordinary officemate, for your advice, for being a superb thesaurus, an expert at GMT, and for always making me laugh! To **Harald Steiner** for the many valuable discussions regarding geodetic techniques. **Steve Taylor** and **Bruce Johnson** for *exceptional* computer support! To the support staff at PGC for making my life so much easier. To **Pam Olson** and the IOS/PGC Library staff for all of your help.

To **Dr. Ian Ferguson**, thank you for all of your support and encouragement through both of my degrees. I have thoroughly enjoyed all of the opportunities that I have had to work with you.

Thank you to all of my friends for their unwavering support. Thank you for encouraging me to pursue my dream and helping me to achieve it. **Kim Sourisseau**, I cannot tell you how much your support has meant to me. Thank you for always making me laugh and for truly understanding me. I love you very much. To my closest friends across the country: **Alison** and **Dave Reis**, **Kristin Salzsauler**, and **Rob Frazer**, thank you for all of your encouragement. To all of my Victoria friends, especially: **Maiclaire Bolton**, **Sheri Molnar**, **Lucinda Leonard**, **Amanda Bustin**, **Claire Currie**, **Liesa Lapinski**, **Roshni Narayan**, **Kumar Ramachandran**, **Michael Riedel**, **Ruben Veefkind**, **Yan Hu**, **Ele Willoughby**, **Asmaa Anwar**, and **Liliane Carle**, thank you for the friendship over the past few years. I could not have asked for better people to share this time with.

I would like to thank my family: **Dad**, **Mom**, **Chris**, **John**, **Pat**, **Angela**, **Tim**, **Jeff**, and **Patrick**. Thank you for your emotional and financial support and for always believing in me. I love you all. Finally, I thank my husband **Rob**. You are my motivator, my happiness, and my inspiration. Thank you for believing in me. I love you.

To

My Dad

Thank you for sharing with me your love of science.

CHAPTER 1

Introduction

This thesis is an investigation of the current vertical crustal deformation occurring at the northern end of the Cascadia subduction zone (CSZ), near southern Vancouver Island. Present day vertical motions derived from four independent observation techniques provide a basis for interpretation of the neo-tectonics of this region, where the Juan de Fuca plate (JdF) is subducting beneath North America.

1.1 Cascadia Subduction Zone

The northern Cascadia margin is dominated by the CSZ, where the JdF plate is underthrusting the North American plate (NA) at approximately 40 mm yr^{-1} in a northeasterly direction [*DeMets and Dixon, 1999*]. The interaction of these plates results in the potential for great thrust earthquakes to occur in the region [e.g. *Hyndman, 1995a*]. However, it is difficult to determine the exact nature of this interaction (e.g. extent of coupling between the plates) because the last earthquake of this type occurred in 1700 [*Satake et al., 1996*], well before instrumentation of the region. Past regional deformation studies [e.g. *Dragert et al., 1994*] assume that the plate interface is fully locked over a distance of 60 km downdip of the deformation front, with an additional 60 km downdip for a zone of linear transition from full to zero slip deficit. Information about the geometry of the locked and transition zones comes from elastic deformation models of the region [e.g. *Hyndman and Wang, 1993*; *Flück et al., 1997*]. An updated elastic deformation model [*Wang et al., 2003*] suggests that the transition zone extends further landward than in previous models [e.g. *Flück et al., 1997*], but still indicates that coseismic slip would be limited to approximately the seaward half of the transition zone.

The limit of coseismic rupture in the most recent model is based on an exponential decrease in slip deficit rate downdip of the locked zone, and so ¾ of the backslip rate decrease would occur in the seaward portion.

1.2 Project Objectives

On a broad scale, this project is part of a program set up to monitor vertical crustal deformation related to subduction processes on Canada's west coast. The last comprehensive analysis of vertical deformation data for the southern Vancouver Island region [*Dragert et al., 1994*] included tide gauge data up to ~1990, precise leveling surveys in 1978, 1984, 1986, and 1990, as well as relative gravity surveys in 1986 and 1990. The earlier repeat leveling surveys and tidal data (up to 1984) were also analyzed by *Holdahl et al.* [*1989*]. Since then, another ~10 years of monthly mean sea level records have accumulated, repeat precise leveling surveys were carried out in 1994 and 2002 across southern Vancouver Island, and a repeat relative gravity survey was completed in 2002 with the addition of co-located absolute gravity stations. As well, repeat absolute gravity measurements at 2 coastal stations on the island between 1995 and 2002 are included in the analysis, where measurements made up to the year 2000 were first reported by *Lambert et al.* [*2001*]. In addition, significant improvement in the precision of vertical GPS positioning since the *Dragert et al.* [*1994*] study allows for ~8 years of vertical measurements at two coastal stations to be included in this analysis. Finally, repeat leveling surveys carried out in 1928, 1955, 1958, 1982, 1983, and 1993 on the mainland were included in the analysis to extend the across-margin vertical deformation profile for this study into the backarc. The earlier data sets were first analyzed by *Holdahl et al.* [*1989*].

The main objective of this thesis is to utilize the most recent vertical deformation data to determine the current spatial deformation pattern across the northern Cascadia margin. Observed deformation rates can then be compared to theoretical rates calculated from the latest dislocation models.

Results of this study are particularly important for constraining the geometrical limit (downdip of the deformation front) of the locked portion of the subducting plate, which could impact calculations for the maximum magnitude of future megathrust events as well as seismic hazard assessments for the region. On a smaller scale, localized deformation patterns could help to identify stress buildup along crustal faults on southern Vancouver Island and the adjacent mainland.

1.3 Thesis Outline

In Chapter Two, a review of the tectonic and geological setting as well as existing geophysical studies of the study region are presented. Chapters 3 through 6 provide background and analysis results for the GPS, leveling, gravity, and tide gauge geodetic methods, respectively. Each chapter reviews how the respective methods are used to determine vertical movements in crustal deformation studies, the data sets used, methodology for the analysis of these data sets, analysis results, and a brief discussion of the results. Chapter 7 focuses on four main areas: (1) a summary of the results given in Chapters 3 through 6 with discussion centering around reconciliation of results from the different methods, (2) comparison of the summarized results with theoretical vertical crustal motions from dislocation models of the CSZ [*Flück et al., 1997*; *Wang et al., 2003*], (3) implications of the comparison between observed and theoretical deformation rates and interpretation of observed rates with the tectonics and geology of the study region, and (4) implications of these results for seismic hazard of the northern Cascadia margin. Chapter 8 is a summary of final conclusions for this thesis.

CHAPTER 2

Tectonic and Geological Setting of Western Canada

2.1 Tectonic Setting

The study area for this thesis (Figure 2.1) is western North America, where the tectonic regime is characterized by the relative motions of three lithospheric plates, the large Pacific (PA) and NA plates and the smaller intervening JdF plate system. The coastal region from northern California to southern British Columbia is dominated by the Cascadia subduction zone, a convergent plate margin, where the relatively young (~10 My) JdF plate is subducting beneath the NA plate (Figure 2.2). To the north and south of the CSZ, strike-slip faulting (with a small component of convergence) is dominant along the Queen Charlotte-Fairweather and San Andreas fault systems, respectively (Figure 2.1).

Present day convergence of the JdF plate relative to North America occurs at an average rate of 40 mm yr^{-1} in approximately a northeasterly direction [*DeMets and Dixon, 1999*]. Estimates of the geometry of convergence have typically been based on completing a vector triangle between JdF/PA spreading and PA/NA motion (e.g. derived from global solutions) [*Riddihough, 1984*]. However, at the northern and southern ends of the subduction zone, the subduction process has become complicated. The Explorer plate to the north has been interpreted to move independently [*Keen and Hyndman, 1979*], although present-day plate motions could be reorganizing such that the eastern portion of the Explorer plate is becoming attached to North America [*Rohr and Furlong, 1995*]. The Gorda plate to the south is deforming internally. The convergence rate may be similar to the JdF plate [*Wilson, 1986*], or alternatively, part of this region could no longer be undergoing subduction [*Riddihough, 1984*].

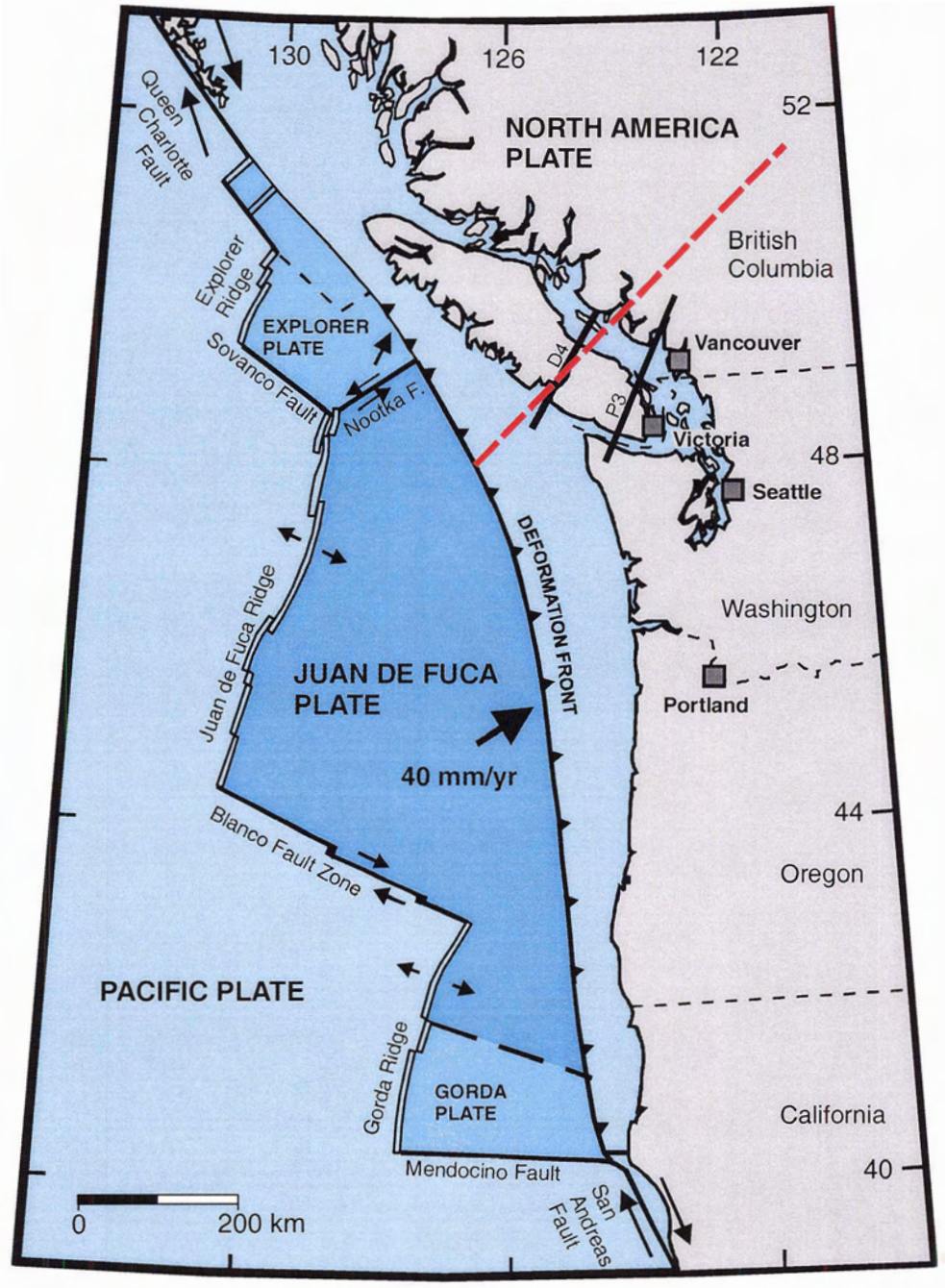

Figure 2.1. Tectonic setting of western North America. The Cascadia subduction zone is shown, where the Juan de Fuca plate is subducting beneath the North American plate. The dashed line indicates the approximate location of the profile that elevation, gravity, and heat flow data, as well as earthquake locations, are projected onto. This profile was also used to calculate model response with distance from the deformation front. The solid lines (D4 and P3) indicate the approximate locations of tomographic vertical velocity sections in Figures 2.11 and 2.12 [adapted from *Hyndman, 1995b*].

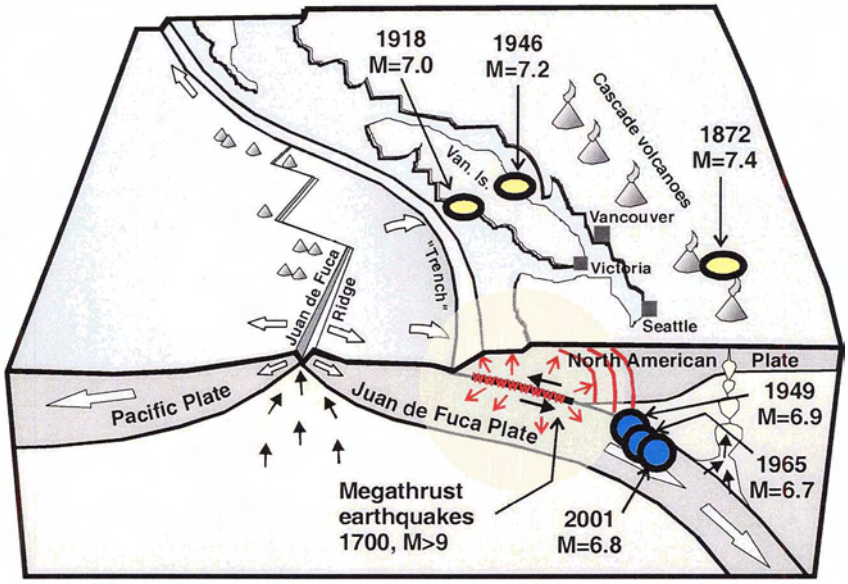

Figure 2.2. Cross-section cartoon of the northern Cascadia subduction zone. Earthquakes shown are discussed in text [modified from *Hyndman et al., 1996*].

2.2 Earthquake Hazards

Large earthquakes (M>6), which comprise the principal seismic hazard in the CSZ, occur in 3 distinct zones: deep (>50 km depth) earthquakes within the subducting slab, shallow (<30 km depth) earthquakes within the continental crust, and megathrust earthquakes, which occur at the boundary between the NA and JdF plates. Only large earthquakes of the first two types have been recorded in the northern CSZ. The largest recorded intraslab earthquakes occurred in 1949 (M=6.9), 1965 (M=6.7) [e.g. *Rogers and Crosson, 2002*] and 2001 (M=6.8) [*Staff of the Pacific Northwest Seismograph Network, 2001*; *Bustin et al., 2004*; *Pacific Northwest Seismograph Network, 2004*]. While the background seismicity of shallow crustal earthquakes is generally high, the three largest observed events of this type have occurred in regions with few small earthquakes (Figure 2.3). The 1918 (M=7.0) [*Cassidy et al., 1988*] and 1946 (M=7.2) [*Rogers and Hasegawa, 1978*] events occurred beneath central Vancouver Island, and the 1872 (M=7.4) [*Malone and Bor, 1979*] inland event near the international border. Of these, only the 1946 event has been reported as having a possible correlation with observed surface faulting (Beaufort Range fault; see Figure 2.3) [e.g. *Rogers and Hasegawa, 1978*].

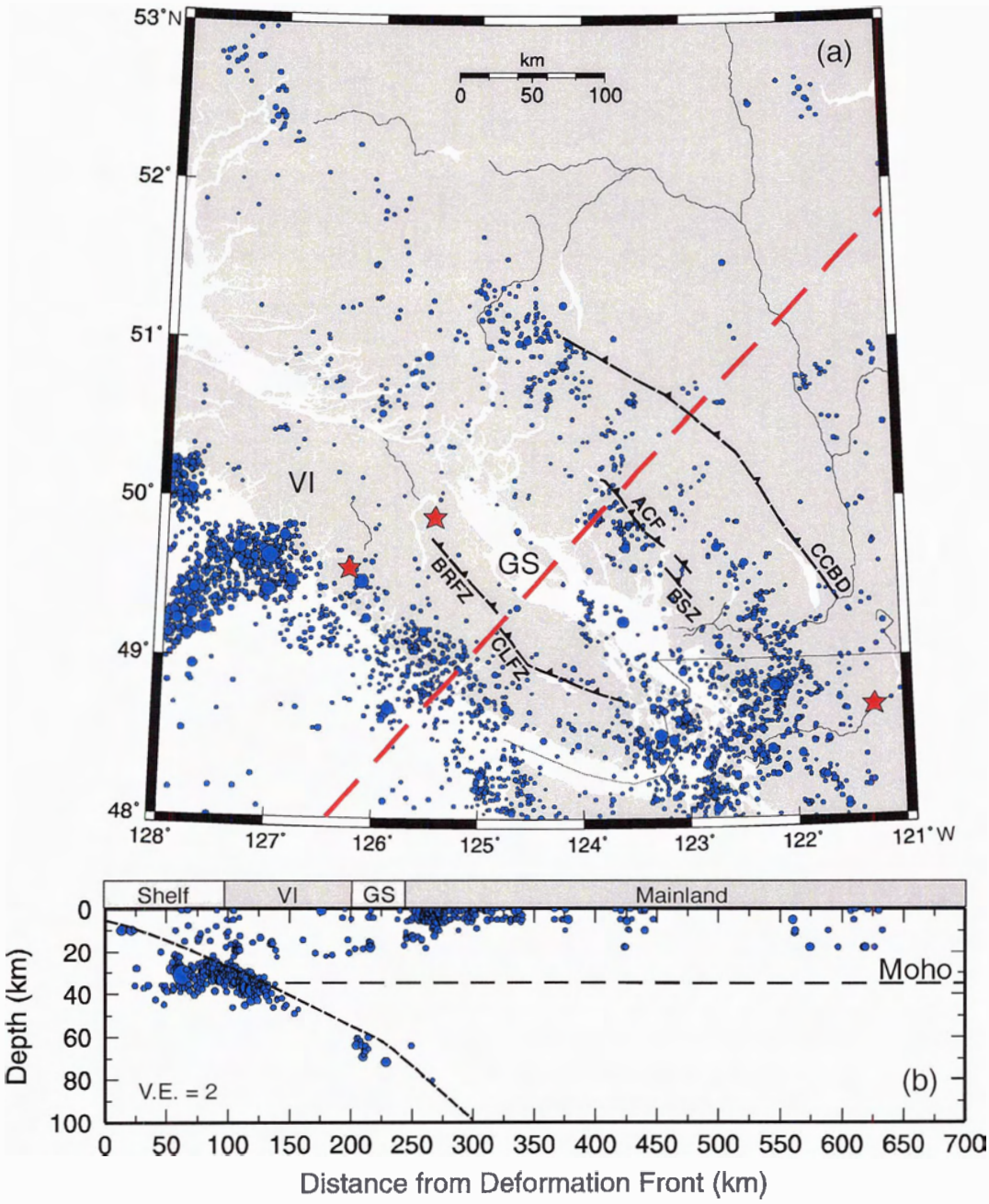

Figure 2.3. (a) Map view and (b) 100 km wide cross-section showing seismicity in the northern Cascadia subduction zone between 1985 and 2001. The dashed line in (a) shows the location of the cross-section, where the downgoing plate is defined by the earthquake locations (approximate location shown by short-dashed line). Crustal earthquakes occur to a maximum depth of approximately 30 km in the region. The Moho is approximated at 35 km depth (long-dashed line). Major historic crustal earthquakes (see Figure 2.2) are shown as stars on the map. BRFZ = Beaufort Range fault zone; CLFZ = Cowichan Lake fault zone; ACF = Ashlu Creek fault; BSZ = Britannia shear zone; CCBD = Central Coast Belt Detachment fault; VI = Vancouver Island; GS = Strait of Georgia.

During the time of written history (~200 years), no megathrust events have been observed along the Cascadia margin [*Rogers, 1988a*; *Hyndman, 1995a*; *Hyndman et al., 1996*]. The last major thrust event is concluded to have occurred in January, 1700 [*Satake et al., 1996*; *2003*]. Possible explanations previously given for the lack of these earthquakes are that convergence no longer occurs along the margin, that subduction is occurring through smooth, stable sliding, or that the thrust fault is locked [*Rogers, 1988a*]. Evidence to discount the first two explanations includes folding and faulting of young sediments at the base of the continental slope (imaged with seismic reflection data), paleoseismic observations of past megathrust events, and present-day measurements of elastic strain build-up along the margin, consistent with stress accumulation across a locked subduction fault [*Rogers, 1988a; 1988b*].

Surface crustal deformation occurs as stress accumulates for any of the 3 types of large earthquakes. For the deep intraslab events, associated surface strain rates that precede such events have not yet been resolved with current technology, although ~1 cm coseismic offsets have been observed for the most recent (2001) earthquake [*GPS Analysis of Olympia quake at RPI, 2004*; *Bustin et al., 2004*]. Surface deformation that accompanies stress accumulation for shallow crustal earthquakes may be resolvable but requires dense monitoring arrays because of the limited spatial extent of the stress anomaly and slow strain rates.

Because of the large extent of the locked zone and rapid convergence rate, the surface deformation that characterizes stress accumulation of a megathrust event dominates the coastal margin. The basic process that produces this deformation is simple and can be represented by an elastic rebound model with two main stages: interseismic and coseismic (Figure 2.4) [e.g. *Hyndman and Wang, 1993*; *Dragert et al., 1994*; *Hyndman, 1995a; 1995b*]. Continuing convergence during the interseismic stage results in the elastic bending and buckling of the continental crust as the seaward edge of the continent gets pulled down. This in turn produces an upward bulge landward and a shortening of the crust across the margin, where the magnitude and spatial pattern is directly related to the location and geometry of the locked zone. As this process

continues, elastic strain accumulates where the plate interface is locked. In the coseismic stage, earthquake rupture of the locked portion of the thrust fault results in the uplift of the seaward portion of the continent, a collapse of the bulge, and horizontal extension across the outer margin.

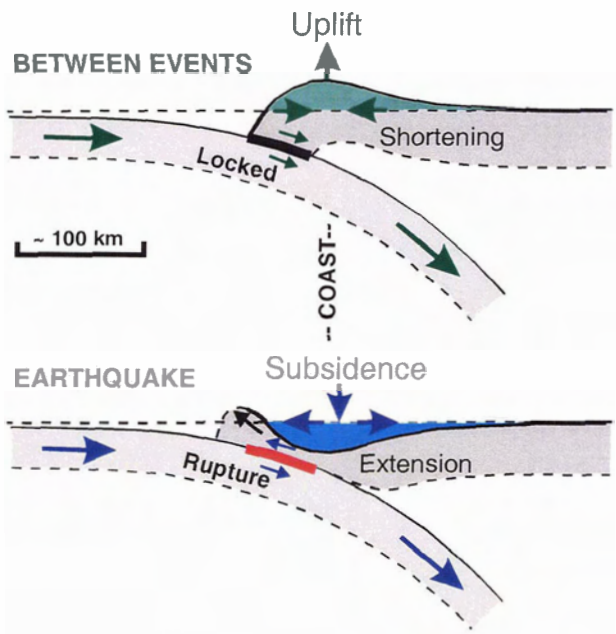

Figure 2.4. Crustal deformation observed during the interseismic (upper) and coseismic (lower) periods of the megathrust earthquake cycle. The cycle shown assumes an elastic accumulation of strain that will be recovered during an earthquake rupture on the thrust fault [modified from *Dragert et al., 1994*; *Hyndman et al., 1996*].

Recent research [e.g. *Dragert et al., 2001*; *Rogers and Dragert, 2003*; *Dragert et al. 2004*] has identified a region of shorter-term strain accumulation (~14.5 months) and release (over a period of a few weeks) across the subduction thrust downdip of the locked zone. Slow slip events occurring in this region of episodic tremor and slip (ETS) are assumed to be part of the tectonic process along the margin contributing to long-term tilting.

2.3 Tectonic Elements and Geology of the Southern Canadian Cordillera

The geological structure of western North America may be divided into five morphological belts (Figure 2.5): the Insular Belt, Coast Belt, Intermontane Belt, Omineca Belt and the Fold and Thrust Foreland Belt. In the context of this study, it should be noted that although all belts have been subject to extensive Cretaceous-Tertiary tectonic activity, most present day seismic and volcanic activity is limited to the Insular and Coastal Belts. The majority of vertical deformation surveys used in this study were performed within these two belts; however, the repeat leveling data on the mainland (Chapter 4) extends into the Intermontane Belt.

The Insular Belt includes the present Pacific continental margin, encompassing Vancouver Island and the Queen Charlotte Islands. As summarized by *Gabrielse et al. [1991]*, the overall geology of Vancouver Island comprises Paleozoic, Mesozoic and Cenozoic volcanic arc rocks, and oceanic and clastic wedge assemblages. The Coast Belt comprises fault-bounded island arc and oceanic terranes [*Journeay and Friedman, 1993*]. Granitic and metamorphic rocks of the Coast Plutonic Complex define the geology of the belt in the southwestern region. The deformed Upper Cretaceous and Tertiary clastic wedge of the Nanaimo Assemblage overlies the belt in this region. To the east, the Coast Belt is underlain mainly by Mesozoic volcanic and sedimentary rocks [*Friedman et al., 1995*]. The Intermontane Belt in southern British Columbia consists of volcanic and sedimentary rocks, which are not as highly metamorphosed nor as deeply eroded as those of surrounding belts [*Gabrielse et al., 1991*].

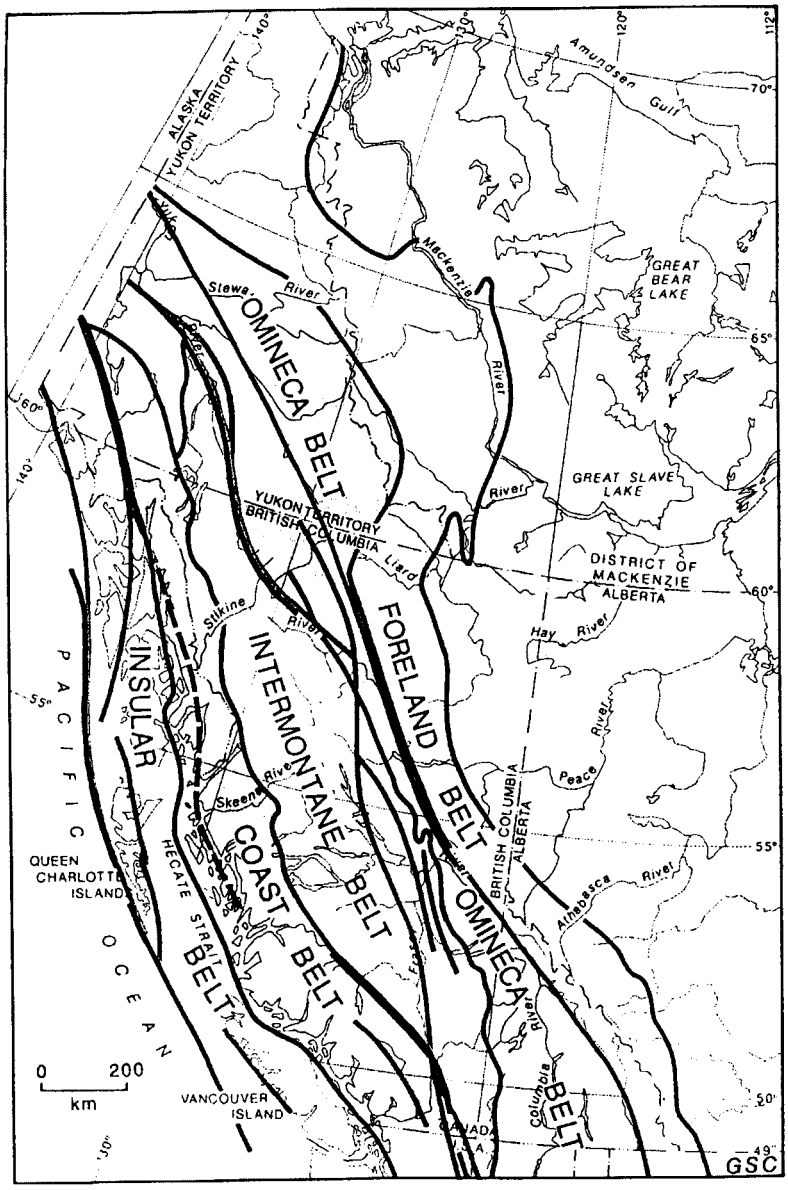

Figure 2.5. Tectonic elements of the Canadian Cordillera, including morphogeological belts and regional strike-slip faults [*Gabrielse et al., 1991*].

2.4 Geology of Vancouver Island and Adjacent Mainland

Vancouver Island can be divided into three (exotic) terranes: Wrangellia, Pacific Rim, and Crescent (Figure 2.6). Much of the island is underlain by Wrangellia, which is composed of marine volcanic and sedimentary rocks of Devonian to Jurassic age. The terrane, extending along the Pacific margin from Oregon to south-central Alaska, was emplaced during the middle Cretaceous [*Monger and Price, 1979*]. To the southwest of Wrangellia, the Mesozoic Pacific Rim Terrane consists of Triassic-Jurassic arc volcanics and an overlying, thick sequence of Jurassic-Cretaceous sediment-rich mélanges [*Muller, 1977*; *Brandon, 1989*; *Dehler and Clowes, 1992*], which outcrop along the central west coast of the island. According to *Hyndman et al.* [*1990*], emplacement of the Pacific Rim Terrane is thought to have occurred shortly before or at the same time as low-pressure metamorphism of the Leech River Complex (a component of the terrane), at about 42 Ma. Outboard of the Pacific Rim Terrane lies the Paleocene to Early Eocene aged Crescent Terrane. Composed of basalt flows, breccia, tuff and volcanic sandstones cut by gabbro and diabase intrusions [*Massey, 1986*], the terrane rocks outcrop on southwestern Vancouver Island and the Olympic Peninsula [*Dehler and Clowes, 1992 and references therein*]. *Johnston and Acton* [*2003*] state that the accretion of the final (Crescent) terrane must pre-date or be coeval with the deposition of sandstone and conglomerate of the latest Early Eocene to Oligocene Carmanah Group, which are undeformed and unconformably overlie the sutures of the three terranes. Emplacement of the Crescent and Pacific Rim Terranes were also inferred [*Hyndman et al., 1990*] to correspond with initiation of the modern Cascade volcanic arc (42 Ma).

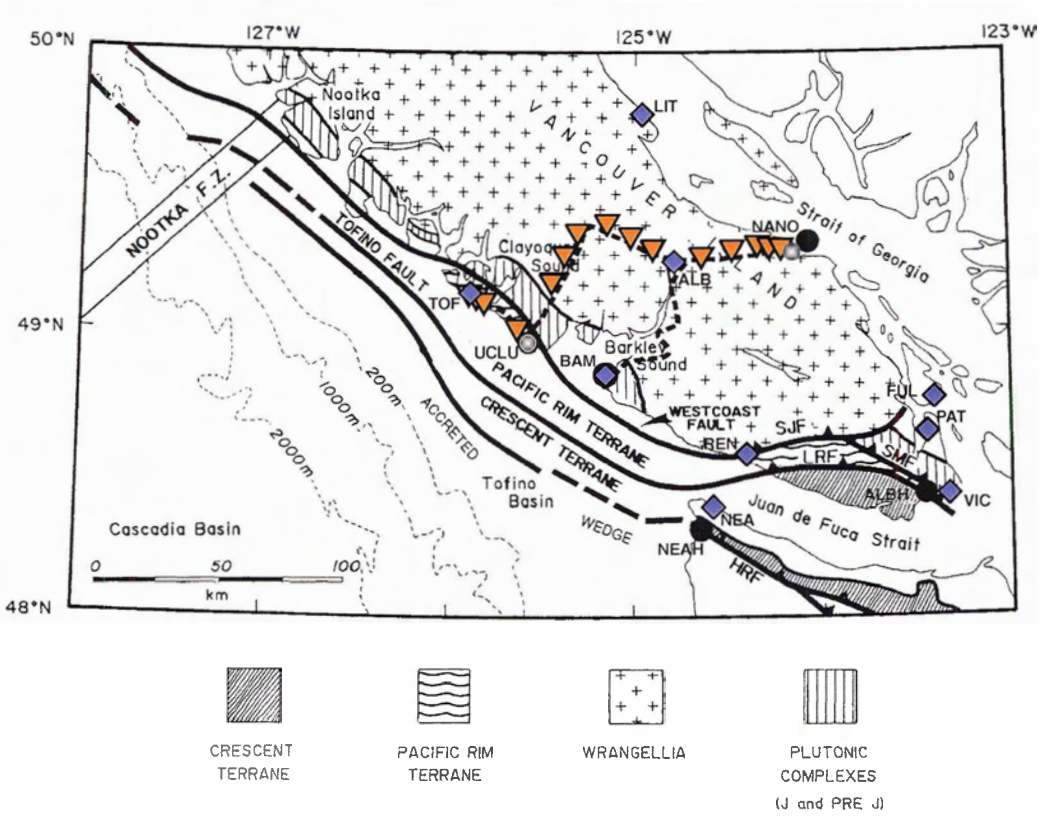

Figure 2.6. Generalized physiography and geology of Vancouver Island showing the Wrangellia, Pacific Rim and Crescent Terranes. Faults are shown as thick, solid lines, broken where inferred. HRF = Hurricane Ridge fault; LRF = Leech River fault; SJF = San Juan fault; SMF = Survey Mountain fault. Approximate locations of vertical deformation surveys are overlaid. Short-dashed lines are leveling transects; large black dots outlined in yellow are continuous GPS (WCDA) stations; diamonds are tidal stations; starburst dots are absolute gravity stations; inverted triangles are repeat relative gravity stations [modified from *Dehler and Clowes, 1992*].

Figure 2.7 illustrates the regional geology of southern Vancouver Island [after *Muller, 1977*]. The oldest rocks on Vancouver Island are volcanic and marine sediments of the Upper Paleozoic Sicker Group [*Muller, 1977*]. Overlying this is the basaltic lava sequence (pillow basalt, massive basaltic lava, dykes, and sills) and sediments of the Triassic aged Karmutsen Formation [*Yorath et al., 1999 and references therein*]. These form the bulk of the rocks underlying central Vancouver Island. On the east coast of the island are rocks of the Nanaimo Group, consisting of marine conglomerate, sandstone and shale [*Muller and Jeletzky, 1970; England, 1989; Kurtz et al., 1990*; *Yorath et al.,*

1999]. This group and the underlying basement have been shortened and thickened through deformation along the Cowichan fold-and-thrust belt [*England and Calon, 1991*].

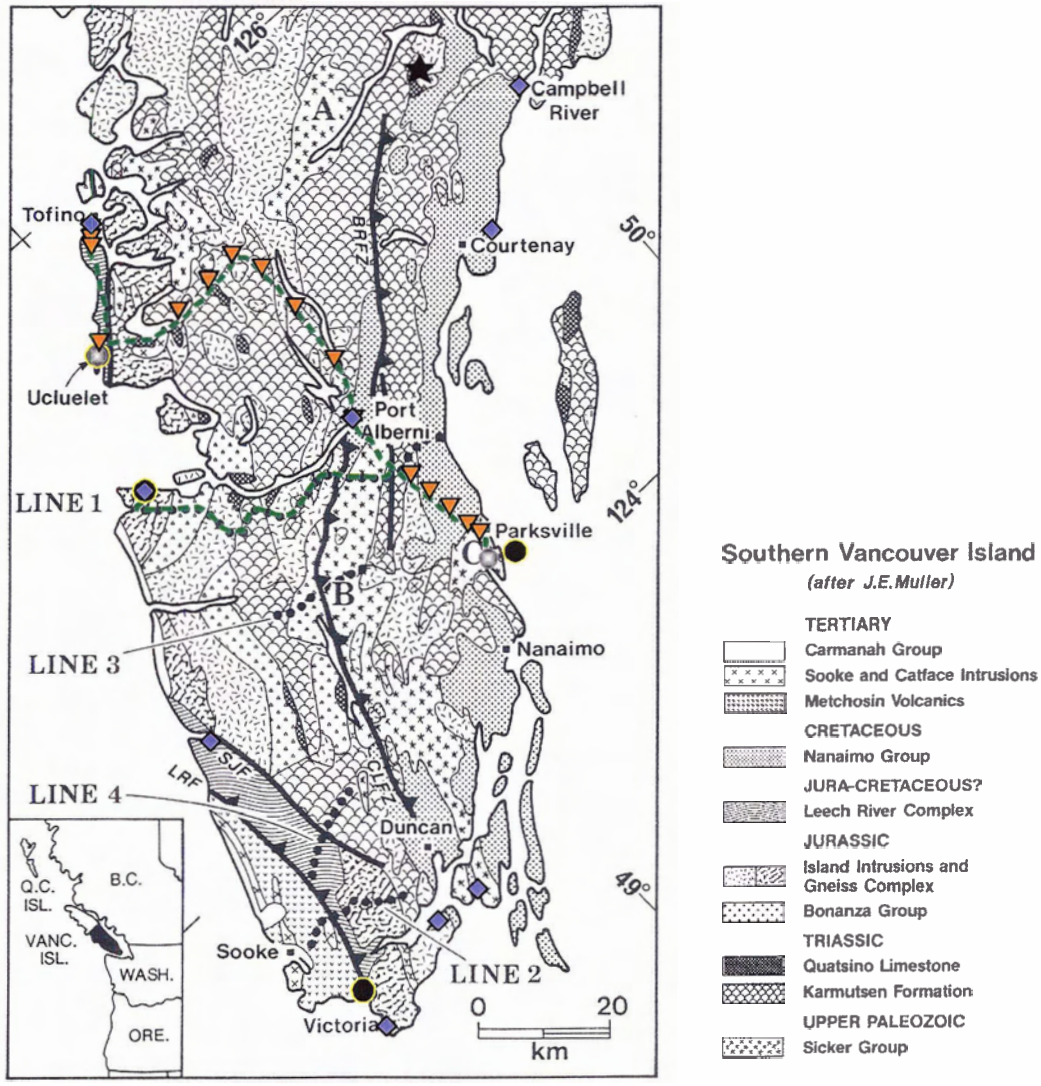

Figure 2.7. Regional geology of southern Vancouver Island. Black dotted lines indicate locations of Lithoprobe seismic profiles. Approximate locations of vertical deformation surveys are overlaid. Green dashed lines are leveling transects; large black dots outlined in yellow are continuous GPS (WCDA) stations; diamonds are tidal stations; starburst dots are absolute gravity stations; inverted triangles are repeat relative gravity stations. SJF = San Juan fault; LRF = Leech River fault; CLFZ = Cowichan Lake fault zone; BRFZ = Beaufort Range fault zone. A = Buttle Lake uplift; B = Cowichan Lake uplift; C = Nanoose uplift [modified from *Yorath et al., 1985*, after *Muller, 1977*].

On the adjacent mainland, the southern Coast Belt has been divided into three regions [*Journeay and Csontos, 1989*; *Journeay and Friedman, 1993*] by the Coast Belt thrust system (CBTS), based on mapping results of *Monger* [*1990; 1991*] and *Journeay* [*1990*]: the western, central and eastern coast belt domains (Figure 2.8). *Journeay and Friedman* [*1993*] describe the western Coast Belt domain (WCB) as having a relatively simple structural style consisting of layers of folded rocks being stacked along thrust faults. The geology of the WCB is described by *Friedman et al.* [*1995*] as comprising mainly plutonic rocks. The WCB is separated from the central Coast Belt (CCB) (Figure 2.8) by a steeply dipping reverse fault (Central Coast Belt detachment (CCBD); Figure 2.8 [*Journeay and Friedman, 1993*]). The geology of the CCB is summarized as including metamorphosed island arc and oceanic as well as metasedimentary rocks [*Journeay and Friedman, 1993*]. Lithologic assemblages in this zone have been correlated with terranes of the western and eastern Coast Belts [*Journeay and Friedman, 1993*; *Journeay and Mahoney, 1994*]. The boundary between the CCB and eastern Coast Belt domain (ECB) is the northwest striking thrust and oblique-slip faults of the Bralorne-Kwoiek fault system (BF and KF; Figure 2.8) [e.g. *Journeay, 1990*]. *Journeay and Friedman* [*1993*] summarize the details of the ECB as encompassing a variety of fault-bounded tectonic assemblages, comprising oceanic, arc-derived volcanic and sedimentary rocks. East of the Coast Belt, geology of the Intermontane Belt in the area where data is used in this study is detailed in *Gabrielse et al.* [*1991*].

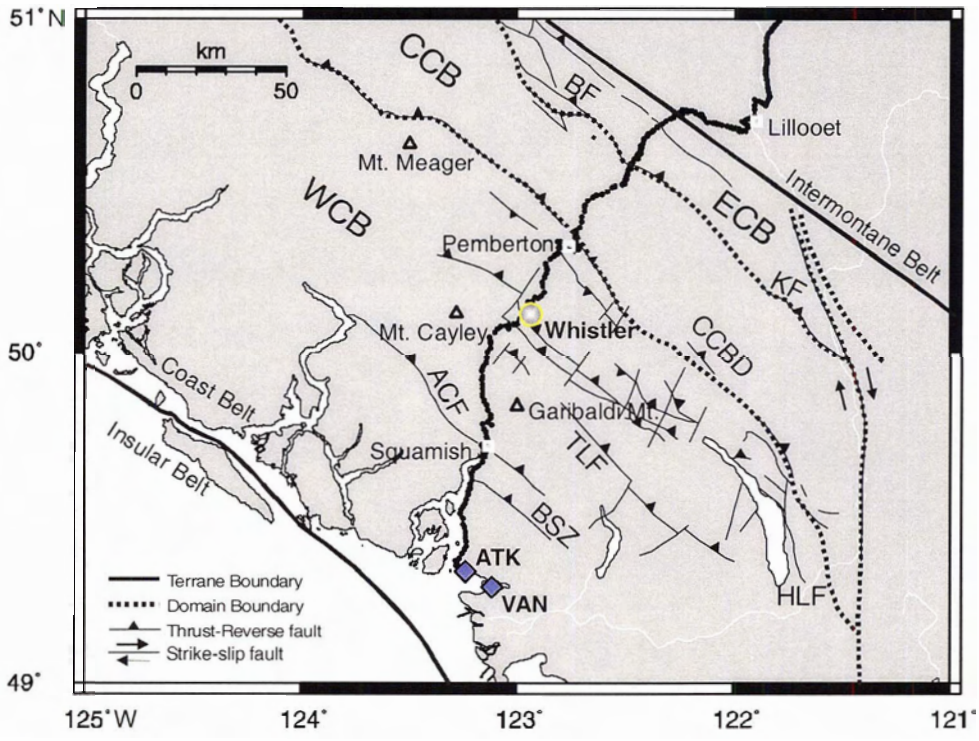

Figure 2.8. The Coast Belt of the southern Canadian Cordillera, showing the western, central and eastern domains as well as Terrane boundaries and known crustal faults [modified from *Friedman et al., 1995*]. Black dots indicate approximate position of Williams Lake leveling line; diamonds are tide gauge stations; starburst dot is continuous GPS station. TLF = Thomas Lake fault; HLF = Harrison Lake fault. Remaining abbreviations are as in text and Figure 2.3.

2.5 Regional Geophysics

Existing geophysical data used to investigate the large-scale structure and processes of the Cascadia margin include gravity, magnetics, multichannel seismic reflection, seismic refraction, seismicity, and heat flow.

2.5.1 Gravity and Magnetics

Gravity data [after *Riddihough, 1979*] for the Cascadia margin indicate parallel bands of low and high anomalies oriented along the trend of Vancouver Island (Figure 2.9). The main gravity low in the western portion of the study area is located over the sediment filled trough at the base of the continental slope and the high over Vancouver

Island (Figure 2.9a) [*Hyndman et al., 1990*; *Hyndman, 1995b*]. On the mainland, the gravity anomaly is consistently low along the leveling profile (Figure 2.9a). However, there is a steep gradient between the coast and approximately Squamish (Figure 2.9b). Similarly, the main trends of the magnetic anomalies are aligned parallel to the Vancouver Island coast (Figure 2.10). On the mainland, a magnetic high is observed from the coast to approximately Squamish.

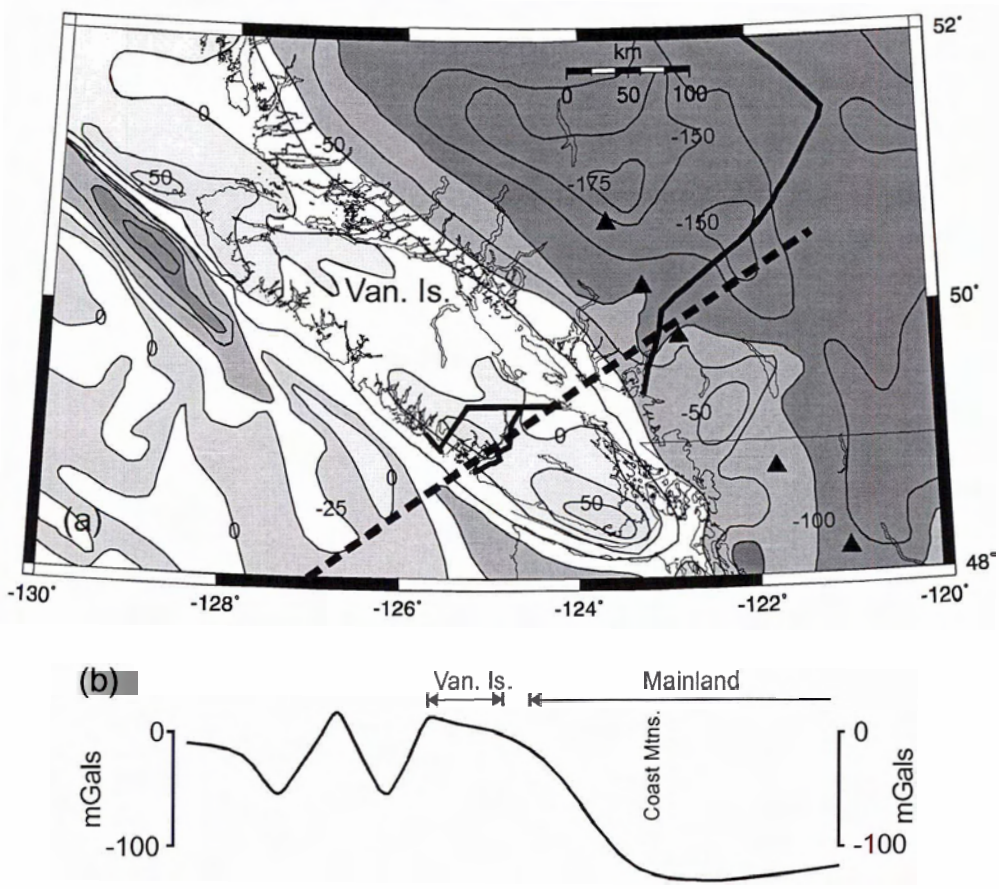

Figure 2.9. (a) Gravity anomaly map of the Cascadia subduction zone (in mGals), Free Air at sea and Bouguer on land [after *Riddihough, 1979*]. Triangles show location of Quaternary volcanic centers. Thick solid lines show approximate location of repeat leveling lines. (b) Across margin gravity anomaly profile, location shown as thick dashed line on (a) [modified from *Keen and Hyndman, 1979*].

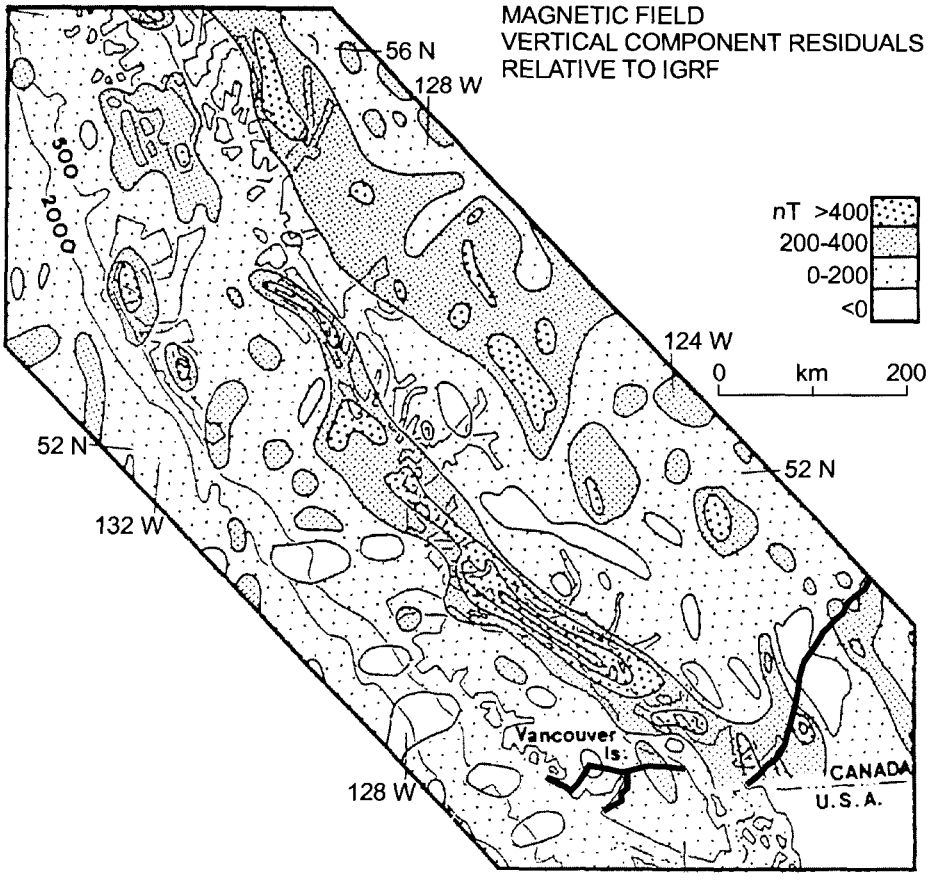

Figure 2.10. Magnetic anomaly map of southwestern British Columbia along the contact between the coast Insular Belt and inland Coast Plutonic Complex [after *Coles and Currie, 1977*]. Thick solid lines show approximate location of repeat leveling lines [modified from *Keen and Hyndman, 1979*].

2.5.2 Seismic Investigations

Multichannel seismic reflection lines across the continental shelf and slope in 1985 and 1989 provided vital information on the structure of the Cascadia Margin. Reflection lines offshore Vancouver Island provided a continuation of the 1984 Lithoprobe Vibroseis reflection lines. The main features imaged by these investigations are [as summarized by *Hyndman et al., 1990*; *Hyndman, 1995b*]: (i) the top of the oceanic crust, (ii) the fold and thrust belt at the base of the continental slope, (iii) the Tofino Basin on the continental shelf, and (iv) the Crescent Terrane, bounded seaward by a possible fossil trench.

Seismic refraction experiments were conducted across the Vancouver Island margin from the deep sea to the mainland, and along the length of the island [*Spence et al., 1985*]. These experiments provided deep velocity structure beneath the continental shelf and slope. The main results of these investigations are: (i) definition of the subducting oceanic crust and (ii) a shallow high-velocity zone beneath the island that is bounded by layers of low-velocity ("C", at 18 km, and "E", at 30 km depth) [*Hyndman et al., 1990*].

Characteristics of the "E" layer, in particular, have been the focus of several studies [e.g. *Hyndman, 1988*; *Calvert and Clowes, 1990*] and have played an important role in interpretations of the structure and tectonic processes occurring along the Cascadia margin [e.g. *Calvert, 1996*]. *Calvert* [*1996*] summarizes proposed explanations for the E reflections as having a "structural" origin, where the layer represents layered mafic or sedimentary rocks [*Yorath et al., 1985*; *Green et al., 1986*; *Clowes et al., 1987*] or a "non-structural" origin, where the layer represents sheared sediments [*Calvert and Clowes, 1990*] that are trapping fluid rising from the subducting plate [cf. *Hyndman, 1988*].

Seismic tomography is another tool utilized to investigate the large-scale structure of the CSZ. In the context of this study, *Ramachandran* [*2001*] and *Ramachandran et al.* [*in press; submitted*] utilized controlled source (SHIPS) and earthquake data to provide a detailed velocity structure from the Olympic peninsula to mainland British Columbia (Figures 2.11 and 2.12). Deep (<70 km depth) crustal structure results (Figure 2.11) [*Ramachandran, 2001*; *Ramachandran et al., submitted*] illustrate the depth of the down-going Juan de Fuca plate changing from ~28 km beneath the northwestern tip of the Olympic peninsula to ~40 km beneath the centre of south Vancouver Island. Detailed shallow (<15 km depth) crustal structure results (Figure 2.12) [*Ramachandran, 2001*; *Ramachandran et al., in press*] illustrate the location of the major contacts between the Crescent, Pacific Rim and Wrangellia terranes, and the Coast Plutonic Complex. *Ramachandran* [*2001*] also suggests a correlation of the Leech River fault at the northern terminus of the Crescent Terrane with seismicity and interpreted it as being active.

Another recent study, by *Zhao et al.* [*2001*], details the velocity structure of Vancouver Island. A main result of their study shows a low P-velocity zone near the location of the 1946 earthquake (e.g. Figure 2.2) beneath central Vancouver Island.

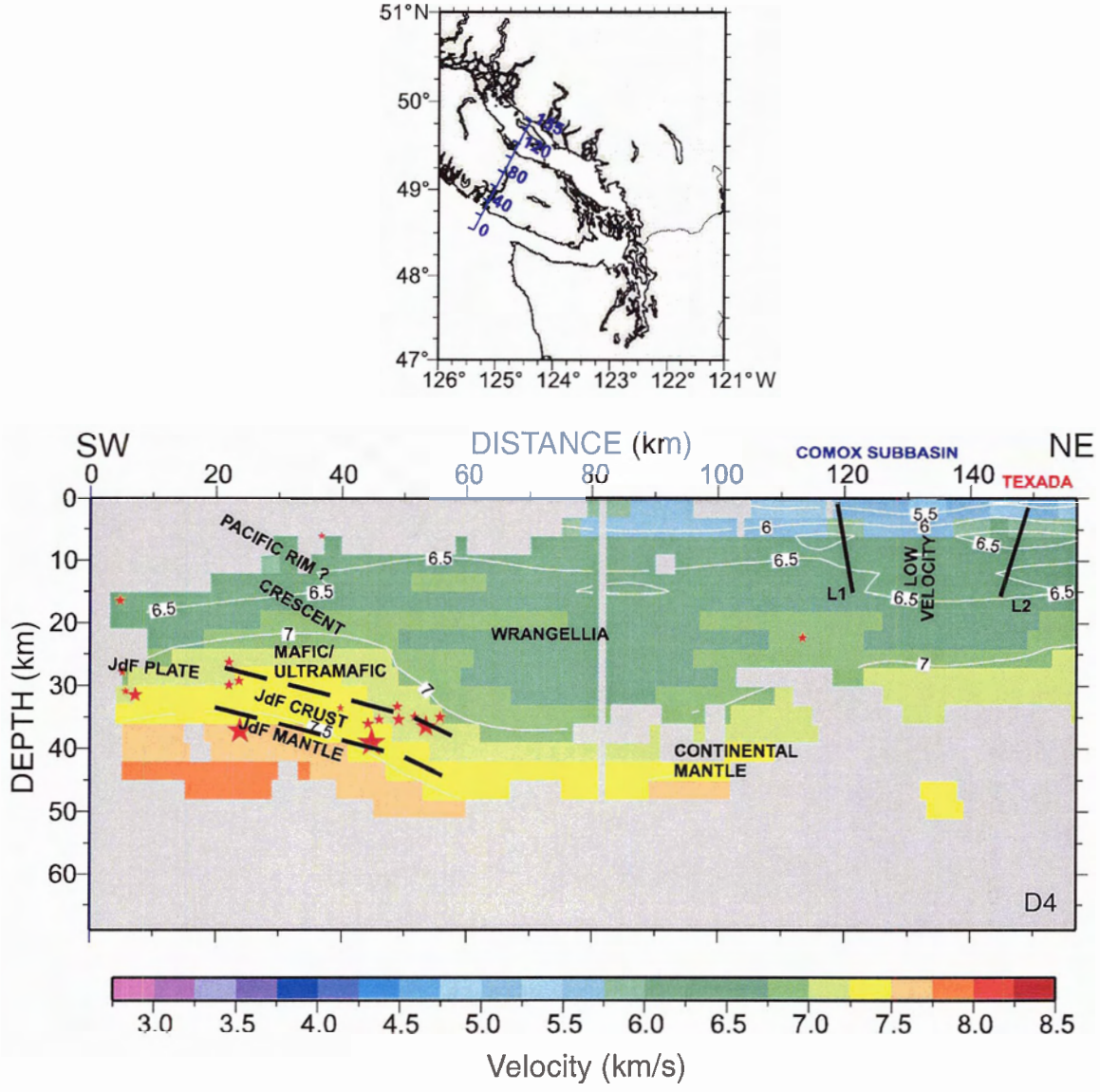

Figure 2.11. NE-SW vertical velocity section (D4) showing the deep crustal structure from the Olympic peninsula to mainland British Columbia. Stars indicate the location of earthquakes. L1 and L2 indicate the boundaries of a low velocity zone [modified from *Ramachandran, 2001*].

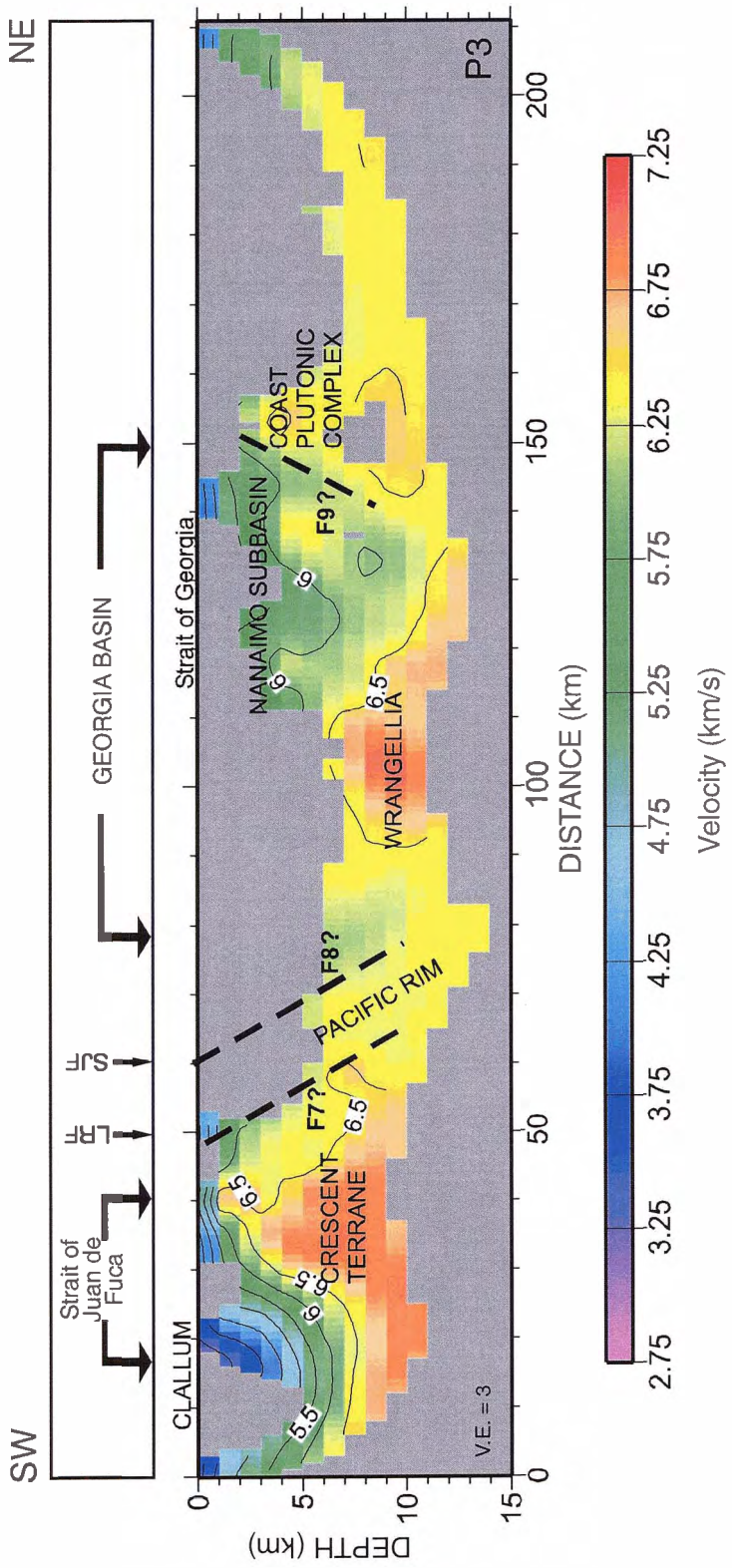

Figure 2.12. NE-SW vertical velocity section (P3) showing the shallow crustal structure from the Olympic Peninsula to mainland British Columbia (see Figure 2.1). F7 is the interpreted subsurface face of the Leech River fault (LRF), F8 is the interpreted contact location between the Pacific Rim Terrane and Wrangellia rocks (San Juan fault, SJF). F9 is the interpreted contact between Wrangellia rocks and the Coast Plutonic Complex [modified from *Ramachandran, 2001*].

A recent study [*Nedimović et al., 2003*], combining results from reflection and tomographic studies of the northern Cascadia margin, compared differences in the reflection character along the plate interface with the spatial extent of the locked, transition, and stable sliding zones. They found that the locked zone correlates well with a narrow package of thrust reflections, the transition zone with a zone of gradual thickening of the reflection band (E-layer), and the stable sliding zone, which is the location of recently discovered ETS events [*Dragert et al., 2001*; *Rogers and Dragert, 2003*], with the fully developed E-zone reflection package. In the scope of this study, which is in part focused on the geometry of the locked and transition zones, these results indicate that the landward extent of the locked zone could be located 25-30 km closer to land and the transition zone could be narrower than the estimates from dislocation models [e.g. *Flück et al., 1997*; *Wang et al., 2003*]. This might then be observed in the vertical deformation observations as a broader peak of uplift across Vancouver Island, with the maximum shifted landward relative to current model predictions.

2.5.3 Seismicity

Crustal earthquakes (Section 2.2) in the northern CSZ are concentrated in a region from Puget Sound, Washington to southwestern British Columbia (Figure 2.3). These earthquakes result from north-south compression [*Hyndman et al., 2003*], where the Oregon forearc is moving to the north against Vancouver Island and the Coast Mountains. The maximum temperature for crustal earthquake failure (350°C) [*Hyndman and Wang, 1993*] limits these earthquakes to the upper 30 km of the continental crust.

The distribution of intraslab seismicity between 1985 and 2001 was recently investigated by *Bolton* [*2003*], who summarized that earthquakes occurred in two distinct concentrations: beneath the west coast of Vancouver Island and beneath Georgia Strait and Puget Sound. Bolton concluded that the seismicity beneath the west coast of Vancouver Island was concentrated between 25 and 40 km depth, where focal mechanisms indicated both normal and strike-slip faulting. Stress tensors for the former

indicated north-south compression and east-west tension. Earthquakes in the Georgia Strait/Puget Sound concentration occur to a maximum depth of 80 km and were analyzed in two groups: small (M<4) and larger (M>5) earthquakes. For the small earthquakes, focal mechanism and stress analysis indicated normal and strike-slip faulting, with near-vertical compression and down-dip tension for the former. Focal mechanism results for the larger earthquakes indicated normal faulting with down-dip tension.

2.5.4 Heat flow

Heat flow data for the southern British Columbia region was obtained from offshore wells in the continental shelf, boreholes on land and from marine heat flow probing of soft sediments in fjords along the southwestern British Columbia coast [cf. *Lewis et al., 1988*; *Hyndman and Lewis, 1995*]. Along the transect in Figure 2.1, heat flow from the continental slope to ~20-30 km west of the Garibaldi Volcanic Belt decreases from ~90 mW m^{-2} to ~30 mW m^{-2} (Figure 2.13). Heat flow values then abruptly increase eastward toward the volcanic belt to values of 60-80 mW m^{-2} [*Lewis et al., 1988*; *Hyndman and Lewis, 1995*]. The estimated accuracies for the borehole heat flow measurements are ±10 to ±20%, depending on borehole depths, water circulation, and the number and quality of thermal conductivity measurements [*Hyndman and Lewis, 1995*].

On Vancouver Island, the radioactive heat generation for surface rocks is low, averaging ~0.4 μW m^{-3} [*Lewis et al., 1988*]. In Figure 2.13, the average heat flow, approximated by the dashed line, takes into account average heat generation for crustal rocks of the backarc (2-5 μW m^{-3}; *Hyndman and Lewis* [*1995*]), but not for the low value generated by rocks on Vancouver Island.

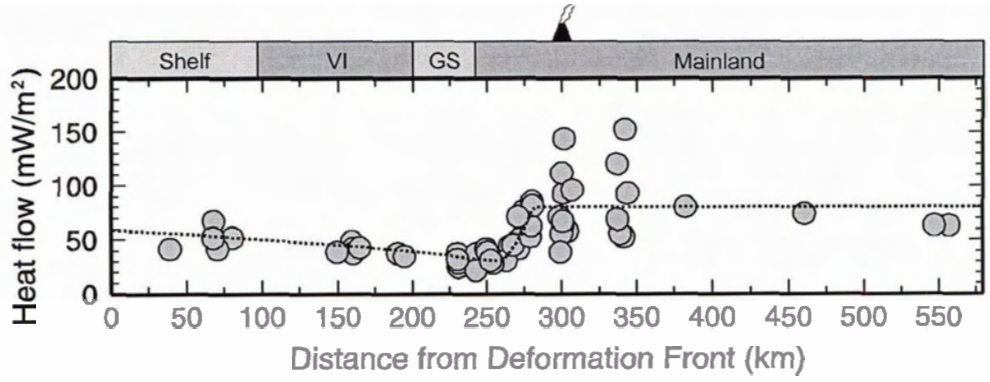

Figure 2.13. Heat flow data across southern Vancouver Island and the adjacent mainland, projected along the profile in Figure 2.1. The dashed line indicates the general trend of the data. The average heat flow for the backarc is based on results corrected for crustal heat generation. Spikes in the trend over the projected location of the volcanic arc (~300 km from the deformation front) were not included. VI = Vancouver Island; GS = Strait of Georgia [modified from *Hyndman and Lewis, 1995*].

CHAPTER 3

Global Positioning System

3.1 Introduction to GPS

The global positioning system (GPS), comprised of 24 high altitude satellites distributed over 6 orbital planes, transmits radio signals that can be used for precision positioning and navigation on the Earth's surface. Originally designed for military use, the capability to establish automated networks over large regions and have stations in remote locations has allowed GPS to be widely used and to become an integral part of deformation studies. GPS has been used on the west coast of Canada to examine crustal deformation since the early 1990s [e.g. *Dragert et al., 1995; Miller et al., 2001*]. However, due to the higher precision of the horizontal measurements compared to the vertical (~ factor of 3), these studies focused mainly on the former component. Only now have sufficient data been collected in this region to reduce errors such as to allow interpretations of vertical deformation rates. This chapter explores the basic methodology of GPS positioning and the results of over 8 years of continuous vertical component data from a subset of network stations on the west coast of Canada.

3.2 GPS Positioning

GPS positioning works on the basis of three-dimensional triangulation: the position of the receiver can be calculated if the distance between the satellites in the GPS constellation and receiver, and the exact position of the satellites are known. The distance to satellites is determined by precise timing of the travel-time of the radio signals. Four

satellites are needed to determine position, three for the triangulation calculations and the fourth to calculate the clock offset between the satellites and receiver.

Factors affecting the accuracy of GPS positioning include the following: satellite geometry, satellite redundancy, accuracy of ionospheric and tropospheric delay estimates, accuracy of satellite orbits, accuracy of earth tide models, the multipath environment of the site, the type of receiver and antennas used, the duration of data analyzed and the methods of analysis. Position accuracy can range from 10's of meters as in hand-held GPS units to a few millimeters as in precision crustal motion monitoring. In the former case, position is based on single-frequency code-determined, uncorrected pseudorange estimates using broadcast orbit information. In the latter case, position is based on dual-frequency, phase-determined, corrected pseudoranges using precise satellite orbits. In addition, the accuracy of horizontal versus vertical positioning is typically 2-3 times as high, mainly due to the 360° azimuthal distribution of satellites for horizontal constraint and the strong correlation of path delay estimates with vertical position.

3.3 Observables and Potential Error Sources

Pseudoranges rather than true distances are the observables resulting from GPS tracking, typically because the ground receivers use imprecise crystal clocks subject to drift rather than precisely set, stable atomic clocks [*Hofmann-Wellenhof et al., 2001*]. As well, GPS signals are subject to unknown propagation delays associated with variable troposphere conditions. The pseudoranges are affected by both systematic and random noise. The sources of error can be classified into satellite, propagation medium, and receiver related errors (e.g. Table 3.1).

Table 3.1. Range biases [*Hofmann-Wellenhof et al., 2001*].

Source	Effect
Satellite	Orbital errors, Clock bias
Signal propagation	Tropospheric refraction, Ionospheric refraction
Receiver	Antenna phase centre variation, Clock bias, Multipath

Systematic errors can be greatly reduced either through modelling or combining observables. For example, differencing between receivers can largely eliminate biases related to the satellites and receiver biases can be eliminated by differencing between satellites [*Hofmann-Wellenhof et al., 2001*]. Errors introduced by site conditions, such as multiple reflections of the signal (Figure 3.1) can be minimized through careful survey and analysis procedures. This might include positioning of the instrumentation such that the distance from possible reflecting surfaces is maximized, and checking for systematic shifts in position correlated with satellite geometry in data analysis.

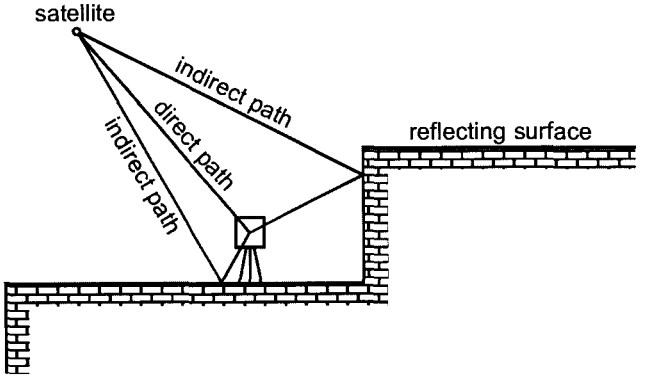

Figure 3.1. Schematic diagram of multipath effect. This effect results from multiple reflections of the signal where interference between the direct and reflected signals is mainly random [*Hofmann-Wellenhof et al., 2001*].

Another source of error in GPS measurements is due to ionospheric and tropospheric refraction. The ionosphere, a series of layers of charged particles located 50 km to 1000 km above the earth, acts as a dispersive medium for GPS signals. The result is a difference between the group and phase velocities, specifically, a group (code measurement) delay and a phase (carrier) advance [*Hofmann-Wellenhof et al., 2001*]. However, because signal propagation is frequency dependent, ionospheric effects can be removed using dual frequency techniques.

The troposphere, a part of the lower neutral (non-ionized) atmosphere, is located from the surface of the earth to ~50 km above the surface. This layer is a non-dispersive medium with respect to GPS signals and therefore signal propagation is frequency

independent. Propagation delay caused by the troposphere can be divided into two source categories: dry delay (accounting for 90% of the effect), which is a function of atmospheric thickness, and wet delay (accounting for 10%), which is a function of water vapour content [*Hofmann-Wellenhof et al., 2001*]. Signals from satellites low on the horizon have a proportionally longer travel path through the atmosphere than signals from satellites at zenith and therefore accumulate a larger delay. The average tropospheric bias will be absorbed into the clock bias as the receiver position is solved, causing an overestimate of the delay for high elevation satellites and an underestimate for low elevation satellites. To minimize this effect, high-precision GPS analysis software solves for a path delay that has a 1/cosZ dependence, where Z is the zenith angle of a satellite. Nonetheless, the correlation of tropospheric delay and antenna height remains a chief contribution to the larger error in the estimates of the vertical component in precise GPS positioning.

3.4 Application of GPS to Regional Crustal Deformation Studies

3.4.1 GPS Network

Differential GPS methods are used in this study to determine regional crustal deformation in the northern CSZ. Positions of permanent benchmarks are measured with respect to a reference station. The location of the reference station is chosen to be far from the deforming areas (i.e. located on nearly stable North America) yet close enough such that many errors are common between stations and thus automatically removed in the data processing stage (Figure 3.2).

The reference station used in this study is located near Penticton, British Columbia at the Dominion Radio Astrophysical Observatory (DRAO). Permanent markers located across southwestern British Columbia (Figure 3.3) referenced to this station constitute the Western Canada Deformation Array (WCDA) [*Dragert et al., 1995*], a network of automated, continuous GPS tracking stations operated by the Pacific

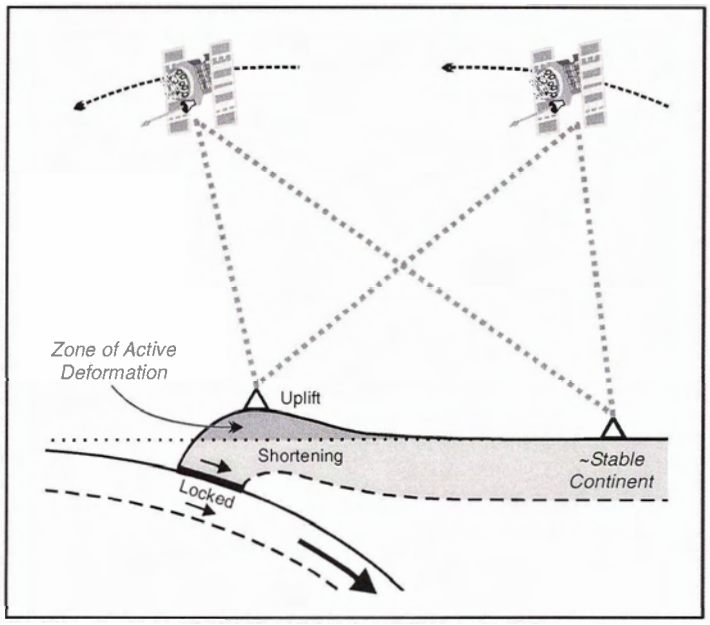

Figure 3.2. Regional-scale differential GPS [*Henton, 2000*].

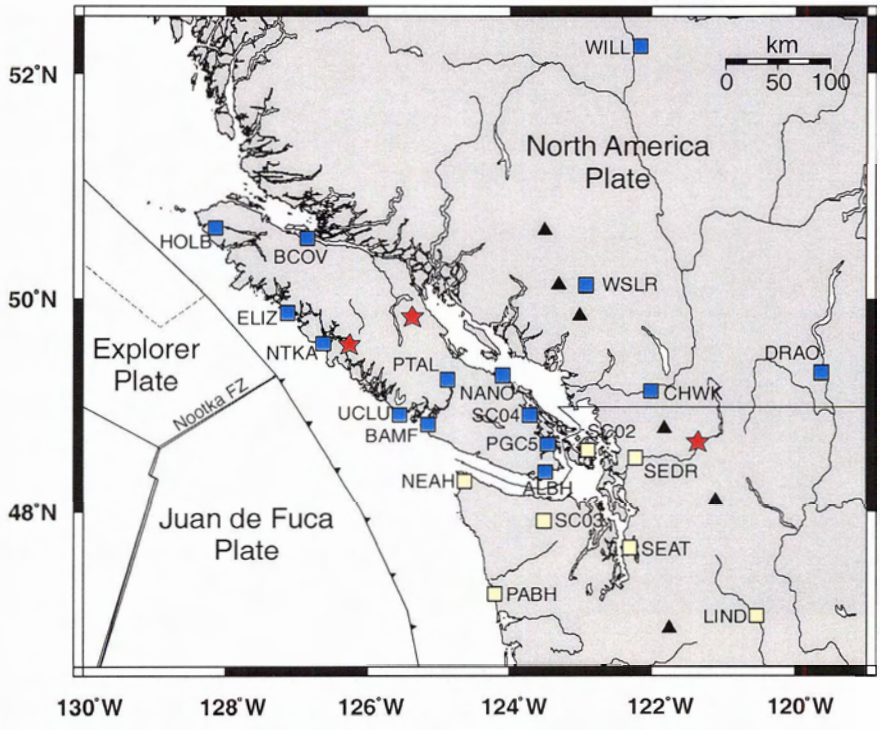

Figure 3.3. Continuous GPS tracker sites (blue squares) of the Western Canada Deformation Array (WCDA) and selected sites (yellow squares) from the Pacific Northwest Geodetic Array (PANGA). Stars indicate the approximate location of major crustal earthquakes (see text and Figure 2.2).

Geoscience Centre (PGC) office of the Geological Survey of Canada (GSC). Established in 1991 with the initiation of DRAO, the network now consists of 15 continuously monitoring stations on the west coast of Canada. The monumentation at most stations consists of a concrete pier (Figure 3.4) or a stainless steel pedestal (Figures 3.5), anchored to bedrock, with a geodetic-quality choke-ring antenna mounted on a forced centre base.

This study focuses on the relative vertical motion of two WCDA stations (Figure 3.6), UCLU (Ucluelet) and NANO (Nanoose Harbour), which define the net tilting across southern Vancouver Island. A secondary set of stations, NEAH (Neah Bay) and ALBH (Albert Head), are used to describe the net relative vertical motion between the west coast of the Olympic peninsula and the southern tip of Vancouver Island. However, only the UCLU-NANO difference can be compared directly with results from repeated leveling surveys (Chapter 4) and repeated precise gravity measurements (Chapter 5). An alternate comparison that can be used for both sets of stations comes from crustal deformation determined using long-term monthly mean sea level trends (Chapter 6) between Tofino (TOF) and Point Atkinson (ATK) and between Neah Bay (NEA) and Victoria (VIC) (see Figure 3.6).

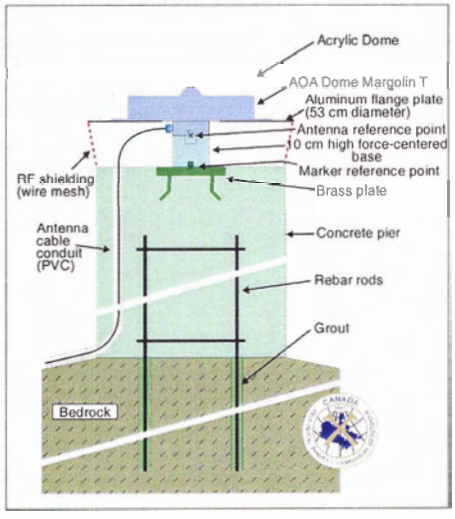

Figure 3.4. Schematic illustration showing the concrete pier construction of a WCDA monument (modified from a *figure courtesy of Michael Schmidt, Geodynamics Group, PGC-GSC*).

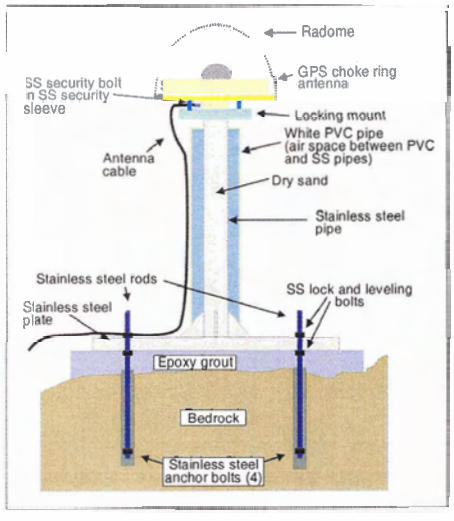

Figure 3.5. Schematic illustration showing the stainless steel pedestal construction of a WCDA monument (modified from *a figure courtesy of Michael Schmidt, Geodynamics Group, PGC-GSC*).

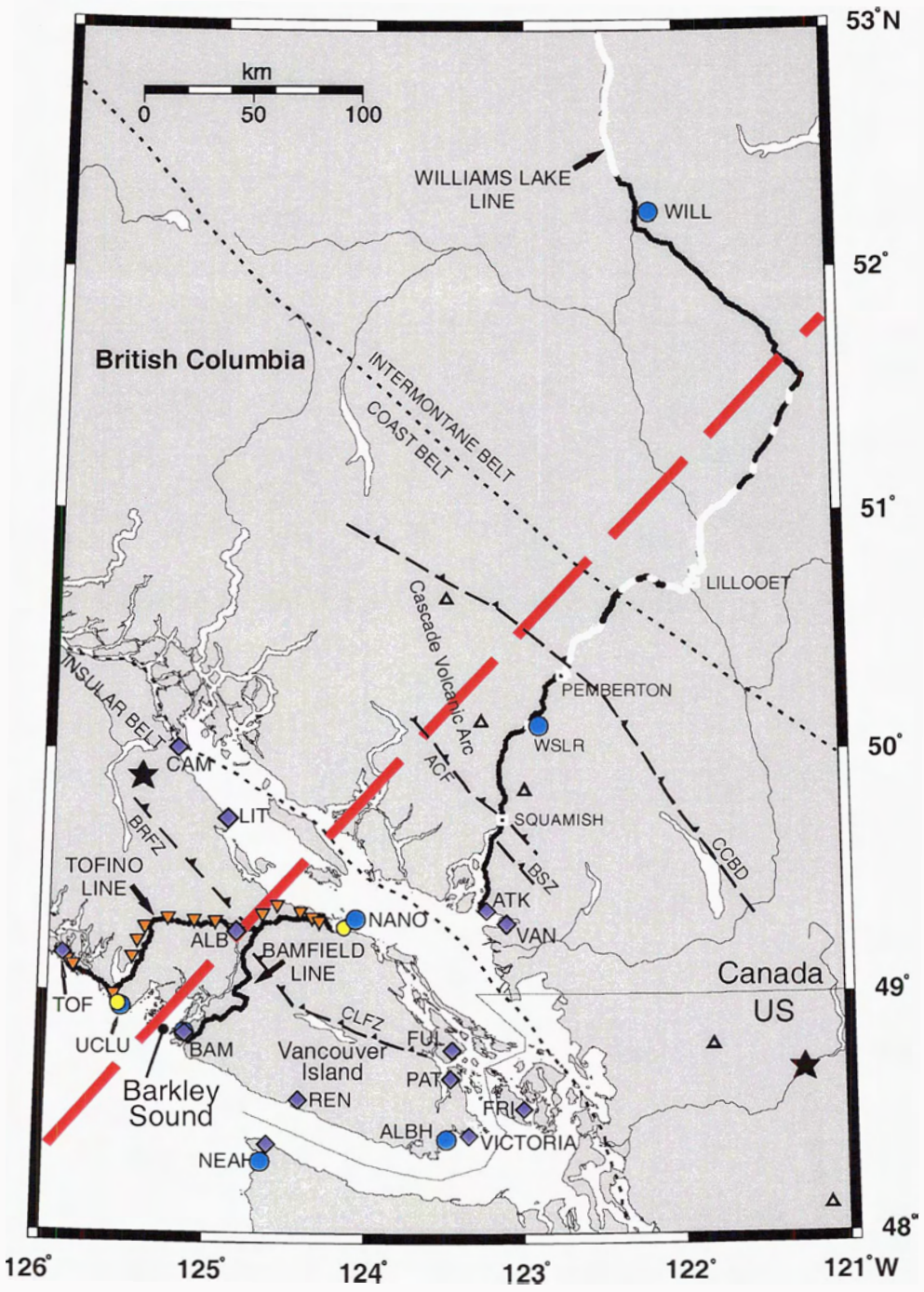

Figure 3.6. Locations of vertical deformation surveys across the northern Cascadia subduction zone. Black (elevation changes available) and white (no elevation changes available) dots are benchmark locations along leveling lines; inverted triangles are relative gravity stations; yellow dots are absolute gravity stations; blue dots are continuous GPS (WCDA) stations; diamonds are tidal stations. Thick dashed line is across-margin profile as in Figure 2.1. Thin, short-dashed lines indicate morphological Belt boundaries (Figure 2.5). Thin long-dashed lines are selected known crustal faults (Figure 2.8). Stars show locations of major historical crustal earthquakes (Figure 2.2). Abbreviations as in Figures 2.7 and 2.8.

3.4.2 Methodology - GPS

Continuous GPS Station Data Processing

Daily variations in the vertical component of continuous GPS data from January 1, 1995 to March 15, 2003 were used in this study to investigate the net tilt across southern Vancouver Island across two profiles: UCLU to NANO in the north of the study area and NEAH to ALBH, near Victoria, in the south (Figure 3.6). The continuous GPS station data were processed as part of the WCDA network processing at the PGC-GSC. Processing is done using the Bernese GPS Software Version 4.2 [*Beutler et al., 2002*], where the data are binned into 24 hour time periods. Solutions of relative positions are obtained using an L3 (ionospheric free) phase, double-difference baseline strategy with fixed ambiguities, applying ocean loading corrections and estimating tropospheric delay [*Dragert et al., 2000*; *Mazzotti et al., 2002*]. The output of the analysis is captured in a series of summary files for each station on a year-by-year basis, which include daily variations in latitude, longitude, and height with respect to the reference station DRAO. Using these values, differences were calculated between stations to obtain the motion in the north, east, and up directions. However, before the differences between stations were calculated, outliers (values $>3\sigma$ of the trend) were removed from the data sets.

Linear Regression of Continuous Baseline Data

Analysis of the position time series trends from the WCDA sites used two approaches: linear regression of time series from individual stations, and linear regression on differenced output between pairs of stations. The time series have been corrected for recognized datum-offsets (steps), which are typically related to equipment changes, antenna changes, RF (radio frequency) skirt installation or replacement, or dome installation or replacement. These parameters for the reference station (DRAO) were not included in the regressions because they are common to all sites and the effect of such offsets should therefore cancel in the differencing process. As well, the initial regressions

did not solve for annual variations or for slow slip events (Section 2.2) occurring at a ~14.5 month interval on the deep portion of the interface of the thrust fault in the northern CSZ [*Dragert et al., 2001*; *Miller et al., 2002*]. Slow slip events are assumed to be part of the tectonic process along the margin contributing to long-term tilting, and the annual variations are assumed, in the initial regressions, to be similar at all stations in close proximity to each other (as in this study) and will therefore be removed or minimized by the differencing process. Nonetheless, *Henton* [*2000*] demonstrated that the vertical component time series for the four WCDA sites under discussion contained annual signals with amplitudes ranging from 1 to 4 mm. However, his results are based on a different analysis technique and less precise orbits. Henton also showed that spectral components changed with time. The suggestion is that annual signals may be dependent on analysis technique or may be time variant. It is, however, worthwhile to test the impact of such signals on the current time series and as such, a secondary analysis was completed, which included fitting a 365.25-day period sinusoid. For descriptive purposes, regression analysis that has not included the seasonal signal will be referred to as Case 1 and analysis that has included a seasonal signal as Case 2.

Datum-offsets due to instrumental set-up changes were removed by fitting step functions during the linear regressions. As noted in *Henton* [*2000*], the time of occurrence of these steps is well documented, but their magnitudes are not known independently. However, an iterative process was used in this study to estimate the steps that made a significant contribution to offsetting the time series. This process involved iteratively estimating offsets for all times that equipment was modified at the respective station and subsequently removing them one by one if the standard error for the parameter was three-times larger than the step magnitude. This was repeated until all remaining step estimates had magnitudes $>3\sigma$. An adjustment to the time series was then made for all days after the equipment modification. Step magnitudes of the final height parameters ranged from 1.72±0.35 mm to 20.07±0.76 mm for Case 1 and from 1.52±0.35 mm to 21.12±0.69 mm for Case 2.

Correcting for Reference Station and North America Plate Motions

General interpretations of the GPS data are affected by vertical motion at DRAO with respect to North America. If there is vertical motion at DRAO, then it must be accounted for to obtain the true vertical component of the tectonic signal, which is the overall goal of this study. Therefore, 1.20±0.50 mm yr^{-1} (up; nominal ITRF2000 solution for DRAO [*Altamimi et al., 2002*]) has been added to all uplift rates (defined here as the vertical velocity at the measurement location) for the individual stations as determined from linear regression analysis. It is assumed that there is no component of vertical motion from DRAO remaining in the differenced results. Additional information about the vertical motion at this site can come from absolute gravity measurements; however, at this time no velocity is available from that method.

As well, day-to-day site position estimates with respect to the fixed reference station will include motion due to North America plate rotation. Therefore, using a recent GPS-derived North America Euler vector [*Sella et al., 2002*], a vertical rate correction was derived for each of the four GPS stations [*H. Dragert, personal communication*] discussed in this chapter. These motions were subtracted from the calculated uplift rates of the respective sites. The corrected uplift rates (see Section 3.4.3) can then be directly compared to observations from the other geodetic techniques used in this study (see Chapters 4 and 6) to determine deformation patterns.

Revising Error Estimates for WCDA Stations

The error estimates obtained from the linear regressions of GPS data are based on a random error model and are usually considered overly optimistic. Therefore, in this study a combined random error, random walk, and flicker noise model [cf. *Mao et al., 1999*; *Mazzotti et al., 2003*] has been applied to all error estimates for both Cases 1 and 2. The revised error estimates were calculated for each station or pair of stations based on the daily scatter in each of the time series.

Potential Antenna Phase Centre Bias

A potential bias in the GPS results may arise from the antenna phase centre at one or more of the stations in this study. A recent study [*Morken et al., 2003*] compared height estimates at NEAH between 1998 and early 2004 with and without the use of phase calibration maps. The trend calculated from the difference between the observations (mapped results minus unmapped results) (-0.64 ± 0.02 mm yr^{-1}) indicates that a correction of the same magnitude should be added to the observed tectonic trend at this station. That is:

$$Neah\ Trend\ (corrected) = Neah\ Trend\ (uncorrected) + 0.64\ \text{mm}\ yr^{-1}$$

The topic is not pursued further in this study. However, it is recognized that although the correction at NEAH may not be significant, it opens the question of similar biases being present at other stations.

3.4.3 GPS Results

Single GPS Stations

Figures 3.7 and 3.8 show the Case 1 (Section 3.4.2) daily variations in the vertical component of the WCDA baselines for this study. The plots display linear trends over time, from which uplift rates are inferred. In both figures (3.7 and 3.8), the seasonal variations described in Section 3.4.2 are evident. These, however, do not appear to bias the long-term trend estimates since the time series span multiple cycles of the signals (cf. Tables 3.2 and 3.3).

Uplift rates were calculated by linear regression analyses of the Case 1 and Case 2 daily variations (Tables 3.2 and 3.3). The focus for Case 2 results is on the seasonal signal components (amplitude and phase) as well as how day-to-day scatter before and after day 2000 (June 24, 2000) of the time series (based on a qualitative assessment of the time series) compares to scatter in the Case 1 time series.

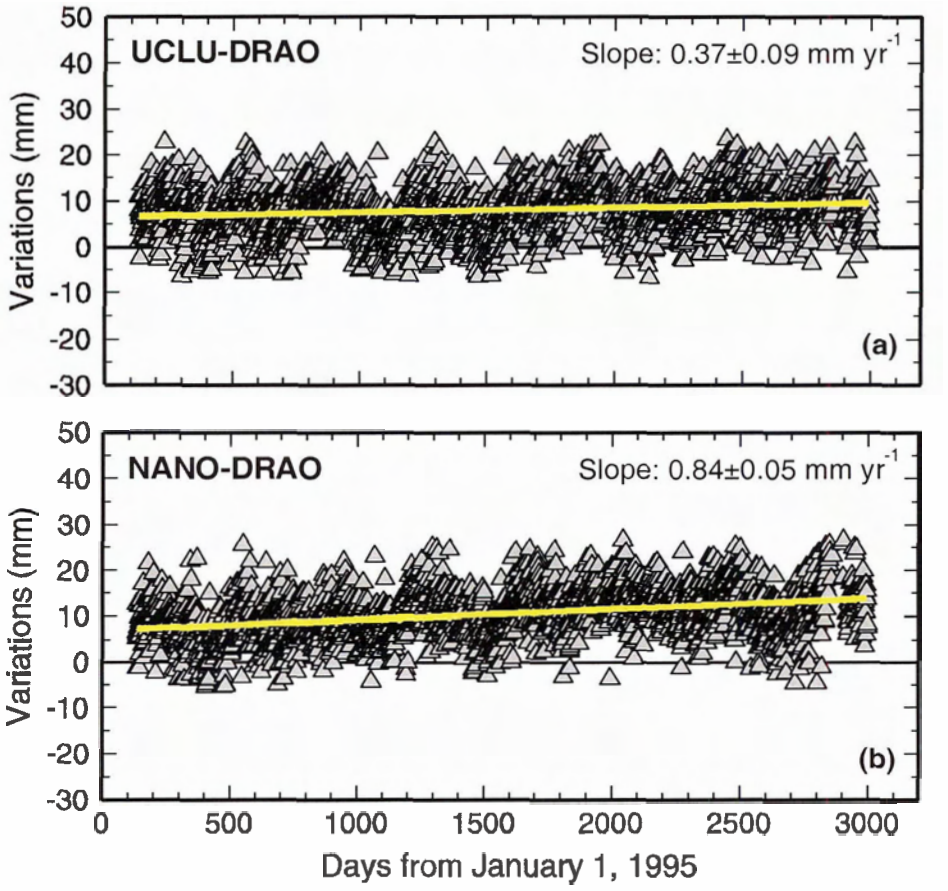

Figure 3.7. Daily height variation time series of the continuous GPS stations (a) Ucluelet and (b) Nanoose between 1995 and 2003 relative to the reference station DRAO. Slope values with standard errors of the raw data trends, from regression analyses, are shown.

Figure 3.7a shows the daily variations in the vertical component for UCLU with respect to the reference station (DRAO). The Case 1 long-term uplift rate resulting from regression analysis and corrected for NA plate- and DRAO- motions as well as the revised error estimate (see Section 3.4.2) is 2.53±1.14 mm yr^{-1} (Table 3.2). Day-to-day scatter for Case 1 is reduced to 4.74 mm in the later half of the time series from 5.23 mm before day 2000.

The Case 2 long-term uplift rate is 2.54±1.14 mm yr^{-1} (Table 3.3). For all time periods, there is a decrease in the day-to-day scatter from Case 1 to Case 2. Day-to-day scatter is also reduced in the later half of the time series, as is the amplitude estimate of the annual signal (Table 3.4).

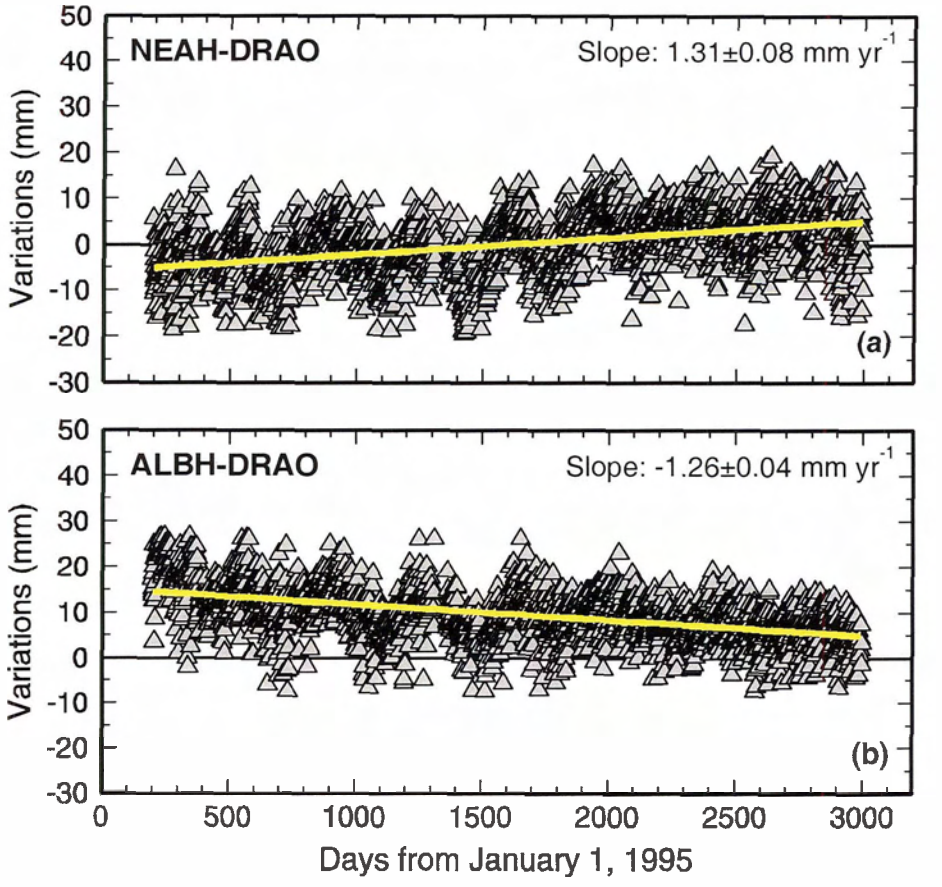

Figure 3.8. Daily height variation time series of the continuous GPS stations (a) Neah Bay and (b) Albert Head between 1995 and 2003 relative to the reference station DRAO. The Neah Bay time series has been zero-meaned. Slope values with standard errors of the raw data trends, from regression analyses, are shown.

Figure 3.7b shows the daily variations in the vertical component for NANO with respect to DRAO. The Case 1 long-term uplift rate at this station indicates a corrected (see Section 3.4.2) uplift rate of 2.70±1.12 mm yr^{-1} (Table 3.2).

Case 2 regression analysis indicates a corrected (see Section 3.4.2) uplift rate of 2.67±1.08 mm yr^{-1} (Table 3.3). Unlike the UCLU time series, the seasonal signal amplitude (Case 2) and the scatter (for both Cases 1 and 2) increase slightly (Table 3.4) after day 2000 of the time series.

Table 3.2. Case 1 Uplift rates of WCDA stations corrected for NA- and DRAO-motions.*

Station	Relative Uplift Rate (mm yr^{-1})	Standard Error on Trend (mm yr^{-1})[1]	Combined Error (mm yr^{-1})[2]	NA-Motion Correction (mm yr^{-1})[3]	Corrected Uplift Rate (mm yr^{-1})[4]	rms Error (mm yr^{-1})[5]
UCLU	0.37	0.09	1.03	-0.96	2.53	1.14
NANO	0.84	0.05	1.00	-0.66	2.70	1.12
NEAH	1.31	0.08	1.20	-1.00	3.51	1.30
ALBH	-1.26	0.04	1.01	-0.81	0.75	1.13

*Uplift rate refers to vertical velocity of the station.
[1]Standard error on the linear trend from Case 1 regression analysis.
[2]Error including combined random error, random walk, and flicker noise model [*Mao et al., 1999*; *Mazzotti et al., 2003*].
[3]NA-motion corrections are subtracted from the relative uplift rates.
[4]Uplift rates corrected for DRAO-vertical motion (1.20 mm yr^{-1} [*Altamimi et al., 2002*]) and NA-motion.
[5]rms error for the NA- and DRAO-motion corrected uplift rates.

Table 3.3. Case 2 Uplift rates of WCDA stations corrected for NA- and DRAO-motions.*

Station	Relative Uplift Rate (mm yr^{-1})	Standard Error on Trend (mm yr^{-1})[1]	Combined Error (mm yr^{-1})[2]	NA-Motion Correction (mm yr^{-1})[3]	Corrected Uplift Rate (mm yr^{-1})[4]	rms Error (mm yr^{-1})[5]
UCLU	0.38	0.09	1.02	-0.96	2.54	1.14
NANO	0.81	0.05	0.96	-0.66	2.67	1.08
NEAH	1.44	0.07	0.95	-1.00	3.64	1.07
ALBH	-1.21	0.04	1.13	-0.81	0.80	1.24

*Note as in Table 3.2.
[1-5]Notes are the same as those in Table 3.2.

Figure 3.8a shows the daily variations in the vertical component for NEAH with respect to DRAO. The Case 1 long-term uplift rate, corrected for NA- and DRAO-motions, indicates an uplift rate of 3.51±1.30 mm yr^{-1} (Table 3.2).

The Case 2 long-term corrected (see Section 3.4.2) uplift rate is 3.64±1.07 mm yr^{-1} (Table 3.3). As with UCLU, the seasonal signal amplitude (Case 2) and scatter (Cases 1 and 2) decrease (Table 3.4) after ~day 2000 of the time series.

Table 3.4. Seasonal signal and day-to-day scatter results for WCDA stations.

Station	CASE 1		CASE 2				Time Period[1]
	rms Scatter (mm)	Variance (mm^2)	rms Scatter (mm)	Variance (mm^2)	Amplitude (mm)	Phase (radians: $-\pi/2$ to $\pi/2$)	
UCLU	5.07	25.71	5.02	25.18	1.06	0.03	1
	5.23	27.39	5.06	25.60	1.95	-0.33	2
	4.74	22.47	4.65	21.63	1.39	-1.25	3
NANO	4.93	24.28	4.73	22.38	1.97	0.81	1
	4.84	23.46	4.57	20.85	2.26	0.35	2
	5.09	25.89	4.68	21.93	2.91	-1.46	3
NEAH	5.94	35.33	5.59	31.28	2.87	-0.43	1
	6.06	36.69	5.58	31.11	3.32	-0.44	2
	5.72	32.70	5.53	30.59	2.07	-0.37	3
ALBH	5.00	25.02	4.73	22.37	2.92	0.79	1
	5.42	29.35	4.97	24.72	3.14	0.33	2
	4.17	17.36	4.05	16.40	1.41	1.16	3

[1]Indicates what part of the time series the regression was performed on: 1 = full length of time series (day 1-2996); 2 = day 1-1999; 3 = day 2000-2996.

Figure 3.8b shows the daily variations in the vertical component for ALBH with respect to DRAO. The long-term uplift rate, corrected for NA- and DRAO-motion, indicates uplift at a rate of 0.75±1.13 mm yr^{-1} (Table 3.2). As with UCLU and NEAH, after ~day 2000 of the time series, there is a reduction in the daily scatter (Table 3.4).

The Case 2 corrected long-term uplift rate is 0.80±1.24 mm yr^{-1} (Table 3.3). This is the only case where the combined error has increased with the addition of a seasonal signal. However, there is still a reduction in the daily scatter from Case 1. The daily scatter for Case 2 between time periods is also decreased in the later portion (after ~day 2000) of the time series, as with UCLU and NEAH.

Paired GPS Stations

Figure 3.9 shows the differences of the daily variations in the vertical component between pairs of stations, all of which are individually referenced to DRAO. As with the individual station time series, the differenced daily variations display linear trends, the slope of which is used to determine the net relative uplift rate (outer coastal station relative to inner coastal station). There is a distinct difference between the trends derived from the pairs of GPS stations in the northern (Figure 3.9a) and the southern (Figure 3.9b) part of the study area. To the north (UCLU-NANO), the differenced uplift rate is -0.18±0.90 mm yr^{-1} (Table 3.5). This is a contrast to the difference in uplift rates to the south (NEAH-ALBH) 2.86±0.94 mm yr^{-1} (Table 3.5). Table 3.6 shows the results of the seasonal signal and day-to-day scatter tests for the differenced (paired station) vertical component. For all cases of the paired-station regressions, the full time series were used.

Table 3.5. Differential raw and NA-motion corrected uplift rates for WCDA stations.

Station Pairs	Raw Differential Uplift Rate (mm yr^{-1})	Error on Trend (mm yr^{-1})[1]	Differential NA-Motion Correction (mm yr^{-1})	NA-Motion Corrected Differential Uplift Rate (mm yr^{-1})	Error on Trend (mm yr^{-1})[2]
UCLU-NANO	-0.48	0.04	-0.30	-0.18	0.90
NEAH-ALBH	2.66	0.04	-0.19	2.86	0.94

[1]Error from linear regression of raw differential daily height variations.
[2]Error including combined random error, random walk, and flicker noise model [*Mao et al., 1999*; *Mazzotti et al., 2003*].

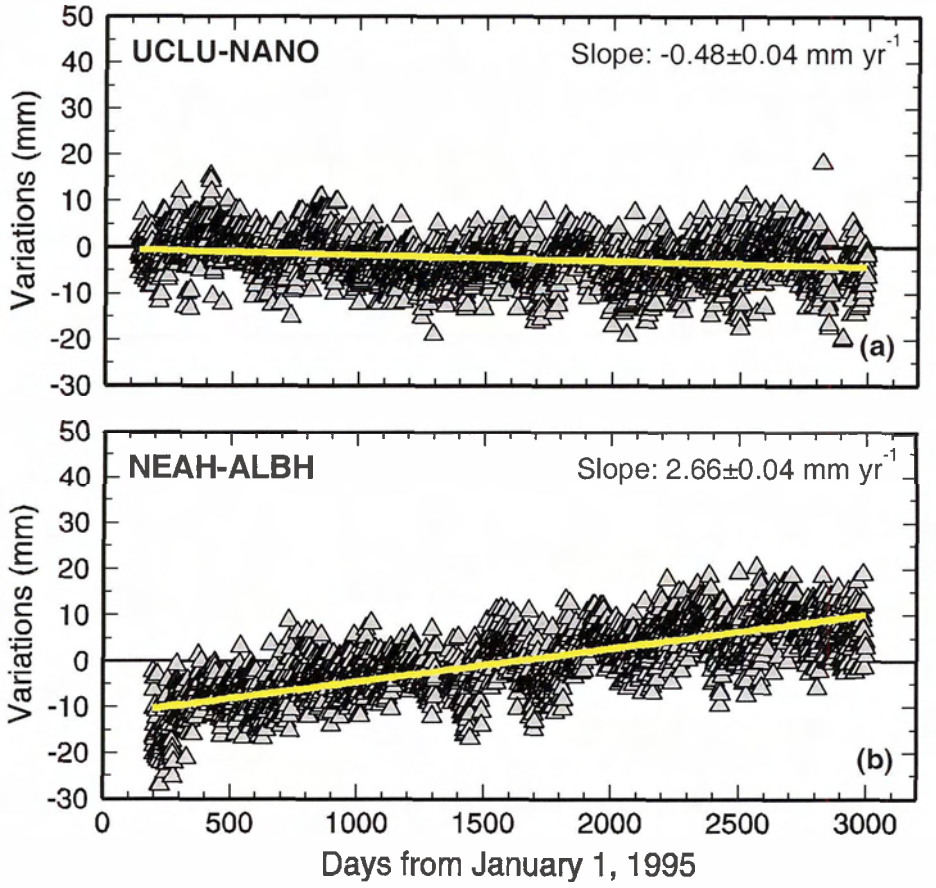

Figure 3.9. Difference in the daily height variations between the continuous GPS stations (a) Ucluelet and Nanoose and (b) Neah Bay and Albert Head between 1995 and 2003. The Neah Bay-Albert Head time series has been zero-meaned.

Table 3.6. Seasonal signal and day-to-day scatter results for paired stations.

Paired Stations	CASE 1		CASE 2			
	rms Scatter (mm)	Variance (mm^2)	Amplitude (mm)	Phase (radians: $-\pi/2$ to $\pi/2$)	rms Scatter (mm)	Variance (mm^2)
UCLU-NANO	4.43	19.61	1.56	-1.33	4.29	18.40
NEAH-ALBH	4.68	21.91	2.41	1.33	4.36	18.98

3.4.4 Discussion of Continuous GPS Results

Discussion of Seasonal Signals

The seasonal signals observed in all of the individual stations time series are probably not true sinusoids since the amplitudes are not uniform over the length of the time series (Table 3.4). Nonetheless, a decrease in the variance (see Table 3.4) at the individual and differenced stations resulting from inclusion of a seasonal signal in the regression indicates that fitting even a poor sinusoid in the analysis reduces scatter. In any case, inclusion of a seasonal signal in the analyses does not greatly affect the slopes of the time series (cf. Tables 3.2 and 3.3).

Single GPS station Discussion

Analysis of over 8 years of continuous GPS data, from four stations around southern Vancouver Island, suggests uplift throughout the region on the order of 1-4 mm yr^{-1} (Table 3.3). This is generally consistent with the previous results from other methods [e.g. *Dragert et al., 1994*; *Wigen and Stephenson, 1980*].

Paired GPS Station Discussion

Differential uplift rates between pairs of continuous GPS stations suggests that although non-tectonic effects cannot be totally ruled out, the tilt rate across the coastal margin at UCLU is less than expected, based on results from other methods [see *Dragert et al., 1994*], and is distinctly different from the tilt rate between NEAH and ALBH (Table 3.5). Possible explanations include a secondary deformation signal affecting observations along one of the two transects, a 3-dimensional tectonic regime (along the margin), or potential antenna phase centre bias as discussed for NEAH (see Section 3.4.2).

CHAPTER 4

Leveling

4.1 Introduction to Leveling

Vertical deformation of the Earth's crust can be measured most directly by observing changes in the relative elevation of permanent markers (benchmarks), which in many cases are installed for use in basic vertical control surveys (leveling surveys). This chapter will begin by exploring the basic methodology of leveling surveys and the errors encountered in measuring elevations. The primary objective of this chapter is to present results from three repeat leveling surveys, two across southern Vancouver Island and the other on the adjacent mainland across the Coast Belt into the Intermontane Belt.

4.2 Measuring Elevations

The elevation of a benchmark is defined as the vertical difference above or below a datum (e.g. Figure 4.1) or a level surface (e.g. geoid) [*Davis et al., 1981*]. The technique used to obtain benchmark elevations consists of taking a series of foresight readings (where the elevation is unknown) and backsight readings (where the elevation is known) along a line using a level and graduated rod (Figure 4.2). The difference in elevation between two benchmarks is the sum of the differences between the backsight taken on a given point and a foresight taken on a successive point [*Davis et al., 1981*].

"Absolute" elevations along a survey line are determined by establishing a reference benchmark (or zero reference for heights along the survey line), at which the elevation above sea level is known (e.g. Figure 4.1). The height (H_R) of the reference benchmark above mean sea level can be calculated by [*Vanicek and Krakiwsky, 1986*]:

$$H_R = H_{MSL} + \Delta H_{BM-TG}$$

where H_{MSL} is the mean sea level height and ΔH_{BM-TG} is the height between the benchmark, BM, and zero level of the tide gauge, TG.

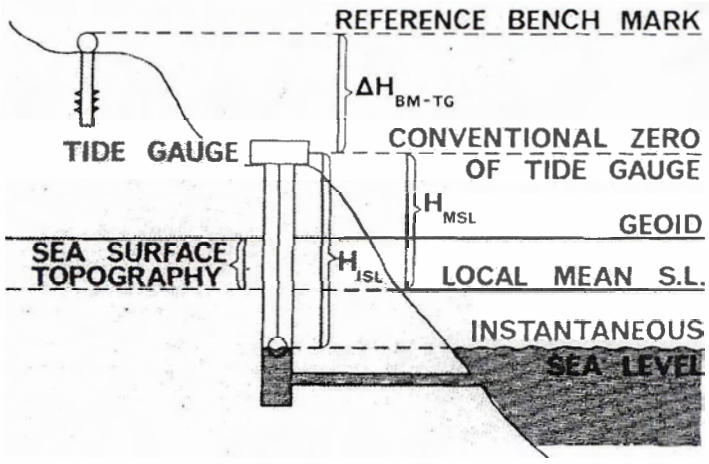

Figure 4.1. Establishment of height of reference benchmark [*Vanicek and Krakiwsky, 1986*].

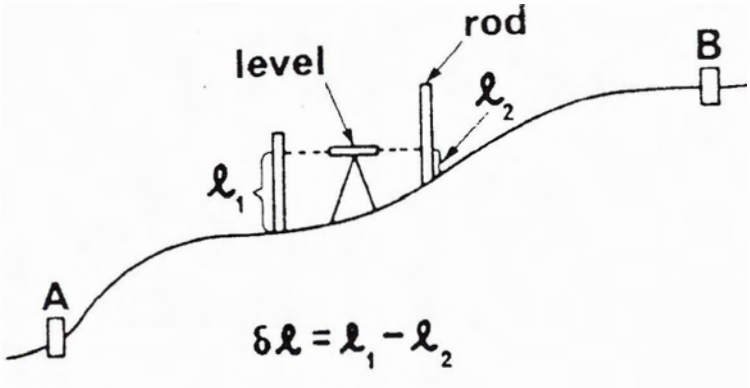

Figure 4.2. Schematic diagram illustrating one setup in the leveling procedure designed to measure the elevation difference between two established benchmarks, A and B [*Vanicek et al., 1980*]. Symbols are as in text.

4.3 Surveying Errors

The following is a brief outline of errors that can accumulate during leveling surveys. For a detailed account of the history of data collection procedures and their impact on data quality, the reader is referred to *Gareau [1986]*. Table 4.1 summarizes some of the errors relevant to leveling surveys.

4.3.1 Random Errors

Random errors in leveling data can originate from imprecise measurements or imperfections in the equipment. These errors can be minimized through survey procedures such as measuring two runs of the line (forward and backward) and using double-scale rods. If the random errors of a measured elevation difference, Δl, between two adjacent benchmarks are statistically independent, the standard deviation of the height difference, $\sigma_{\Delta l}$, can be written as:

$$\sigma_{\Delta l} = \sigma_0 K^{1/2}$$

where K is the distance between the two benchmarks, in km, and σ_0 is the unit standard deviation per 1 km [*Vanicek et al., 1980*; *Vanicek and Krakiwsky, 1986*].

4.3.2 Systematic Errors

The degree of precision for leveling measurements depends on survey methods, survey instrumentation, and survey conditions (e.g. weather). High precision (special order) leveling data are generally corrected for these systematic errors, arising from the above sources, based on laboratory calibrations or theoretical bases.

Table 4.1. Errors in Leveling [modified from *Davis et al., 1981*].

Source	Type	Cause	Remarks	Procedure to eliminate or reduce
Instrumental	Systematic	Line of sight not parallel to axis of level tube	Error of each sight proportional to distance[a]	Adjust instrument; balance sum of backsight and foresight distances
		Rod not standard length (throughout length)[b]	May be due to manufacture, moisture, or temperature; error usually small	Standardize rod and apply corrections, same as for tape
Personal	Random	Bubble not centered at instant of sighting	Error varies as length of sight	Check bubble before making each sight
		Rod not held plumb	Readings are too large; error of each sight proportional to square of inclination[a]	Wave rod, or use rod level
		Faulty turning points	...	Choose definite and stable points
Natural	Random	Temperature	May disturb adjustment of level	Shield level from sun
	Systematic	Earth's curvature	Error of each sight proportional to square of distance[a]	Balance each backsight and foresight distance; or apply computed correction
	Random	Variations in atmospheric refraction	Error of each sight proportional to square of distance[a]	Same as for Earth's curvature; take short sights, well above ground; take backsight and foresight readings in quick succession
	Systematic	Settlement of tripod or turning points	Observed elevations are too high	Choose stable locations; take backsight and foresight readings in quick succession; alternate order of sights

[a]Error of each sight is systematic, but the resultant error is the difference between the systematic error for foresights and that for backsights; hence, the resultant error tends to be random.
[b]Uniform wear of the bottom of the rod causes no error.

The following sub-sections describe some of the systematic errors that arise during leveling surveys and, in some cases, corrections that have been applied to the data sets in this study. While the magnetic correction is briefly described, it has not been applied to the data in this study, due to the non-magnetic nature of the equipment used for surveying since the 1980s [see *Gareau, 1986*].

Unequal (residual) Refraction

Perhaps the most significant error affecting precise leveling data is residual refraction, which is caused by a layering of moisture content and temperature in the atmosphere (e.g. Figure 4.3). The error associated with this effect is thus heavily dependent on the line of sight distance, slope of the ground (long line of sight and small slope enhance error), and weather conditions at the time of the measurement. One form of the refraction correction can be calculated as [*Vanicek and Krakiwsky, 1986 and references therein*]:

$$\delta H_R = A \Delta T \Delta S^2 \delta l$$

where ΔT is the temperature difference, in degrees Celsius, between two chosen elevations (z_1, z_2) above the ground, in meters; ΔS is the sight length, in meters; δl is the observed elevation difference between the two locations, in meters; and

$$A = \frac{4.76 \times 10^{-4}}{z_1^c - z_2^c}\left[\frac{-1}{1+c}\left(z_1^{c+1} - z_2^{c+1}\right) + z_0^c\left(z_1 - z_2\right)\right]$$

in millimeters per meter cubed and per degree Celsius. As well, z_0 is the elevation of the instrument above the ground and c is the exponent from the relation between temperature and elevation above the ground:

$$T = a + bz^c$$

This is also dependent on the altitude, z, of the temperature measurement location and the height of the instrument above the ground. Typically, z_0, z_1, and z_2 are 1.5 m, 0.5 m, and 2.5 m respectively. However, the above form of this correction can only be applied to

surveys after 1983 [*Gareau, 1986*], when measuring temperature gradients became standard practice in surveying. Before this, the model of *Holdahl* [*1981*] was applied to correct historical data using records of solar radiation, cloud coverage, wind speed, the albido and ground moisture [*Gareau, 1986*].

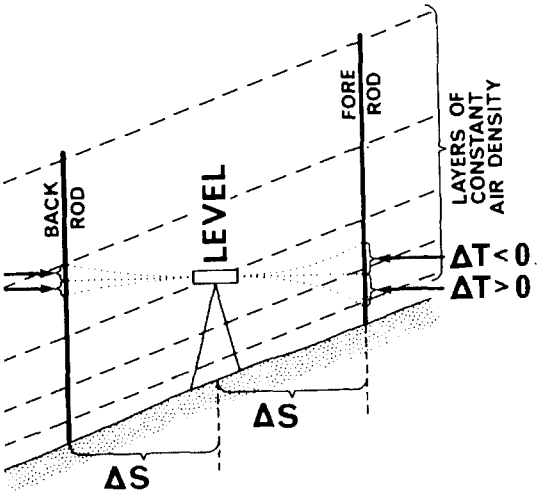

Figure 4.3. Character of residual refraction [*Vanicek and Krakiwsky, 1986*]. Symbols are as in text.

Rod Scale

Rod errors are also heavily height and slope dependent [*Vanicek et al., 1980*]. The leveling rod may be a source of systematic error in one of two ways: it is not a standard length, or there is expansion or contraction of the rod. The former becomes a systematic error that varies directly as the difference in elevation if the error is distributed over the length of the rod. It can be corrected for by comparing the rod with a standard rod length. The latter is due to a change in the moisture content or temperature, which causes the rod to expand or contract. Corrections for this error can be made based on observed temperatures of the rod [*Davis et al., 1981*]. As suggested by *Vanicek et al.* [*1980*], because rod errors are height and slope dependent, they should be detectable by correlations between the topography and measured elevation differences.

Astronomic

The astronomic correction accounts for temporal movements of level surfaces that result from attracting forces of the sun and moon. The effect on level surfaces from celestial bodies is, therefore, a large spatial-scale effect, although it is related to the local time that the survey is conducted [*Balazs and Young, 1982*]. The average magnitudes of the corrections are on the order of 10^{-2} mm.

Orthometric

The orthometric correction accounts for convergence of level surfaces at different elevations. As level surfaces are a function of gravity, a given level or equipotential surface is farther from sea level at the equator than at a point near the poles. In terms of leveling surveys, lines running north-south that are at different elevations will be referenced to different level surfaces. The correction (in meters) can be calculated as [*Davis et al., 1981*]:

$$\text{correction} = -0.005288 \sin 2\phi h \Delta\phi \text{arc}1'$$

where ϕ is the latitude at the starting point, h is the mean sea level elevation (meters) at the starting point, and $\Delta\phi$ is the change in latitude, in minutes, between the two points (positive in the direction towards the north pole).

The orthometric correction for elevation data in this study was supplied by the Geodetic Survey of Canada, Ottawa, Canada for only the 1994 and 2002 surveys along the Bamfield leveling line (Figure 3.6). The magnitudes of the corrections are very small (10^{-3} to 10^{-6} mm) and the nature of the error makes it unlikely to change with time. Therefore, elevation changes with time should not be dependent on this correction.

Magnetic

The magnetic correction accounts for a deflection of the compensator in 'self-leveling' surveying instruments under the influence of the earth's magnetic field. *Gareau*

[*1986*] compares the effect of the magnetic field on the compensator to that of a dampened pendulum. Under the influence of gravity, the pendulum would hang in the direction of the plumb line (Figure 4.4), but with a magnetic field present the pendulum would be deflected from the vertical by an angle δ. The magnitude of deflection will depend on construction and net magnetization of the instrument, the direction of line of sight (maximum magnitude in the northern direction), intensity of the field, and inclination of the field.

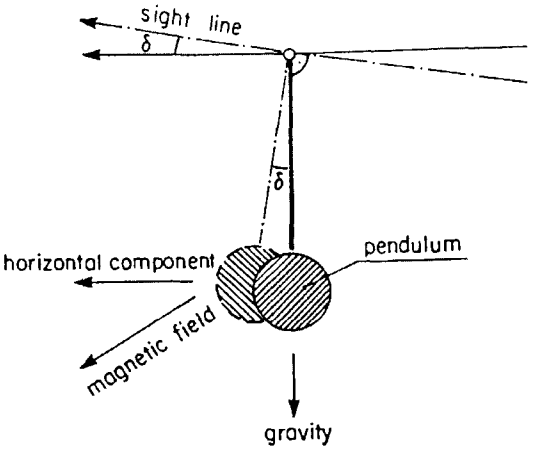

Figure 4.4. Effect of Earth's magnetic field on a stationary pendulum [*Gareau, 1986*].

Since the magnetization of the compensator can change with time (via temperature changes, shocks, or exposure to strong magnetic fields), it is generally impossible to calibrate this effect. The presence of magnetic field bias can be detected by correlating changes in elevation with magnetic azimuths of leveling sections.

Ocean Loading

A systematic error can also arise from ocean (or tidal) loading. As the ocean waters move, periodically the earth becomes loaded and unloaded, causing displacement, tilt, and gravity changes [*Pagiatakis, 1990*]. The effects of tidal loading can be separated into three components [*Zschau, 1976*]:

i) A tilt due to the gravitational attraction of the excess water masses.

ii) A primary load tilt resulting from elastic deformation of the Earth's surface.

iii) A secondary load tilt resulting from the change in direction of the local gravity vector caused by a redistribution of mass.

Typically, this error is only accounted for in gravity and GPS data analyses [e.g. *Lambert et al., 1998*; *Dragert et al., 2000*] along the west coast of Canada. However, it may play an important role for tilt measurements determined from leveling techniques in this region. While ocean tide loading effects have not been calculated for sites in this study, *Lambert et al.* [*1998*] state that displacements due to ocean tide loading can be at the tens of millimeters level. Therefore, if a differential effect occurred across south-central Vancouver Island, it is possible that significant transient tilts could be induced, thereby biasing survey measurements for short-line sections normal to the coast.

4.4 Benchmark Stability

Apart from the random and systematic errors of leveling measurements, the stability of benchmarks used in a survey is also considered when determining the quality of data. In this study, identification of benchmarks no longer usable for precise leveling was made through reconnaissance surveys. Questionable (e.g. unstable) markers were then omitted from the survey and in some cases new markers were established.

The identification of questionable changes in elevation due to ground instability can be aided by examining the type of benchmark used. Benchmarks cemented into bedrock are generally robust and therefore reflect genuine changes in regional crustal elevations. Benchmarks mounted on soil posts might respond to local ground conditions (e.g. frost, variations in soil moisture, vibration, ground slumping [*Holdahl et al., 1989*]) and are more likely to reflect non-tectonic changes in elevation. In this study, most of the benchmarks used are set in rock (outcrops or road-cuts).

4.5 Application of Leveling Surveys to Regional Crustal Deformation Studies

4.5.1 Leveling Survey Data Sets

Releveling data from two distinct regions were used to investigate tilt across the Cascadia margin: the first on southern Vancouver Island and the second on the adjacent mainland (Figure 3.6). Repeat leveling surveys on Vancouver Island were conducted along two transects, the Tofino and the Bamfield leveling lines (Figure 3.6). The Tofino line is located between Tofino, on the west coast, and Nanoose Bay on the east coast of the island. Surveys were conducted in 1978, 1986, 1990 and 2002. The 1978 data set was not used in this study because of unknown magnetic effects on the instrument. The Bamfield line is located between Bamfield on the west coast and Port Alberni in central-to-eastern Vancouver Island. Surveys along this line were conducted in 1984, 1990, 1994, and 2002. The transect located on the southern British Columbia mainland (Williams Lake leveling line) between Point Atkinson and Williams Lake was surveyed to various extents in 1928, 1955, 1958, 1982, 1983, and 1993. All leveling surveys were carried out by the Geodetic Survey of Canada, Ottawa, Canada.

To facilitate comparison between observed data sets and uplift patterns predicted from current elastic dislocation models (see Chapter 7), all leveling results were projected onto a transect perpendicular to the Vancouver Island margin (Figure 2.1) between 48.15°N/126.23°W and 53°N/119°W. It should be noted that since the northern portion of the leveling line runs obliquely to this transect, the projected elevation changes may be affected by three-dimensional processes or structure.

4.5.2 Methodology - Leveling

Analysis of the elevation data in this study followed that of *Dragert et al.* [*1994*]. Corrections described in Section 4.3.2 were calculated by the Geodetic Survey of Canada, Ottawa, Canada, and in this study were applied to the raw, instrumental data. Corrected elevation data differences between adjacent benchmarks are obtained by

averaging a forward run and a backward run between benchmarks. Elevations of each benchmark are calculated by assigning an elevation to a reference benchmark and summing the cumulative differences to each subsequent benchmark (Section 4.2). To facilitate comparisons of elevations from one survey to the next, the reference benchmark should be stable and also be included in each survey. The final product for each leveling survey is a topographic profile plotted against the cumulative distance along the survey line, or in this study, the projected distance from the deformation front.

Changes in relative elevations, Δh, over different time periods are calculated by differencing topographic profiles from each survey with respect to an arbitrary 'reference epoch' survey, usually the initial survey of a given leveling line:

$$\Delta h = h_2 - h_1$$

where h_1 is the old reference height and h_2 is the new observed height. In this study, the reference surveys for the Tofino, Bamfield, and Williams Lake leveling transects were those carried out in 1986, 1984, and 1928/1983 (combined), respectively.

The average velocity of each benchmark, Δr, is then found by:

$$\Delta r = \Delta h / \Delta t$$

where Δt is the time elapsed between levelings. Note that all leveling surveys of a particular survey line use a common reference benchmark whose elevation is assumed fixed. This may not be the case, however, and it is common to use tide gauge trends to establish absolute uplift rates.

To describe the uncertainty associated with these values, cumulative errors along the survey lines were estimated from forward and backward leveling misclosures multiplied by $L^{1/2}$ (see Section 4.3.1), where L is the cumulative line distance along the profile, in km.

4.5.3 Leveling Survey Results

Vancouver Island Leveling Results

Results of relative elevation changes (expressed here as uplift rates) determined from repeat leveling across southern Vancouver Island and plotted as the projected distance from the deformation front (see Figure 3.6) are shown in Figure 4.5. Figure 4.5a shows the spatial distribution of uplift rates across the island along the Tofino line. The two epochs for this line, 1986 to 2002 and 1986 to 1990, are referenced to the Tofino tidal station (2.92±0.14 mm yr^{-1}; Chapter 6). They are generally in good agreement at the ends of the line, where results are within the cumulative errors. In the central region of the island (near Port Alberni) the uplift rates for the epochs begin to deviate. The most recent survey indicates a net bulging from 1986 to 2002, with a maximum uplift rate of ~1 mm yr^{-1} relative to the ends of the profile for approximately 40 km along the projected profile (centered over Port Alberni). For the period of 1986 to 1990, net uplift rates of this central region appear significantly lower than at the profile ends. Although it is apparent that the uplift rates across the island may indicate a more complex deformation pattern than a linear decrease from the outer to inner coast, the rates at the two ends of the survey line are very similar and constant for the two estimates. The leveling error estimated from forward and backward misclosures for this line averaged 0.78 mm $K^{1/2}$, where K is the distance in kilometers between two benchmarks. This is significantly better than the required misclosure of 3 mm $K^{1/2}$ [e.g. *Dragert et al., 1994*].

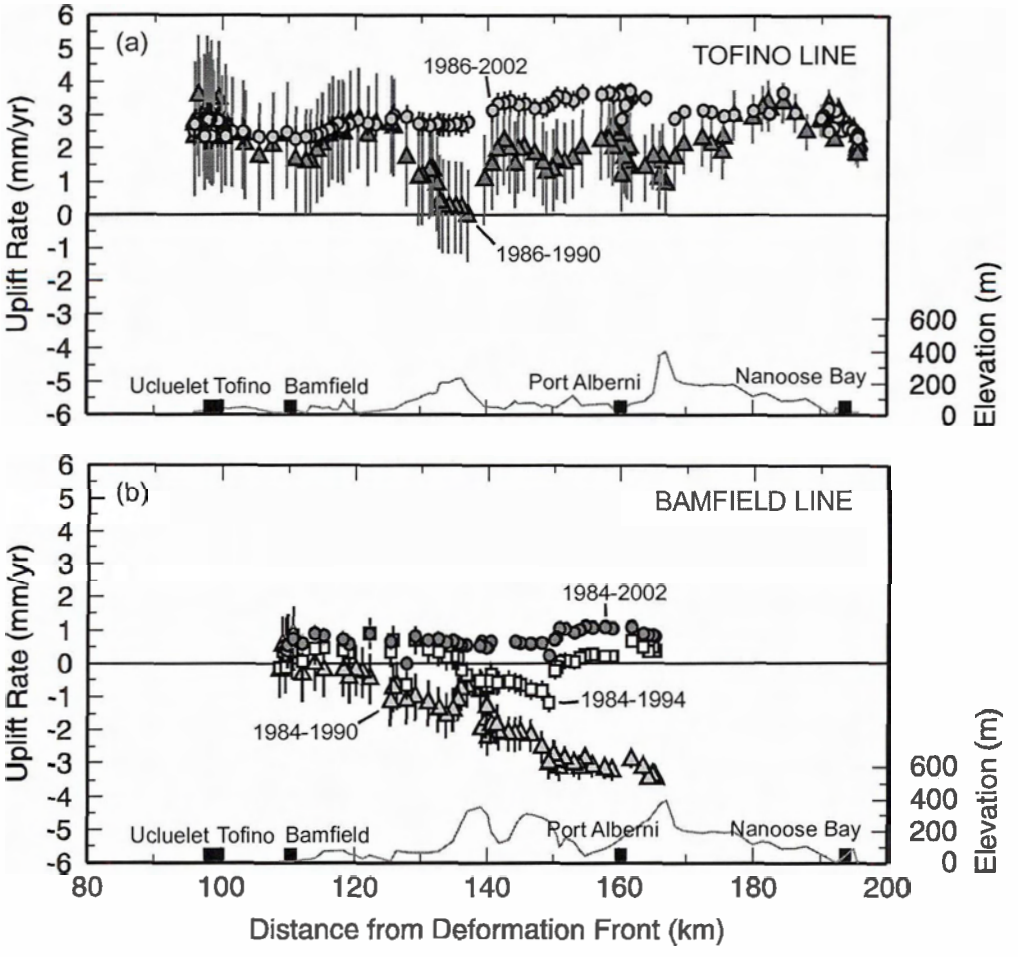

Figure 4.5. Elevation changes along the (a) Tofino and (b) Bamfield leveling lines expressed as uplift rates (left axis) and projected perpendicular to the Vancouver Island margin along the profile shown in Figure 2.1. Uplift rates for the Tofino leveling line are referenced to the Tofino tide gauge station (2.92±0.14 mm yr^{-1}). Rates for the Bamfield leveling line are referenced to the Bamfield tide gauge station (0.86±0.13 mm yr^{-1}). Vertical bars illustrate cumulative vertical errors along the survey lines. Topography profiles (grey lines) for each leveling line are plotted along the bottom of the respective graphs. The elevation scale is shown on the right axis.

A leveling profile for a subset of elevation data along the Tofino leveling line between Tofino and Ucluelet (parallel to the strike of the island; Figure 3.6) was re-analyzed to investigate any differences in uplift rates between Tofino and Ucluelet. These data indicated only a minor amount of tilt (<0.5 mm yr^{-1}) for both the 1986 to 1990 and 1986 to 2002 time periods.

Figure 4.5b shows the spatial distribution of uplift rates across the island along the Bamfield line, where all time periods were referenced to the Bamfield tidal station at an

uplift rate of 0.86±0.13 mm yr^{-1} (Chapter 6). Net uplift rates over the two longer time periods (1984 to 1994, and 1984 to 2002) are in good agreement for the majority of the line. They deviate over the mid-section of the line, with net uplift rates from 1984 to 2002 being almost constant along the line while the net uplift rates from 1984 to 1994 are up to ~1 mm yr^{-1} lower. As with the Tofino line, there is little difference in uplift rates between the two ends of the line for both time periods. Note, however, that the Bamfield line only covers the western two-thirds of the island, with Port Alberni being at the eastern terminus. Results for the shortest time interval (1984 to 1990) are distinctly different from the longer intervals. While the relative uplift pattern is consistent with those of the longer epochs for the eastern end of the survey line, the absolute rates are ~4 mm yr^{-1} lower for the shorter time period. The uplift rates for the 1984 to 1990 time period increase in a relatively linear fashion to a maximum of ~4.0 mm yr^{-1} higher at the western end, near Bamfield, compared to the eastern end [as shown in *Dragert et al., 1994*]. Smaller scale features along the leveling line for this period include a sudden increase in the net uplift rate nearly 150 km from the deformation front, approximately the same location as a sudden decrease in net uplift rate for the other two time periods. There is also a distinct bulge feature in the 1984 to 1990 epoch that will be discussed further in Section 4.5.4. Similar to the Tofino line, the Bamfield line had a significantly better average misclosure (0.69 mm $K^{1/2}$) than that required with special order leveling (3 mm $K^{1/2}$).

Mainland Leveling Results

Results from the mainland leveling line (Figure 4.6) indicate two main features: (1) a broad region of uplift in the Pemberton area with respect to Point Atkinson on the coast and (2) a section of reduced uplift rates and possible subsidence between Point Atkinson and Squamish. The broad region of uplift appears to start just west of the Garibaldi Volcanic Arc, where the uplift rate increases steeply eastward to a maximum of ~5 mm yr^{-1} near Pemberton. East of this region, uplift rates decrease approximately

linearly towards zero at 580 km distance from the deformation front. The 1983 to 1993 and 1958 to 1983 epochs have been adjusted such that the benchmark at Point Atkinson reflects the uplift rate determined from long-term tide gauge data (0.66±0.11 mm yr^{-1}) at that location (Chapter 6). Uplift rates for the 1983 to 1993 time period are consistent with the vertical estimate (2.36±1.27 mm yr^{-1}) from the Whistler (WSLR) continuous WCDA GPS station (see Figure 3.6) as determined from the global GPS analysis by SOPAC (1.16±1.17 mm yr^{-1}) [*SOPAC, 2003*] and adjusted for vertical motion at DRAO [*Altamimi et al., 2002*]. The 1928 to 1955 and 1928 to 1982 epochs have been adjusted such that the benchmark 28C682J (near the town of Williams Lake) reflects the uplift rate (1.58±0.82 mm yr^{-1}) between 1995 and 2003 of the continuous WCDA GPS station WILL (see Figure 3.6). This rate was adjusted from the calculated rate (0.38±0.65 mm yr^{-1}) [*SOPAC, 2003*] to reflect absolute uplift at DRAO [*Altamimi et al., 2002*]. The remaining epoch (1928 to 1983) shown in Figure 4.6 is plotted as relative uplift rates due to the absence of a co-located "absolute" reference (e.g. GPS or tidal station). The placement of this epoch along the vertical axis (uplift rate magnitude) is essentially arbitrary, owing to the relative nature of the measurement, and was therefore located to provide continuity in the uplift pattern along the profile.

The secondary feature, along the section of the leveling line between the coast and Squamish, suggests that there is a change in the direction of tilt (1983 to 1993 epoch) such that the top of Howe Sound (Squamish) is subsiding relative to the coast. There is a distinct difference between the two epochs over this section, where the 1983 to 1993 epoch indicates a reduction in uplift rates towards Squamish and the 1958 to 1983 epoch indicates an increase. Due to the later date and longer length along the profile of the 1983 to 1993 epoch, a higher confidence could be applied to this data as opposed to the 1958 to 1983 epoch. As well, the 1958 survey has no systematic error corrections available and may therefore be biased (e.g. by refraction).

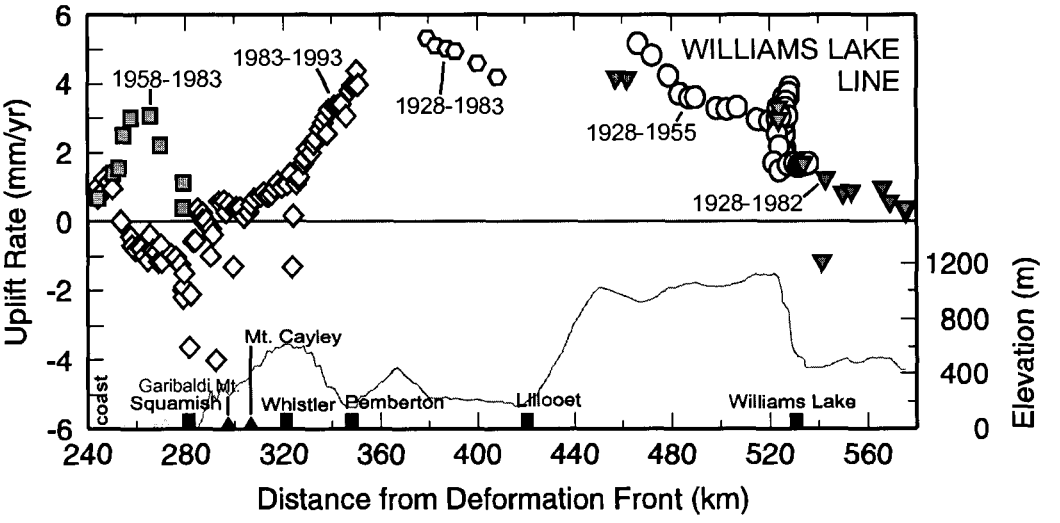

Figure 4.6. Elevation changes along the Williams Lake leveling line expressed as uplift rates (left axis) and projected perpendicular to the Vancouver Island margin along the profile shown in Figure 2.1. Time periods are shown on the figure. Uplift rates for the 1983 to 1993 and 1958 to 1983 time periods are referenced to the Point Atkinson tide gauge station (0.66±0.11 mm yr^{-1}). Rates for the 1928 to 1955 and 1928 to 1982 time periods are referenced to the Williams Lake continuous GPS site (1.58±0.82 mm yr^{-1}). The 1928 to 1983 time period indicates relative uplift rates and data are plotted to illustrate continuity of the trend. A topography profile (grey line) is plotted along the bottom of the graph. The elevation scale is shown on the right axis.

4.5.4 Discussion of Leveling Results

Vancouver Island Leveling Results Discussion

Net uplift rates calculated using repeat leveling data for two survey lines across Vancouver Island indicate very little net across-island tilting over the past 2 decades. However, the difference between the longer- and shorter-term trends may indicate either an unresolved problem with the data sets (possibly related to systematic errors) or a true temporal change in the uplift rates. Although it is unlikely that the linear trend observed in the 1984 to 1990 epoch of the Bamfield line is due to miscalculated corrections, sensitivity tests were carried out to gauge the impact of rod scale and refraction corrections on observed tilt across the margin, for both the Tofino (Figure 4.7) and Bamfield (Figures 4.8) lines. The goal of these calculations was to investigate whether reasonable changes in these corrections for the 1990 survey would: (1) make 1984 to

1990 tilt rates more consistent with those for the longer-period epochs along the Bamfield line; and (2) affect the tilt rate of the two epochs along the Tofino line.

Results of the refraction sensitivity test for the Tofino line (Figure 4.7a) indicate that a factor of 5 or 10 increase in the refraction correction magnitude will increase the net cross-island tilting for the 1986 to 1990 interval. A factor of 10 increase in the rod scale correction magnitude (Figure 4.7b) also results in an increase in the net cross-island tilt for this time frame. While a factor of 5 only increases the tilt by ~1 mm yr^{-1}, the uplift pattern across the island more closely resembles that of the 1986 to 2002 epoch. A magnitude of 5 or 10 increase in the corrections is unrealistic in any case, and therefore suggests that the refraction and rod scale corrections were calculated correctly.

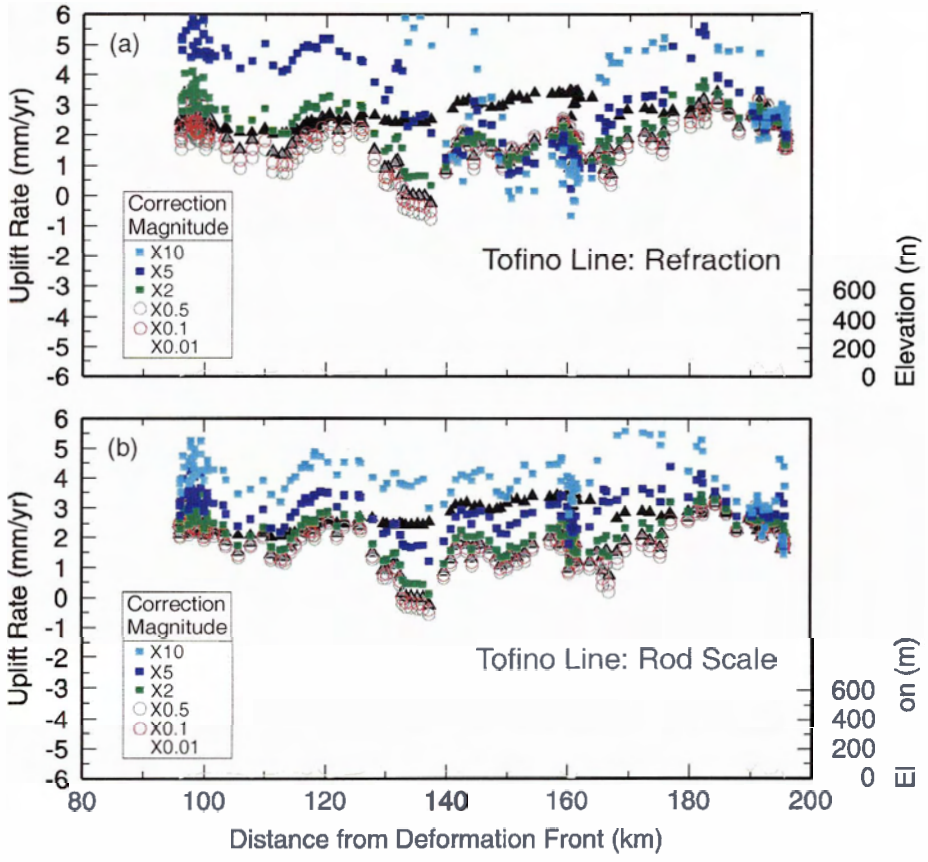

Figure 4.7. 1990 (a) refraction and (b) rod scale correction tests along the Tofino leveling line, for the 1986 to 1990 time period, projected perpendicular to the Vancouver Island margin along the profile in Figure 2.1. Symbols represent recalculated uplift rates for different magnitudes of the corrections (shown in legends) in both figures. Black triangles are the uplift rates with the original corrections applied for the 1986 to 2002 time period and grey triangles for the 1986 to 1990 time period.

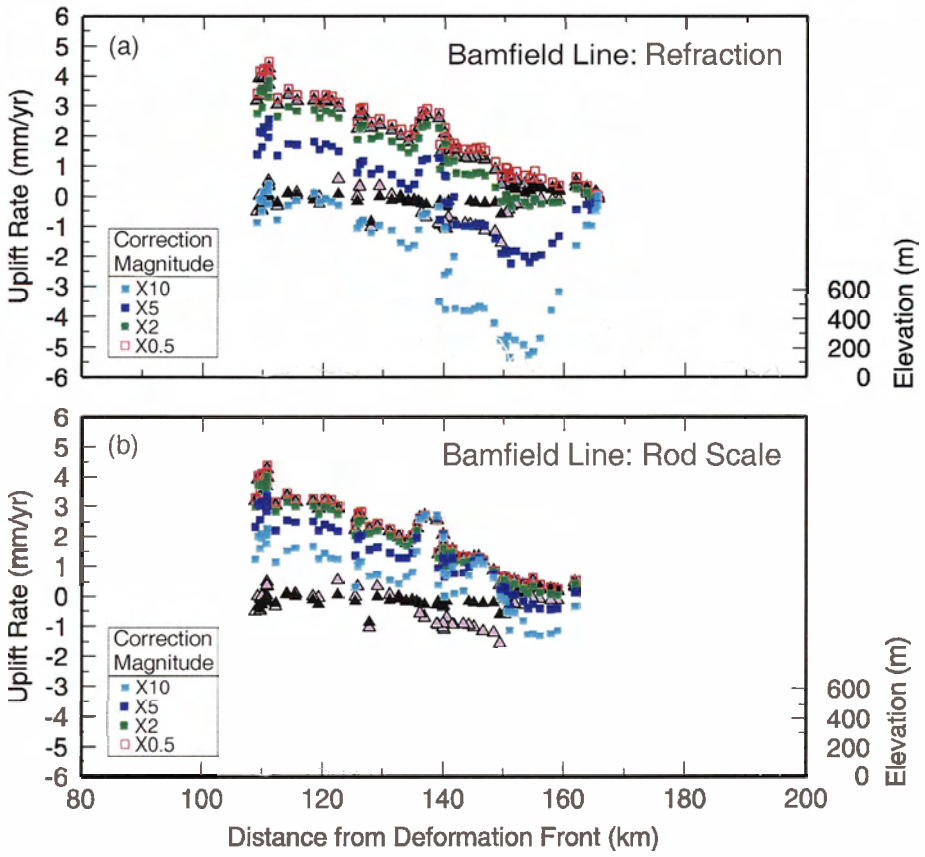

Figure 4.8. 1990 (a) refraction and (b) rod scale correction tests along the Bamfield leveling line, for the 1984 to 1990 time period, projected perpendicular to the Vancouver Island margin along the profile in Figure 2.1. The symbols represent recalculated uplift rates for different magnitude of the corrections (shown in legends) in both figures. Black triangles are the uplift rates with the original corrections applied for the 1984 to 2002 time period, purple triangles for the 1984 to 1994 time period, and grey triangles for the 1984 to 1990 time period.

Results of the refraction sensitivity test for the Bamfield line (Figure 4.8a) indicate that a factor of 5 or 10 increase in the refraction correction magnitude will reduce the net cross-island tilting for the 1984 to 1990 interval. However, the correlation with shorter wavelength topography becomes strongly accentuated. As with sensitivity tests for the Tofino line, a factor of 5 or 10 increase in magnitude is unrealistic and so the refraction correction was probably calculated correctly. An alternate test could be the use of a different refraction model for the 1990 data, one that would take into account the high precipitation that occurred during the survey, which was recorded in the field notes. This, however, was not attempted in this study.

The test for rod scale corrections along the Bamfield line (Figure 4.8b) gave similar results as the refraction test, where a factor of 10 increase in the correction magnitude reduces the across-island uplift rates to a difference of ~2 mm yr^{-1} along the line from ~4 mm yr^{-1} for the 1984 to 1990 interval. As with the refraction test, this is an unrealistic increase in magnitude for the correction and suggests that the rod scale correction was calculated appropriately. There is, however, evidence of a correlation between the rod scale correction and topography between ~135-140 km distance from the deformation front (see Figure 4.5b). At this location, an increase in the topography is mirrored in the 1984 to 1990 epoch and is accentuated with an increasing magnitude of the correction factor (Figure 4.8b). Therefore, while there is no consistent correlation with topography, localized correlations exist [e.g. *Dragert et al., 1994*].

In addition to the broad scale trend in the data, small inconsistencies between the epochs and possible outliers have been addressed by checking the relative stability of the benchmarks (e.g. tablets in bedrock versus helix pipes in soil). Based on benchmark descriptions (indicating a mixture of bedrock and soil sites) outliers were removed; however the minor differences between epochs were not resolved.

It is also noteworthy that results from this study for the shortest time periods from the Tofino and Bamfield lines were compared to the results of *Dragert et al.* [*1994*]. The same data were used in both studies, however, the 1986 to 1990 time period (Tofino line) from this study does not illustrate the ~ 3 mm yr^{-1} of landward tilt observed by *Dragert et al.* [*1994*]. This difference is a result of all available systematic error corrections for the 1986 survey being applied to the raw elevation differences in this study. Specifically, the earlier study did not include refraction corrections to elevation differences for a series of benchmarks at approximately 140 km (projected distance) from the deformation front in the 1986 survey.

Mainland Leveling Results Discussion

As stated previously, many of the standard corrections applied to elevation data were not calculated for the Williams Lake line because of the early survey dates. According to *Gareau* [*1986*] and *Holdahl et al.* [*1989*], leveling data collected after 1982 are corrected for refraction using observed vertical temperature gradients. The result of this is that only the western-most portion of the Williams Lake line (corresponding to the 1983 and 1993 surveys) has been corrected using temperature gradients. Theoretically, corrections can be calculated for historical data, but vital information for the calculations along this leveling line (e.g. time of day) is missing in most cases. This is also noted in *Holdahl et al.* [*1989*], who used the earlier surveys along the Williams Lake leveling line to investigate crustal motion in the region. An interesting feature evident in the elevation data along the Williams Lake line is the series of "dipping" sections between Squamish and Whistler (Figure 4.6). Benchmark descriptions indicate that most of the markers along this section of the line are set in rock, thereby eliminating the possibility of soil settling. Aside from unstable benchmarks, these features could indicate movement due to localized stress accumulation along geological structures (e.g. transcurrent faults). While there are known faults in this area [e.g. *Journeay and Friedman, 1993*; *Friedman et al., 1995*] (see Figure 2.8), it is unlikely that these faults are active. In general, however, leveling data for the Williams Lake transect is considered less robust than data for Vancouver Island due to the early time frame of the surveys and the equipment used along some portions of the line (e.g. instrument having magnetic effect).

CHAPTER 5

Gravity

5.1 Introduction to Gravity

One of the most cost effective sources of data that can be used to measure vertical crustal motion comes from repeated gravity observations, which can be made between distant points more rapidly than observations from other classical geodetic techniques (such as leveling). Localized changes in gravity usually arise from vertical displacement, but also from redistribution of mass within the earth. Changes in gravity observed after major earthquakes (e.g. 1964 Alaskan earthquake) indicate that precise measurements can provide valuable information about crustal deformation associated with earthquakes [e.g. *Barnes, 1966*]. When these gravity measurements are used in conjunction with other vertical geodetic measurements (e.g. repeat leveling or GPS), the nature of the physical processes occurring in the region may also be constrained [e.g. *Dragert et al., 1981*].

Repeat high-precision relative gravity surveys were carried out in 1986 and 1990 [*Dragert et al., 1994*]. A new repeat-survey at 14 stations on Vancouver Island was carried out in 2002 and analyses of these data are presented here. Repeated absolute gravity measurements were carried out at two stations on Vancouver Island between 1995 and 2002, and absolute gravity measurements at 12 of the relative stations were made in 2002. Results of the absolute gravity surveys between 1995 and 2000 were first discussed by *Lambert et al.* [*2001*]. Results for the 2001 and 2002 absolute gravity surveys are presented for the first time in this thesis.

5.2 Absolute and Relative Gravity Measurements

Pendula or free-fall devices can be used to directly measure gravity at a point on the surface of the earth, and thus provide absolute gravity measurements. However, these devices are not as portable or easy to operate as differential gravimeters, which measure the difference in gravity between pairs of points [*Vanicek and Krakiwsky, 1986*]. The measurement of absolute gravity also requires a long observation period (e.g. on the order of days). Accuracies for absolute (averaged over a 24-hr period) and relative gravity measurements are on the order of 1 μGal [*Lambert et al., 1998*] and 3-4 μGal [*Dragert et al., 1981*], respectively. Combining absolute and relative measurements at a subset of network stations establishes a robust absolute datum for all sites. In this study, only the most recent relative gravity survey (2002) was anchored to co-located absolute measurements.

5.3 Non-Margin Tectonics Gravity Variations

5.3.1 Postglacial Rebound

Uplift rates determined using gravity techniques are typically adjusted for the effects of postglacial rebound (PGR), which is the response of the Earth to the decay of ice-sheets [e.g. *James et al., 2000*]. Previous PGR models for the northern CSZ [*Tushingham and Peltier, 1991* (ICE-3G); *James et al., 2000* (Cordilleran)] estimated tilt rates across Vancouver Island ranging from 1.2 mm yr^{-1} to <0.1 mm yr^{-1} (Figure 5.1a and b). These results are based on differing viscosity profiles through the mantle (Figure 5.1d). The ICE-3G model uses an upper mantle viscosity of 10^{21} Pa s and a lower mantle viscosity twice as large. However, this model does not satisfy observed proglacial lake shoreline tilts in the Puget Lowland. Based on the lake shoreline observations, *James et al.* [*2000*] created the Cordilleran model, which uses lower viscosities (<10^{20} Pa s) throughout the whole mantle. To accommodate the observed shoreline tilts and a layered viscosity profile, *Clague and James* [*2002*] revised the ICE-3G and Cordilleran models.

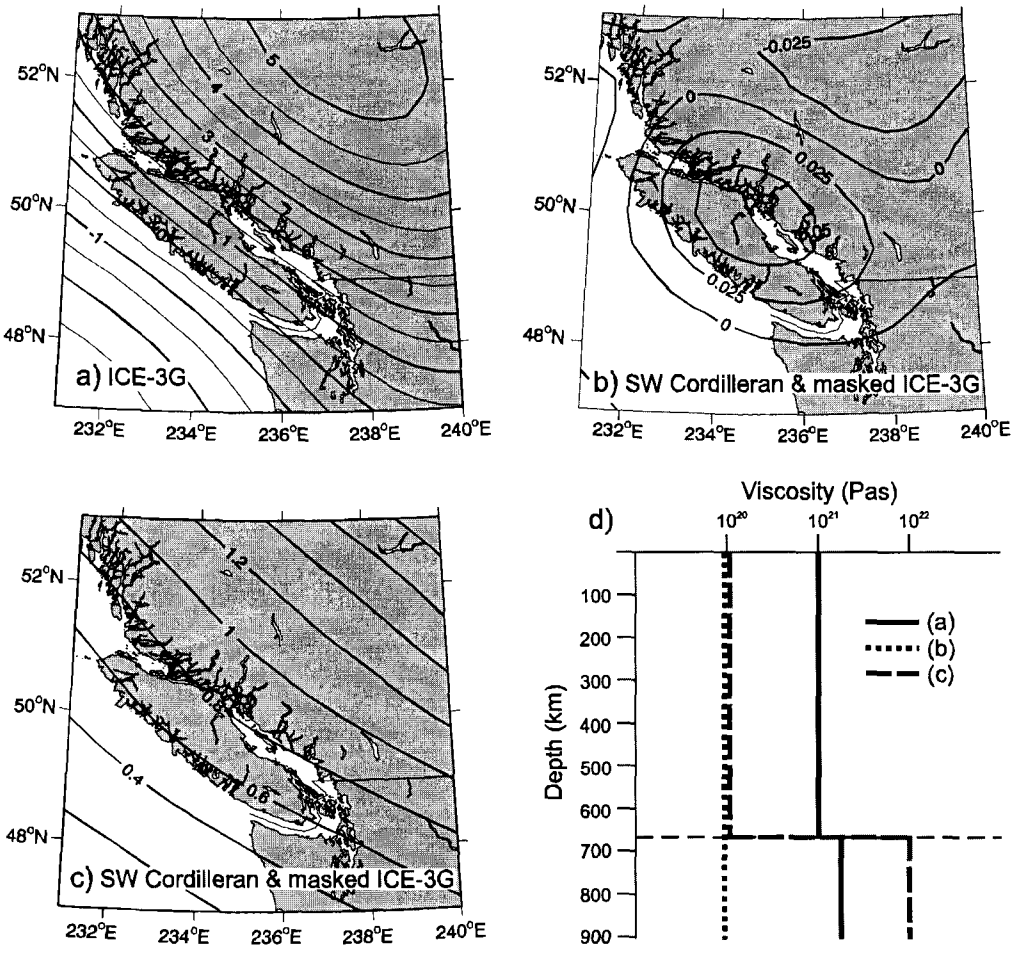

Figure 5.1. Predicted present-day crustal uplift (mm yr^{-1}) for (a) the global ICE-3G model [*Tushingham and Peltier, 1991*] and (b) and (c) a Cordilleran model embedded in a masked version of ICE-3G for two different viscosity profiles shown in (d) [modified from *Clague and James, 2002*].

They fixed the viscosity of the upper mantle at 10^{20} Pa s and set the viscosity of the lower mantle to 100-fold larger (see Figure 5.1d). This updated PGR model of *Clague and James [2002]* is used in the current study. Estimates of contemporary uplift rates from this model are small, ranging from ~0.55 mm yr^{-1} on the outer coast to ~0.80 mm yr^{-1} on the inner coast. This results in a seaward cross-island tilt in the study region of ~0.25 mm yr^{-1} (Figure 5.1c). Therefore, the net across-margin tilt between two stations should not be significantly affected by PGR. Similarly, PGR uplift rates determined for the British Columbia mainland in the region of repeat leveling data in this study range from ~0.80 mm yr^{-1} for the coast to ~1.60 mm yr^{-1} near Williams Lake. Therefore, the tilt

expected as a result of PGR for the mainland with respect to data in this study would be ~0.80 mm yr^{-1}. However, *Clague and James [2002]* caution that the regional shallow mantle viscosity is most likely lower (~$5x10^{18}$ to 10^{19}) and therefore, the results from their study are probably the upper limits of uplift rates due to PGR.

For gravity measurements, it is important to note that both vertical displacements and redistribution of masses are associated with the PGR phenomenon. While no PGR correction is applied to the relative gravity data in this study (it provides only tilt information), the "absolute" tectonic uplift rates are determined by applying the PGR correction values described by *Clague and James [2002]* to the equivalent uplift rates determined from the time series of absolute gravity stations (UCLU and NANO).

5.3.2 Ocean Loading

The main effects of ocean loading were briefly introduced in Section 4.3.2, with the focus on how tilting of the earth's surface could be induced. The ocean tide loading effect on gravity results from the same sources, mainly the gravitational attraction of the extra water masses, an internal redistribution of mass, and a radial displacement of the gravity field [*Lambert et al., 1998*].

Through the use of a global ocean tide model including regional ocean tide effects, *Lambert et al. [1998]* calculated the radial component of displacement and gravity for the main semidiurnal (M_2) and diurnal (K_1) tidal constituents near the Canadian west coast. It was found that after correcting for ocean loading, the M_2 and K_1 constituents have residual gravity amplitudes of at least 2 μGal and 1 μGal, respectively. However, the effect of semidiurnal and diurnal ocean tide loading is significantly reduced through averaging over a 24-hour period. Relative to the precision of day-long absolute gravity measurements (1 μGal), the effects are small. Therefore, in the scope of this study, the ocean loading correction would only be critical if measurements were made over shorter-term (<1 day) periods. Minor amounts of ocean loading on the coasts of Vancouver Island are accounted for in relative gravity data measurements, in which a

series of repeat measurements between a subset of network stations are made within a period of about 6 hours and corrected for linear drift.

5.3.3 Water Table Fluctuations

Precise gravity surveys are also sensitive to the effects of changing groundwater conditions [e.g. *Lambert and Courtier, 2000*]. *Dragert et al.* [*1981*] discuss possible consequences of changing groundwater conditions on gravity measurements on Vancouver Island. They note that bedrock porosities and permeabilities are low around most of the gravity stations on southern Vancouver Island [*Halstead and Treichel, 1966*]. However, high porosities are found in the coastal lowlands along eastern Vancouver Island. Therefore gravity stations in this region could potentially be affected by groundwater fluctuations. The lowlands are composed of glacial and alluvial deposits, containing Quadra sediments (sand, gravel, and silt) with porosities of 30-50% [*Halstead and Treichel, 1966*]. As summarized by *Dragert et al.* [*1981*], seasonal changes on the order of 1 m in groundwater level can occur between April and August in the lowlands region. Using an infinite sheet approximation with 30% porosity, they estimated a 12 μGal seasonal gravity variation for the observed change in groundwater level (1 m). While hydrological information around all sites is still needed to understand what areas are in fact affected, and therefore calculate corrections, *Dragert et al.* [*1981*] suggest that the stations most likely to be affected are in or near the boundary of the lowlands. In the scope of this study, stations potentially affected are then: Brynmarl (BRY), Rathtrevor (RAT), Qualicum Beach (QUA), and to a lesser degree, Little Qualicum Falls (LIT) (see Figure 3.6). It thus seems evident that groundwater corrections for stations situated on hard-rock outcrops with impermeable formations are not as crucial as for stations located in areas with unconsolidated sediments or highly fractured rock. In the latter cases *Lambert and Beaumont* [*1977*] suggest the installation of deep benchmarks, which can double as piezometers.

Currently, only soil moisture readings are being made at the absolute gravity station NANO. These measurements span only the last 3 years, however, and so no correction is yet available. As well, there remains little or no information regarding the deep fluid distribution and movement for this region.

5.4 Gravity Surveys Across the Cascadia Margin

5.4.1 Gravity Data Sets

Repeat, high-precision relative gravity surveys were carried out in 1986, 1990, and 2002 to monitor possible gravity changes associated with contemporary crustal deformation. Relative gravity measurements were taken at the following stations (see Figure 3.6): Nanoose Bay (NAN1), Brynmarl, (BRY), Rathtrevor (RAT), Qualicum Beach (QUA), Little Qualicum Falls (LIT), Arrowsmith (ARR), Tsehaheh (TSA), Sproat Lake (SPR), Taylor Arm (TAY1), Kennedy River (KEN), Canoe Creek (CAN), Larry Lake (LAR), Cox Bay (COX), and Tofino Coastguard (TOF1). At Ucluelet (UCL), relative measurements in 1986 were replaced in 1990 by absolute gravity measurements. As well, measurements were not repeated at QUA or ARR in the 2002 survey.

The relative surveys utilized four LaCoste and Romberg Model-D gravimeters surveying simultaneously. *Lambert et al.* [*1979*] provide an evaluation of these instruments, where the focus of the study was to report the performance of the gravimeters with respect to measuring possible gravity changes associated with seismicity.

Repeat absolute gravity measurements at Ucluelet and Nanoose Bay (for location, see Figure 3.6) between 1995 and 2002 are also used in this study to provide an independent measure of vertical motion occurring on southern Vancouver Island. The measurements were made using an FG5-106 gravimeter (PGC-GSC). In addition to these measurements, an initial set of absolute gravity readings were made in the spring (May/June) of 2002 at 12 of the D-meter stations listed above. The direct connection of

absolute and relative gravity observations at these 12 stations provided an absolute datum for the network sites.

5.4.2 Methodology - Gravity

Relative Gravity Methodology

Gravity values for the 1986 and 1990 survey stations were adjusted such that they are expressed with respect to the mean value of the 2002 survey over common sites. Co-located absolute gravity measurements at the 2002 survey stations provided the opportunity to anchor these relative gravity measurements (for the 2002 survey) to an absolute reference.

Changes in observed gravity values between surveys were transformed to equivalent vertical uplift rates by applying a deformation gravity gradient of –0.19 μGal mm^{-1}, corresponding to a rock density of 2.8 gm cc^{-1} and Poisson's ratio of 0.25 [*Rundle, 1978*]. Errors associated with the differenced gravity results were calculated as root mean squares and scaled by the same factor to provide error bounds for uplift rates. Trends were found for each time period using the linear regression technique.

For comparison to published relative gravity results [*Dragert et al., 1994*], uplift rates were also calculated for the 1986 to 1990 time period. The same method as above was followed, except that the 1990 survey mean served as the reference to which the 1986 survey mean was adjusted.

Repeated Absolute Gravity Methodology

Analysis of absolute gravity values measured at Ucluelet and Nanoose (for location, see Figure 3.6) was undertaken at the Pacific Geoscience Centre (*N. Courtier and A. Lambert, PGC-GSC*). Corrections to the measurements included empirically modelling seasonal variations of groundwater (from precipitation and temperature

information) and allowing for a regional interannual gravity signal [*A. Lambert, personal communication, 2004*].

As with the vertical component of continuous GPS measurements (see Chapter 3), trends were calculated from the time series of each station using the linear regression technique. Equivalent uplift rates were again determined using a deformation gravity gradient of –0.19 μGal mm^{-1} [*Rundle, 1978*], which was applied to the time series trend.

5.4.3 Gravity Results

Relative Gravity Results

Results of relative gravity changes determined from repeat gravity measurements between 1986 and 2002 and between 1990 and 2002 across southern Vancouver Island, referenced to co-located absolute gravity measurements, are shown in Figure 5.2a. Figure 5.2b illustrates these gravity changes as equivalent uplift rates. Both figures present results as a function of projected distance from the deformation front along the profile shown in Figure 2.1.

For both time periods, the gravity results follow a similar pattern along the length of the profile. They indicate subsidence on the western portion of southern Vancouver Island, uplift towards the central portion, and subsidence or minor uplift eastward. Assuming no mass changes, the gravity results indicate a net mean seaward tilt of 3.3±2.6 mm yr^{-1} between 1986 and 2002 and 7.3±3.5 mm yr^{-1} between 1990 and 2002 (between the TOF and BRY stations; uncertainties are given as formal regression errors). Individual site movement is only consistent (within 2σ) between the two time intervals for 60% of the stations. The largest offset of net uplift rates between the two time periods occurs at SPR.

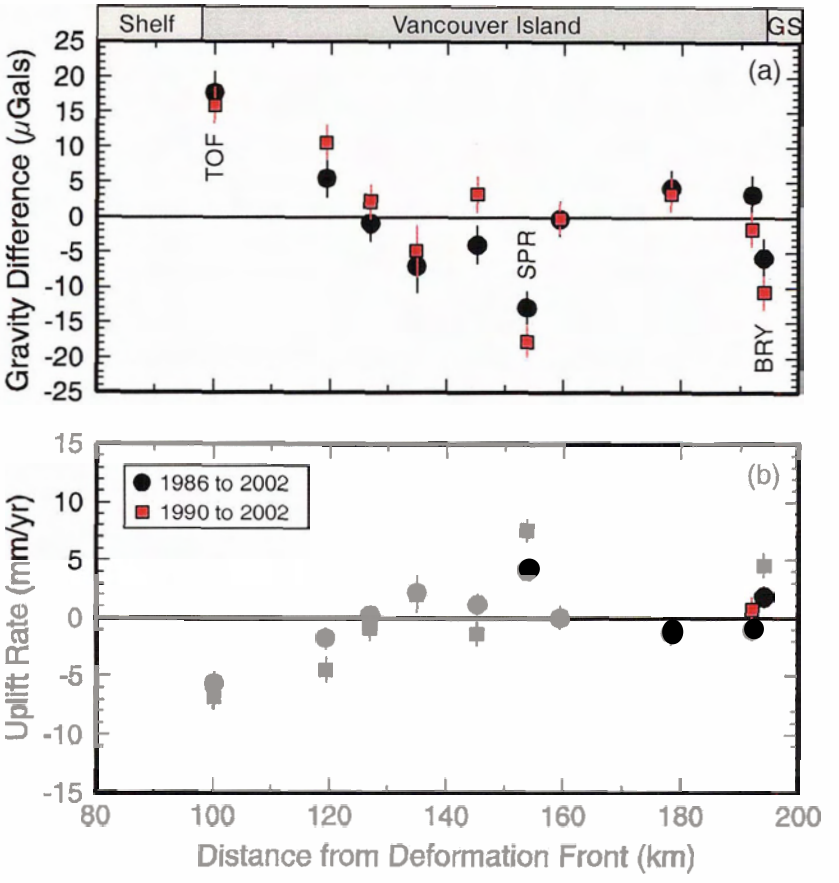

Figure 5.2. Repeat relative gravity results for southern Vancouver Island (see Figure 3.6). Observations are plotted as projected distance from the deformation front along the profile in Figure 2.1. (a) Gravity differences between surveys and (b) equivalent uplift rates (positive is crustal uplift) calculated using a deformation gradient of –0.19 μGal mm^{-1} [*Rundle, 1978*]. 2002 has been used as the reference survey. Vertical bars denote 1σ errors. GS = Strait of Georgia.

Results of relative gravity changes between 1986 and 1990 along the profile in Figure 2.1 are shown in Figure 5.3a and equivalent uplift rates for this time period in Figure 5.3b. The direction of tilt (landward) and the general uplift pattern between stations is consistent with the *Dragert et al.* [*1994*] study; however, the magnitude of differences between some stations (e.g. ARR) appears (qualitatively) larger in this study. *Dragert et al.* [*1994*] results were corrected for PGR according to the model of *Tushingham and Peltier* [*1991*], introducing a landward tilt of ~1.2 mm yr^{-1} (assuming a deformation gravity gradient of 0.2 μGal mm^{-1}). It has since been determined [cf. *Clague and James, 2002*] that regional PGR tilt is <0.2 mm yr^{-1}, obviating the need for a

correction. This may resolve some of the difference between equivalent uplift rates in the two studies. Alternatively, differences could arise from different analysis techniques between the two studies or the rounding of gravity values during analysis.

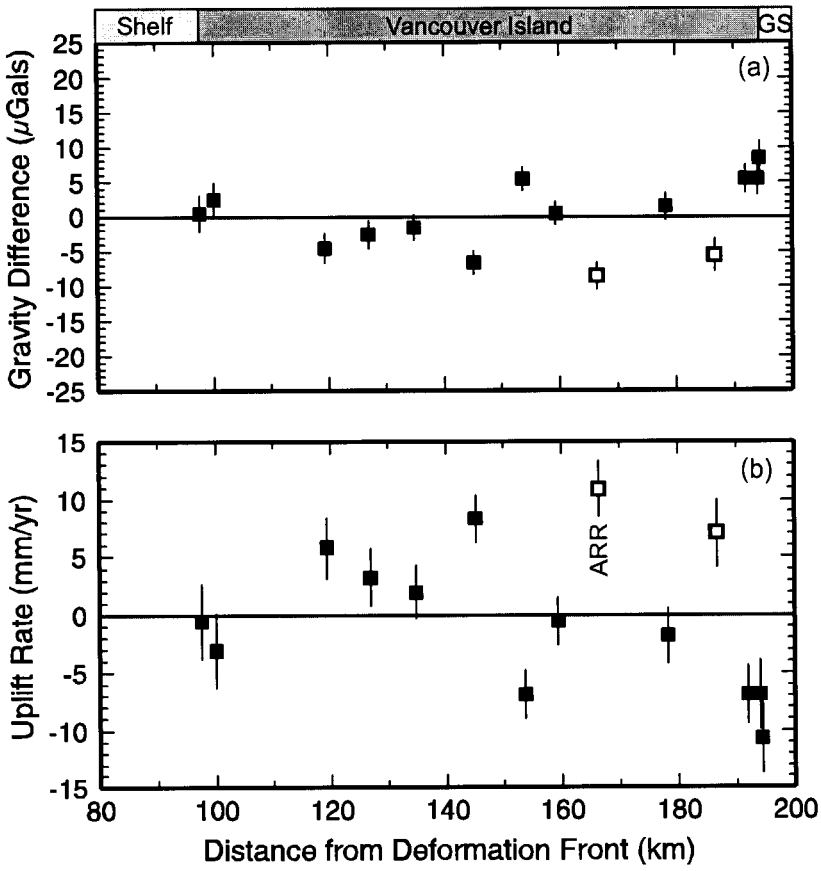

Figure 5.3. Repeat relative gravity results for southern Vancouver Island (see Figure 3.6) between 1986 and 1990. Observations are plotted as projected distance from the deformation front along the profile in Figure 2.1. (a) Gravity differences between surveys and (b) equivalent uplift rates (positive is crustal uplift) calculated using a deformation gradient of –0.19 μGal mm^{-1} [*Rundle, 1978*]. Open symbols represent potentially unstable stations, where local site effects may contribute to gravity observations. Vertical bars denote 1σ errors. GS: Strait of Georgia.

Repeated Absolute Gravity Results

Repeat absolute gravity measurements over time at Ucluelet and Nanoose Bay (*courtesy of A. Lambert, PGC-GSC*; station locations shown in Figure 3.6), are shown in

Figure 5.4. The best-fit linear gravity trend at Ucluelet (-0.50±0.21 μGal yr^{-1}), illustrated in Figure 5.4a, indicates uplift of the west coast of southern Vancouver Island at a rate of 2.56±1.08 mm yr^{-1}. Similar values for the observed gravity trend (-0.62±0.22 μGal yr^{-1}) and equivalent vertical uplift rate (3.17±1.10 mm yr^{-1}) were obtained for Nanoose (Figure 5.4b) on the eastern side of the island. Note that these values have not been corrected for PGR. However, using the PGR results of *Clague and James* [*2002*] (-0.55 mm yr^{-1} for Ucluelet and –0.75 mm yr^{-1} for Nanoose), the equivalent uplift rates would then be 2.01±1.08 mm yr^{-1} and 2.42±1.10 mm yr^{-1}, respectively.

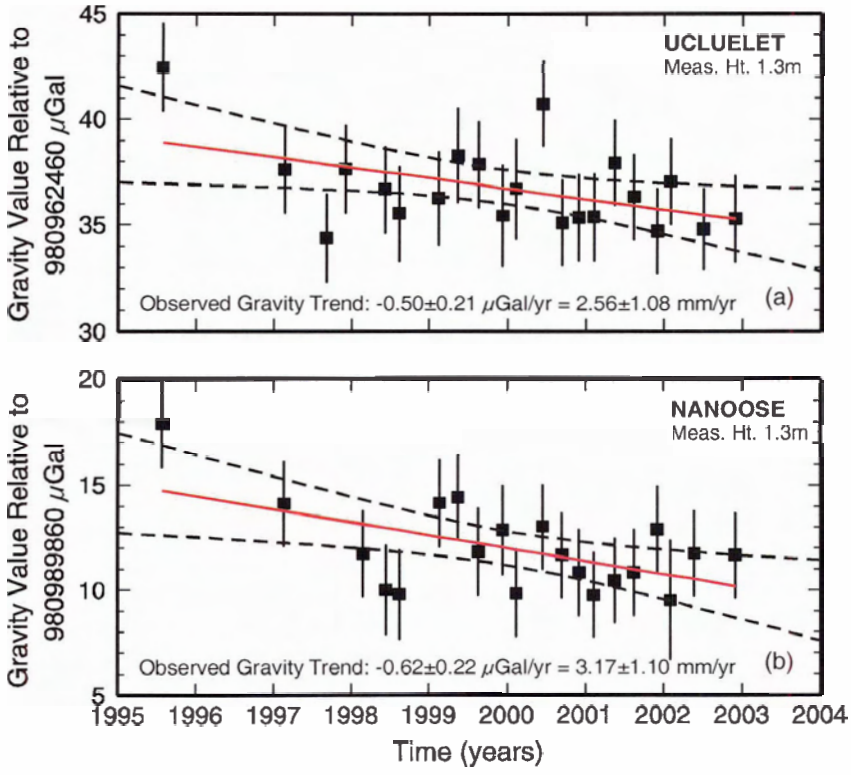

Figure 5.4. Absolute gravity observations at (a) Ucluelet and (b) Nanoose Bay between 1995 and 2002. Values have been corrected for ground moisture variations and a regional interannual signal (T ~6.85 years). Trends over time are expressed in terms of both gravity changes and equivalent uplift rates, using a deformation gravity gradient of –0.19 μGal mm^{-1} [*Rundle, 1978*]. The uplift rates are not corrected for PGR. Positive rates indicate crustal uplift. Vertical bars denote standard errors (*courtesy of A. Lambert, PGC-GSC*).

5.4.4 Summary and Discussion of Gravity Results

Repeat relative and absolute gravity measurements across southern Vancouver Island have been used to provide independent estimates of uplift occurring in the northern CSZ. Equivalent uplift rates were calculated using a deformation gravity gradient of –0.19 μGal mm^{-1} [*Rundle, 1978*]. Based on results from *Clague and James* [*2002*], which indicate little present day tilt across the margin, no differential PGR corrections have been applied in this study. However, absolute gravity results should have a PGR correction applied to estimate absolute uplift rates due to margin tectonics. By applying a correction for PGR, equivalent uplift rates from the absolute gravity stations at Ucluelet and Nanoose are 2.01±1.08 mm yr^{-1} and 2.42±1.10 mm yr^{-1}, respectively.

If assumed to be caused by elevation changes alone, repeat relative gravity results indicate net mean seaward tilting of 3.3±2.6 mm yr^{-1} between 1986 and 2002 and 7.3±3.5 mm yr^{-1} between 1990 and 2002. Both time periods show a consistent pattern across the island, with subsidence (~6-7 mm yr^{-1}) occurring on the western coast and uplift (~3-5 mm yr^{-1}) on the eastern coast. The largest offset of a single station between time periods appears to have occurred at SPR, which is adjacent to Sproat Lake. The first suspicion is that readings at this station have been affected by water level changes in the lake between surveys. However, lake level records indicate that sub-meter lake level changes occurred between the survey years, and with the location of the station relative to the lake, this is insufficient to have a significant effect on the gravity measurements [*A. Lambert, personal communication, 2003*].

While an ambiguity in the DC shift of the uplift rates based on the 3 surveys still exists, the differences of rates at the western and eastern ends do not agree with the absolute gravity results. This strongly suggests temporal effects, possibly caused by mass redistributions. This hypothesis is suggested by a comparison of absolute gravity results and continuous GPS height measurements at Ucluelet during an ETS [*Dragert et al., 2001*; *Rogers and Dragert, 2003*] event. Allowing for offsets coincident with ETS events can reduce the variance of repeated absolute gravity measurements at Ucluelet. Such offsets, if caused by elevation changes, would require uplift of the order of 1 cm. No such

changes in height are seen from the continuous GPS data, suggesting a local bulk mass change during an ETS event [*A. Lambert, personal communication, 2004*]. Such an episodic mass redistribution would result in time-dependent rates for trends in gravity readings at stations across the island. Further insight into this problem may come from similar, comparative observations at the absolute gravity and continuous GPS stations at Nanoose on the eastern coast of Vancouver Island.

CHAPTER 6

Tide Gauge

6.1 Introduction to Tide Gauges

Tide gauges were designed originally for the study and prediction of tidal variations; however, use of the data has expanded over the past century to include studies of monitoring vertical motion of the earth's crust due to tectonic processes [e.g. *Wigen and Stephenson, 1980*; *Dragert et al., 1994*]. Water levels that are recorded at tide gauges over an extended period of time (several decades or more) allow the use of mean sea level (MSL) as a datum from which long-term changes of land level can be determined. These measurements allow continuous observations of solid earth motion over a longer time period than other measurements (e.g. GPS or leveling) and can therefore potentially provide information on long-term and time-varying earth responses to earthquake cycles and changes in surface loading [*Larsen et al., 2003*]. However, tide gauge data are also affected by long-term oceanographic changes, such as El Nino. These signals must be removed form the observations to separate the tectonic vertical motions.

6.2 Tide Gauge Instrumentation

As summarized by *Chelton and Enfield* [*1986*], the classical instrumentation used to collect tidal data is generally designed with filtering techniques that remove short-period fluctuations in water level produced by surface gravity waves. One way in which this is done is to measure the water level in a cylinder with a narrow opening at the bottom, which limits the rate at which the level can change within the cylinder. This, however, can lead to problems such as a spurious data record if the hole becomes

plugged. Other problems with the instruments could include failure of the float device or sinking of the pier on which the tide gauge is located [cf. *Chelton and Enfield, 1986*].

6.3 Potential Error Sources

It is not always easy to distinguish sea level changes due to vertical crustal motion from those driven by atmospheric or oceanic processes. Sea level variations come from a variety of sources, such as [cf. *Vanicek, 1978*; *Vanicek and Krakiwsky, 1986*]: atmospheric pressure variations, dynamic effects of sea-level variations, wind variations, river discharge variations, changes in bathymetric configuration, glacial melt, and long periodic tides.

Short-term variations in sea level can be minimized by using annual means, whereas long-term variations can be minimized by identification and removal of common modes at several stations [*Savage and Plafker, 1991*]. Variability is also present in very long-term changes, which could be due to postseismic relaxation or glacial isostatic adjustment [*Larsen et al., 2003*]. In the scope of this study, where monthly mean sea levels (MMSL) are used, short-term variability is a potential concern.

6.3.1 Eustatic Sea Level Rise

To determine crustal uplift rates from tide gauge data, the effects of global mean sea level rise must be removed. According to *Douglas* [*1991*], published values for global sea level rise for the last century vary between 1 mm yr^{-1} and 3 mm yr^{-1}, with uncertainties ranging from 0.15 mm yr^{-1} to 0.90 mm yr^{-1}. The scatter results from a difference in the data sets and analysis techniques used between studies. The preferred correction for this study is 1.80±0.10 mm yr^{-1} from the global analysis of *Douglas* [*1991*; *1997*]. His analysis was based on station selection criteria including the length and completeness of record, general agreement with surrounding stations over the same time period, and locations free of known tectonic effects.

6.3.2 Postglacial Rebound

The other major correction applied to tide gauge data used in crustal deformation studies is for postglacial rebound. Section 5.3.1 and Figure 5.1c illustrate the rate of PGR in the study region as determined by *Clague and James* [*2002*]. PGR corrections applied to long-term trends determined from the monthly mean sea levels at individual tidal stations used in this study ranged from ~0.50 mm yr^{-1} (Neah Bay) to ~0.80 mm yr^{-1} (Point Atkinson, Vancouver, and Campbell River). Again, no PGR corrections were applied to differential trends between pairs of stations, as there is little tilt expected from this source [*Clague and James, 2002*].

6.4 Application of Tidal Data to Regional Crustal Deformation Studies

6.4.1 Tide Gauge Data Sets

MMSL data from thirteen tidal stations (Figure 3.6) were used to investigate vertical crustal deformation in this study: Tofino (TOF), Port Alberni (ALB), Bamfield (BAM), Port Renfrew (REN), Victoria Harbour (VIC), Patricia Bay (PAT), Fulford Harbour (FUL), Friday Harbour (FRI), Vancouver (VAN), Point Atkinson (ATK), Campbell River (CAM), Little River (LIT) and Neah Bay (NEA). MMSL values for the Canadian stations were obtained from Marine Environmental Data Services (MEDS) and downloaded from the Permanent Service for Mean Sea Level website [*PSMSL, 2003*] for Neah Bay and Friday Harbour. All MMSL values were calculated from hourly tidal heights. To allow for the most robust trend possible, outliers were removed from each station with a cutoff of 3σ (from the trend). The maximum number of outliers removed from a single station was 3 (TOF), and as such, the trends of either individual or differenced stations should not be affected by a reduction of the data set.

In a general sense, analyses of tidal data are dependent on the operating history of the stations. As such, this information (e.g. stability of instrument or datum) was taken into account in this study when choosing the time periods for analysis.

6.4.2 Methodology – Tidal Data

Linear Regression of Tidal Data

Analysis of the MMSL time series for tidal stations around southern Vancouver Island was completed using three approaches to estimate trends at individual stations: linear regression of the time series using raw MMSL data, linear regression of the time series using MMSL data corrected for common oceanographic signals (detailed in the next section), and linear regression on the differenced output between pairs of stations, using both the raw and corrected data sets. The differencing method follows the analysis of *Wigen and Stephenson [1980]*, which involved differencing the MMSL values between a shorter-term or discontinuous station and a long-term reference. The trends for the differenced results were then calculated using the linear regression technique and combined with the trend of the individual long-term reference station to retrieve the trend at the shorter-term or discontinuous station. The only stations for which the differencing technique was used are CAM and LIT.

To determine tilt across the Cascadia margin from tidal heights, linear regression analysis was performed on the differenced time series between Tofino (TOF) and Point Atkinson (ATK) in the northern region of the study area and between Neah Bay (NEA) and Victoria (VIC) in the south. These stations were chosen to provide a direct comparison of uplift rates with those determined from differential GPS analysis (see Chapter 3) in both regions and repeat leveling (Chapter 4) and gravity (Chapter 5) results in the north. Again, linear regressions were performed on the differences determined using raw MMSL data and those corrected for oceanographic signals.

Data Scatter Reduction and Corrections

To reduce variance in the data sets, an oceanographic correction (OC) was applied to the time series of most stations in this study. The correction is based on the assumption that atmospheric and oceanographic signals will be common between stations located in

close proximity to each other. The stations were grouped into inner (ATK, VAN, VIC, PAT, FUL, FRI) and outer (TOF, ALB, BAM, REN, NEA) coastal sites. Regional corrections were obtained by averaging residuals, calculated using regression analysis to remove linear trends from each individual station, for common months within these groups of sites (e.g. Figure 6.1). To calculate the correction for any particular month, MMSL values from at least 3 stations were used.

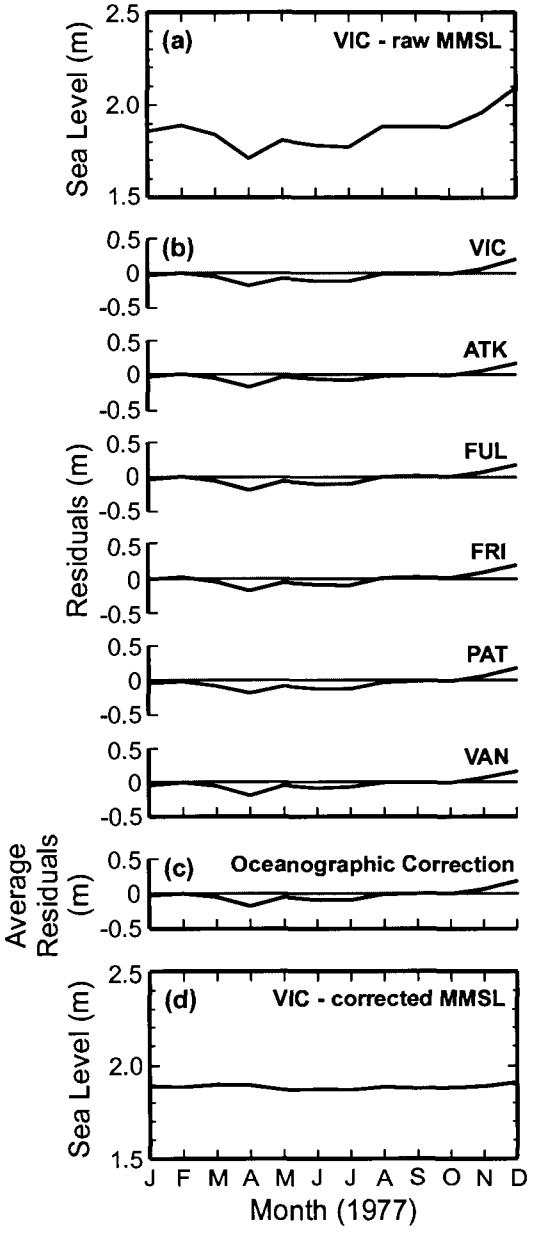

Figure 6.1. Example showing application of the oceanographic correction to one year of MMSL data at Victoria Harbour in 1977. (a) Raw MMSL data for VIC. (b) Residuals for each of the six tidal stations used to calculate the inner coastal oceanographic correction (see text). Residuals were calculated by removing linear trends from the raw data sets. (c) Inner coastal oceanographic correction, calculated by averaging the monthly residuals for the six panels in (b). A minimum of three stations were used to calculate the correction on a month-by-month basis. (d) MMSL data for VIC in 1977 corrected for common oceanographic signals by subtracting (c) from (a).

Two other major corrections were also applied to the MMSL trends: global eustatic sea level rise and PGR. Eustatic sea level rise is the same for all stations in the study region (see Section 6.3.1) and was assumed to cancel for the differenced trends. A PGR correction was applied to each station based on the results of *Clague and James [2002]* (see Sections 5.3.1 and 6.3.2). Thus, the tectonic signal, TS, obtained from the time series of individual tidal stations can be described by:

$$TS = -(T_0 + PGR' - ESL')$$

where T_o is the observed raw MMSL trend, PGR' is the post-glacial rebound correction and ESL' is the eustatic sea level correction. PGR corrections were not applied to differenced trends (see Section 5.3.1).

6.4.3 Tidal Station Results

Single Tidal Station Results

Tables 6.1 and 6.2 summarize the analysis results for individual tidal stations in the southern Vancouver Island region based on the time series shown in Figures 6.2-6.4. The plots display linear trends over time, from which the tectonic uplift rates are calculated. Solid grey and blue lines show the raw MMSL data and trends in Figures 6.2-6.4. Solid red and dashed black lines show the MMSL data corrected for common oceanographic signals (details in next section) and trends.

Table 6.1 summarizes the trends and associated calculated uplift rates for the raw MMSL data. Table 6.2 summarizes the results of subtracting an oceanographic correction (Section 6.4.2) from the MMSL data sets on a month-by-month basis. Using the preferred time periods (see the detailed station descriptions) for trend calculations on the raw data, trends were recalculated for the oceanographic corrected data. In most cases, trends remained within 2σ of the raw data trends and variance was decreased by at least an order of magnitude. Note that Table 6.2 shows only those stations that have had an OC applied.

Table 6.1. Monthly mean sea level trends and crustal uplift rates for raw or reference-station-differenced tide gauge data.

Station Number	Location	Period of Analysis	Sea Level Trend (mm yr^{-1})	Std. Error of Trend (±mm yr^{-1})	Variance (mm^2)	PGR Correction (mm yr^{-1})	Uplift Rate (mm yr^{-1})*	RMS Error (±mm yr^{-1})
07795	Point Atkinson	1950-2002	-0.01	0.23	$7x10^{-3}$	0.80	1.01	0.25
07735	Vancouver	1950-2002	0.60	0.22	$7x10^{-3}$	0.80	0.40	0.24
07330	Fulford	1953-1992	0.23	0.35	$7x10^{-3}$	0.70	0.87	0.36
07277	Patricia Bay	1976-2002	-0.67	0.73	$9x10^{-3}$	0.63	1.84	0.74
9449880	Friday Harbour	1934-2001	1.10	0.16	$8x10^{-3}$	0.70	0.00	0.19
07120	Victoria	1910-2002	0.67	0.10	$8x10^{-3}$	0.60	0.53	0.14
08074	Campbell River	1967-2002	-2.52	0.29	-	0.80	3.52	0.31
07993	Little River	1967-1994	-1.24	0.34	-	0.78	2.26	0.35
08615	Tofino	1940-2001	-1.35	0.25	0.014	0.55	2.60	0.27
08575	Port Alberni	1971-1997	-0.02	0.78	0.011	0.69	1.13	0.79
08545	Bamfield	1970-2002	0.36	0.61	0.013	0.55	0.89	0.62
08525	Port Renfrew	1957-1997	1.24	0.69	0.014	0.55	0.01	0.70
9443090	Neah Bay	1934-2001	-1.60	0.22	0.015	0.50	2.90	0.24

*Uplift refers to the vertical velocity of the stations.

Table 6.2. Monthly mean sea level trends and crustal uplift rates for common ocean-signal-corrected tide gauge data.

Station Number	Location	Period of Analysis	Sea Level Trend ($mm.yr^{-1}$)	Std. Error of Trend ($\pm mm\ yr^{-1}$)	Variance (mm^2)	PGR Correction ($mm\ yr^{-1}$)	Uplift Rate ($mm\ yr^{-1}$)*	RMS Error ($\pm mm\ yr^{-1}$)
07795	Point Atkinson	1950-2002	0.34	0.05	$3x10^{-4}$	0.80	0.66	0.11
07735	Vancouver	1950-2002	0.71	0.04	$2x10^{-4}$	0.80	0.29	0.11
07330	Fulford Harbour	1953-1992	0.40	0.05	$1x10^{-4}$	0.70	0.70	0.11
07277	Patricia Bay	1976-2002	0.05	0.10	$2x10^{-4}$	0.63	1.12	0.14
9449880	Friday Harbour	1939-2001	0.85	0.03	$2x10^{-4}$	0.70	0.25	0.10
07120	Victoria	1914-2002	0.63	0.03	$3x10^{-4}$	0.60	0.57	0.10
08615	Tofino	1957-2001	-1.67	0.10	-	0.55	2.92	0.14
08575	Port Alberni	1971-1997	-0.76	0.19	-	0.69	1.87	0.21
08545	Bamfield	1970-2001	0.39	0.09	-	0.55	0.86	0.13
08525	Port Renfrew	1957-1997	1.72	0.26	-	0.55	-0.47	0.28
9443090	Neah Bay	1957-2001	-1.64	0.09	$3x10^{-4}$	0.50	2.94	0.13

*Uplift refers to the vertical velocity of the stations.

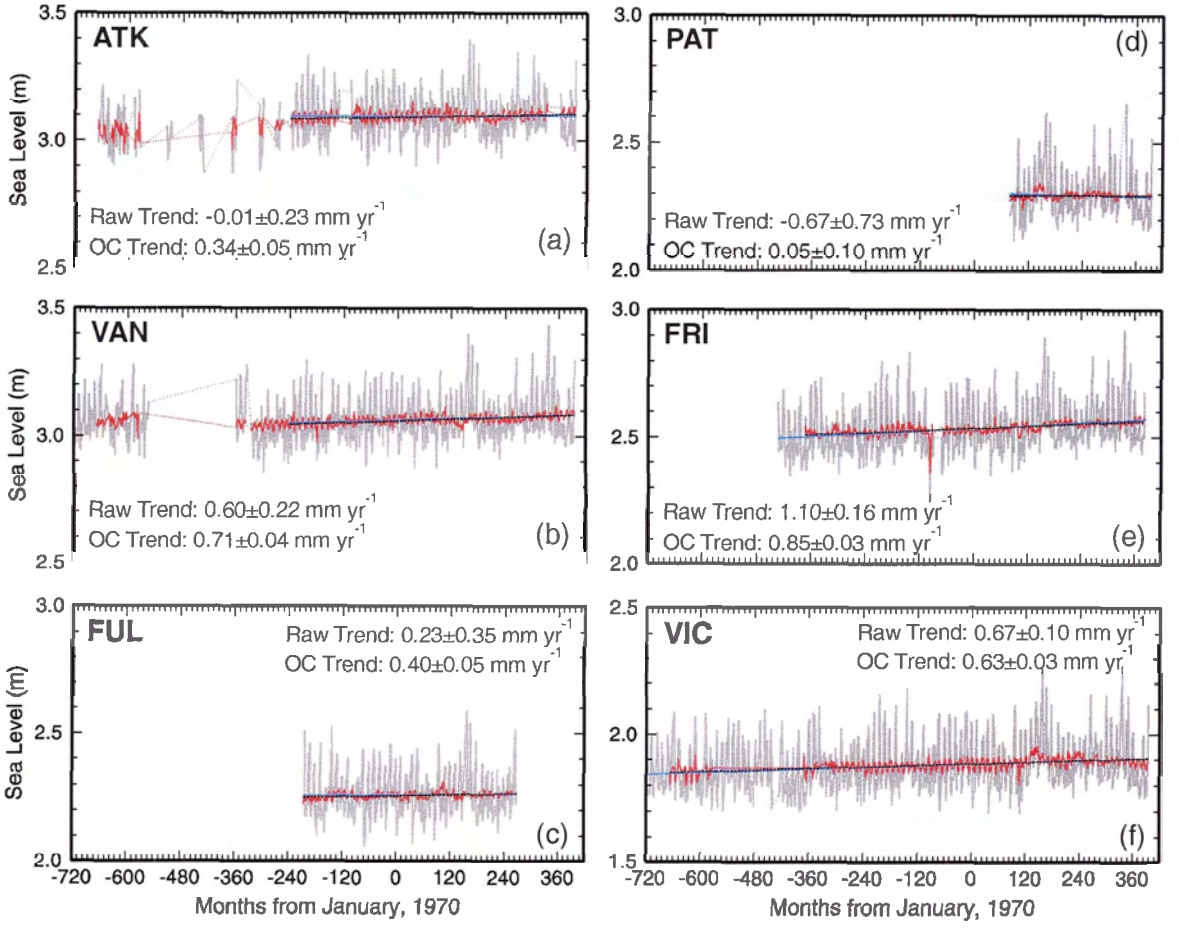

Figure 6.2. MMSL heights for (a) Point Atkinson, (b) Vancouver, (c) Fulford Harbour, (d) Patricia Bay, (e) Friday Harbour, and (f) Victoria Harbour. Solid grey and blue lines (dashed where data is not available) are MMSL heights and trends for the raw data, solid red and dashed black lines are MMSL heights and trends corrected for oceanographic effects (see text). Trend lines are shown for the period over which slopes were calculated. Slope values are indicated on each graph for the raw and oceanographic-signal-corrected (OC) data sets.

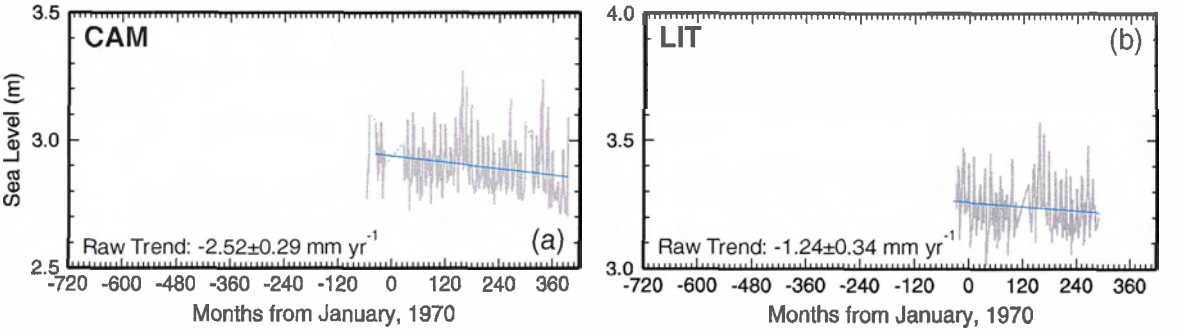

Figure 6.3. MMSL heights (grey line) and trends (blue line) for (a) Campbell River and (b) Little River. Trend lines are shown for the period over which slopes were calculated. Slopes values for the raw data are indicated on each graph. Lines are dashed where MMSL data was not available.

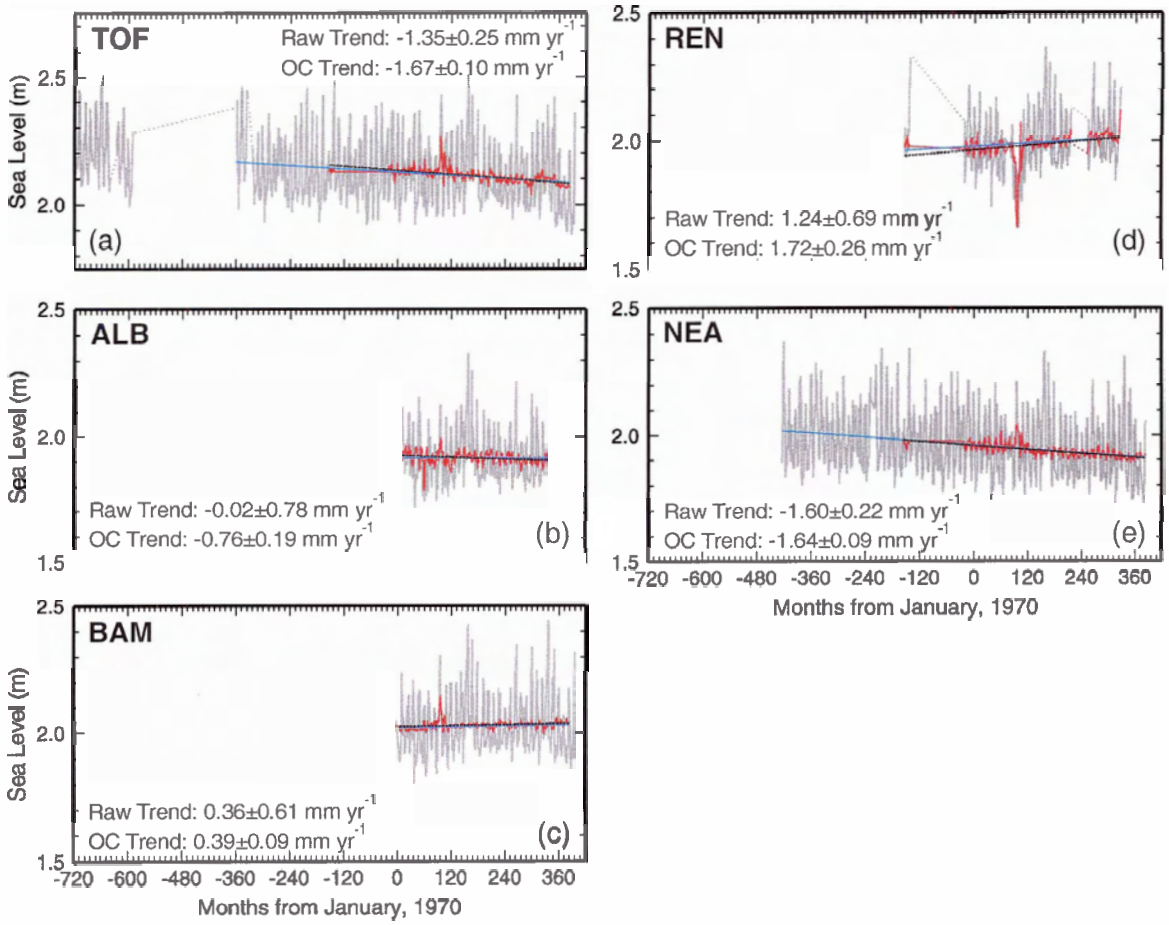

Figure 6.4. MMSL heights for (a) Tofino, (b) Port Alberni, (c) Bamfield, (d) Port Renfrew, and (e) Neah Bay. Solid grey and blue lines (dashed where data was not available) are MMSL heights and trends for the raw data, solid red and dashed black lines are MMSL heights and trends corrected for oceanographic effects (see text). Trend lines are shown for the period over which slopes were calculated. Slope values are indicated on each graph for the raw and oceanographic-signal-corrected (OC) data sets.

For the detailed site discussions that follow, uplift is land up (if positive) relative to sea level and a eustatic sea level correction of 1.80±0.10 mm yr^{-1} [*Douglas, 1991*; *1997*] has been applied to trends at all stations. The RMS errors associated with the uplift rates were calculated using the standard errors of the MMSL trends and the uncertainties associated with the eustatic sea level correction (±0.1 mm yr^{-1}). No uncertainties were assigned to the PGR corrections of *Clague and James* [*2002*]. Station descriptions were obtained partially from *Wigen and Stephenson* [*1980*] and *PSMSL* [*2003*].

Point Atkinson

While MMSL data are available for the Point Atkinson tidal station since 1914, the record is discontinuous until approximately 1950. Furthermore, from 1943 to 1949, the tidal station was at a different location. For these reasons, the trend was calculated from 1950 onward (see Figure 6.2a). A long-term (1950 to 2002) trend (Table 6.1) calculated from the raw data of -0.01±0.23 mm yr^{-1} indicates a decrease in mean sea level on the southern coast of the British Columbia mainland. The associated uplift rate (Table 6.1) is 1.01±0.25 mm yr^{-1}.

Applying the oceanographic correction has reduced variations in sea level height (cf. Tables 6.1 and 6.2). The recalculated long-term trend (Table 6.2) at this station is 0.34±0.05 mm yr^{-1}. The uplift rate, based on this recalculation, is then 0.66±0.11 mm yr^{-1}.

Vancouver

Figure 6.2b shows the raw and oceanographic-signal-corrected time series of MMSL values at the Vancouver tidal station. Based in part on revisions to the elevation datum in the 1950s, the preferred time period for trend calculation is between 1950 and 2002. Correcting for eustatic sea level rise and PGR, the long-term trend from the raw data is 0.60±0.22 mm yr^{-1} and indicates an increase in sea level height. The associated uplift rate is 0.40±0.24 mm yr^{-1}.

Applying the oceanographic correction has reduced variations in sea level height (cf. Tables 6.1 and 6.2). The recalculated trend is 0.71±0.04 mm yr^{-1}, with an associated uplift rate of 0.29±0.11 mm yr^{-1} (Table 6.2).

Fulford Harbour

Figure 6.2c shows the raw and oceanographic-signal-corrected time series of MMSL values for the Fulford Harbour tidal station. Data for FUL is only available between December, 1952 and June 1992, making the record shorter than at other tidal stations in the area. Based on the raw MMSL values at this station, sea level has been

rising at a rate of 0.23±0.35 mm yr^{-1}. The associated uplift rate is 0.87±0.36 mm yr^{-1} (Table 6.1).

As with other stations in the area, variations in the data set were reduced by applying an oceanographic correction (Table 6.2). The recalculated long-term trend is 0.40±0.05 mm yr^{-1}, with a recalculated uplift rate of 0.70±0.11 mm yr^{-1}.

Patricia Bay

Figure 6.2d shows the raw and oceanographic-signal-corrected time series of MMSL values for the Patricia Bay tidal station. MMSL data were available for PAT between 1976 and 2002, with one large data gap in 1997. The long-term trend from raw data is -0.67±0.73 mm yr^{-1} and may be affected by a signal (possibly El Nino) that is present in other time series (e.g. Victoria) for the missing time period in this data set. The uplift rate calculated from the raw data trend between 1976 and 2002 is 1.84±0.74 mm yr^{-1}, which is directionally consistent with other tidal stations in the region. One concern regarding this station is that the sea level values may be affected by different oceanographic effects due to the location of the station in a sheltered area.

After applying the oceanographic correction, the recalculated long-term sea level trend is 0.05±0.10 mm yr^{-1}. The associated uplift rate is then 1.12±0.14 mm yr^{-1} (Table 6.2).

Friday Harbour

Figure 6.2e shows the raw and oceanographic-signal-corrected time series of MMSL values for the Friday Harbour tidal station. The tidal station at FRI has been in operation since 1934, with only one large data gap from October, 1962 to February, 1964. Since 1934 an increase in sea level of 1.10±0.16 mm yr^{-1} has occurred. Accounting for eustatic sea level rise and PGR (Table 6.1), the result is little to no crustal uplift (0.00±0.19 mm yr^{-1}) occurring at this site.

Variations in sea level were reduced by applying the oceanographic correction (cf. Tables 6.1 and 6.2), although there remains a spike in the data set at January, 1962. The

recalculated sea level trend is 0.85±0.03 mm yr^{-1}, with an associated uplift rate of 0.25±0.10 mm yr^{-1}.

Victoria Harbour

Figure 6.2f shows the raw and oceanographic-signal-corrected time series of MMSL values for the Victoria Harbour tidal station. The long-term trend between 1910 and 2002 at VIC indicates a sea level rise of 0.67±0.10 mm yr^{-1}, or uplift rate of 0.53±0.14 mm yr^{-1} (Table 6.1). The data set from the Victoria tidal station is relatively continuous, with no large (≥1 year) gaps in the operating history.

Oceanographic or atmospheric signals are apparent in the time series, but most were reduced or eliminated by applying the oceanographic correction calculated for this area (Figure 6.2f). A particularly strong signal (possibly El Nino) that is common to other stations in the region (e.g. Point Atkinson) at the beginning of 1980 was not completely removed. The recalculated long-term trend at VIC is 0.63±0.03 mm yr^{-1}, with an associated uplift rate of 0.57±0.10 mm yr^{-1}.

Campbell River

Figure 6.3a shows the raw time series for the Campbell River tidal station. One of the shorter-term stations, the trend of MMSL from CAM indicates a decrease in sea level between 1967 and 2002. Monthly MSL data are available beginning in 1965, but are sparse before 1967. As such, the preferred trend was calculated beginning from 1967. The trend (-2.52±0.29 mm yr^{-1}) was calculated with respect to ATK to decrease the standard error. The associated uplift rate for this time period is 3.52±0.31 mm yr^{-1} (see Table 6.1).

No oceanographic correction was applied to CAM due to the location of this station further north than others in this study (see Figure 3.6). While some major common signals with ATK may have cancelled during the differencing process, it should be noted that it is possible that different oceanographic, atmospheric, or even tectonic processes influence the sea level trend.

Little River

Figure 6.3b shows the raw time series for the Little River tidal station. A similar time series to that of CAM is observed for LIT (cf. Figures 6.3a and b), with a shorter operational history (1967 to1993) than other tidal stations in the region. The only large data gap is between January 1979 and November 1980. The MMSL trend (-1.24±0.34 mm yr^{-1}) indicates a decrease in sea level over the 26-year period. As with CAM, this trend was calculated with respect to ATK to reduce the standard error of the trend. The associated uplift rate is 2.26±0.35 mm yr^{-1}. As with CAM, there was no oceanographic correction made to the LIT data due to the station location (see Figure 3.6). It is therefore possible that the sea level trend could be influenced by factors different than those at other stations (see Campbell River description).

Tofino

Figure 6.4a shows the raw and oceanographic-signal-corrected time series of MMSL values for the Tofino tidal station. The tidal station has been in operation since 1910, with data gaps between October 1916 and October 1917; November, 1920 and December, 1939; and in 1942. Large data gaps in the earlier portion of the record and potential site instabilities (based on the location of the reference benchmarks) resulted in the time period 1940 to 2002 being used to calculate the sea level trend (-1.35±0.25 mm yr^{-1}; Table 6.1). The uplift rate is 2.60±0.27 mm yr^{-1} (Table 6.1).

Large variations in sea level have been recorded at this site and signals (possibly El Ninos) are seen repeatedly in the raw data time series (Figure 6.4a). These variations have been greatly reduced by subtracting an oceanographic signal correction determined for the outer coastal stations. The revised trend (-1.67±0.10 mm yr^{-1}; Table 6.2) indicates a greater a uplift rate of 2.92±0.14 mm yr^{-1} (Table 6.2). The corrected trend and uplift rates refer to the time period between 1957 and 2001, since there are insufficient amount of common monthly mean sea level data to calculate the outer coastal oceanographic correction before 1957.

Port Alberni

Figure 6.4b shows the raw and oceanographic-signal-corrected time series of MMSL values for the Port Alberni tidal station. The raw MMSL trend at ALB (-0.02±0.78 mm yr^{-1}; Table 6.1) was calculated for the time period between 1971 and 1997. This indicates uplift at a rate of 1.13±0.79 mm yr^{-1} over the 26-year period.

Only one larger signal (possibly El Nino) is observed in the ALB time series (Figure 6.4b), which occurs in the middle of the time series. However, subtracting a common oceanographic signal reduced high frequency variations, resulting in a MMSL trend of -0.76±0.19 mm yr^{-1} (Table 6.2). The revised uplift rate for ALB is then 1.87±0.21 mm yr^{-1} (Table 6.2).

Bamfield

Figure 6.4c shows the raw and oceanographic-signal-corrected time series of MMSL values for the Bamfield tidal station. Monthly MSL data were available for the Bamfield tidal station from 1970 to 2001. The sea level trend over this period is 0.36±0.61 mm yr^{-1} (Table 6.1). After corrections for PGR and eustatic sea level rise, an uplift rate of 0.89±0.62 mm yr^{-1} was calculated.

High frequency and larger signals (possibly El Nino) have been reduced by subtracting a common oceanographic signal correction. The revised trend for BAM (0.39±0.09 mm yr^{-1}; Table 6.2) and uplift rate (0.86±0.13 mm yr^{-1}; Table 6.2) were calculated for the time period between 1970 and 2001, due to an insufficient amount of common data to calculate the outer coastal oceanographic correction in 2002.

Port Renfrew

Figure 6.4d shows the raw and oceanographic-signal-corrected time series of MMSL values for the Port Renfrew tidal station. MMSL data were acquired for the period of 1957 to 1997. During this time one large data gap exists between 1988 and

1990. The trend (1.24±0.69 mm yr^{-1}) was calculated using the full time period. From this, a small uplift rate of 0.01±0.70 mm yr^{-1} (Table 6.1) was determined.

As with other outer coastal stations, subtracting a common oceanographic signal correction reduced the variance in the data set (cf. Tables 6.1 and 6.2). However, the time series at this station is short relative to other stations in the region. As well, the sea level trend may be influenced by the large signal (possibly El Nino; Figure 6.4d) that could not be completely removed using the oceanographic correction. The resulting sea level trend is 1.72±0.26 mm yr^{-1} (Table 6.2). The uplift rate determined from this is –0.47±0.28 mm yr^{-1} (Table 6.2).

Neah Bay

Figure 6.4e shows the raw and oceanographic-signal-corrected time series of MMSL values for the Neah Bay tidal station. Neah Bay is the longest running "outer coastal" site, with MMSL data available between 1934 and 2001. The sea level trend over this period is -1.60±0.22 mm yr^{-1}, with an associated uplift rate of 2.90±0.24 mm yr^{-1} (Table 6.1). NEA is considered a robust tide gauge station, and the trend does not vary significantly when different time periods are taken.

The variance in the data set was reduced by applying a correction for common oceanographic signals. The revised sea level trend (-1.64±0.09 mm yr^{-1}; Table 2) and recalculated uplift rate (2.94±0.13 mm yr^{-1}; Table 6.2) are not significantly different from the raw MMSL results, even though the analysis period was reduced to 44 years (between 1957 and 2001).

Paired Tidal Station Results

Tables 6.3 and 6.4 summarize the MMSL differences for paired tidal stations around southern Vancouver Island, based on the time series shown in Figure 6.5. All differenced trends and uplift rates refer to the outer-coastal station relative to the inner-coastal station.

As with the individual station time series, the differenced MMSL heights between TOF and ATK (Figure 6.5a) and between NEA and VIC (Figure 6.5b) display linear trends, the slope of which is used to determine the crustal uplift rate. In the case of these differences, the uplift rate is the negative of the sea level trend, and so they have not been included in Tables 6.3 and 6.4. As well, no corrections for PGR or eustatic sea level rise have been applied, as the PGR model of *Clague and James* [*2002*] indicates an insignificant tilt correction across the margin and the latter is the same for all sites. Therefore, the errors associated with the differential uplift rates are the same as those of the differenced sea level trends calculated using linear regression analysis.

Table 6.3. Tilt rates between tidal stations near southern Vancouver Island using raw monthly mean sea level differences.

Station Pairs	Time Period	Differential Uplift Rate (mm yr^{-1})*	Error (mm yr^{-1})
TOF-ATK	1950-2002	1.58	0.17
NEA-VIC	1934-2001	2.57	0.08

*Uplift rate refers to vertical velocity of the station

Table 6.4. Tilt rates between tidal stations near southern Vancouver Island using differenced monthly mean sea levels corrected for oceanographic effects.

Station Pairs	Time Period	Differential Uplift Rate (mm yr^{-1})*	Error (mm yr^{-1})
TOF-ATK	1950-2002	1.97	0.15
NEA-VIC	1934-2001	2.13	0.11

*Uplift rate refers to vertical velocity of the station

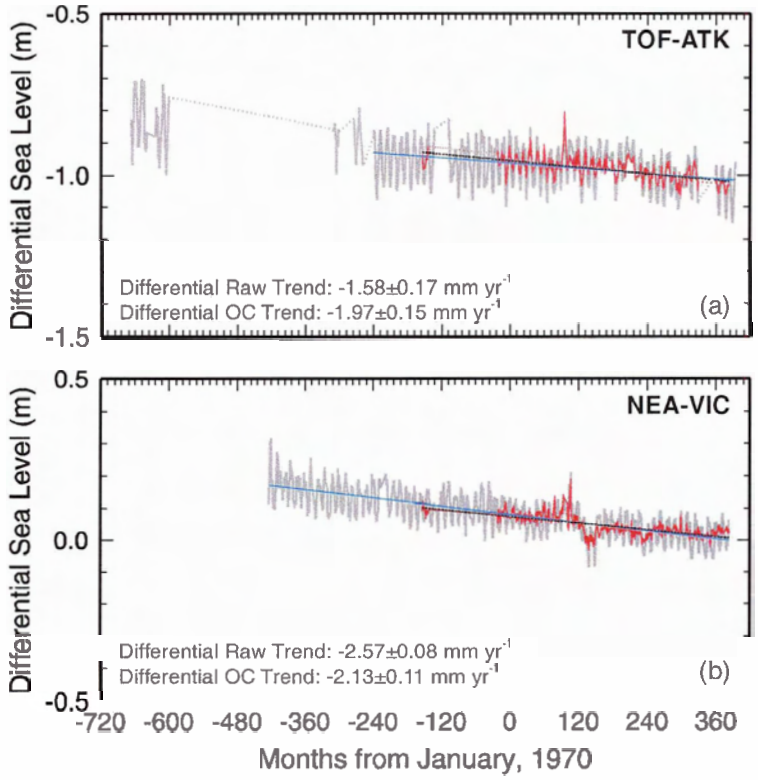

Figure 6.5. Differenced monthly mean sea level heights between (a) Tofino and Point Atkinson and (b) Neah Bay and Victoria. The solid grey and blue lines (dashed where differences were not able to be taken) are differenced MMSL heights and linear trends using the raw data, solid red and dashed black lines are differenced MMSL heights and trends using data corrected for oceanographic effects (see text). Slope values are indicated on each graph for the differenced raw and oceanographic-signal-corrected (OC) data sets.

Figure 6.5a illustrates the differential sea level trends between Tofino and Point Atkinson using raw MMSL data as well as those corrected for oceanographic signals (see Section 6.4.2). From the raw MMSL data, a differential sea level trend of –1.58±0.17 mm yr^{-1} was calculated for the time period between 1950 and 2001, reflecting differential crustal uplift at a rate of 1.58±0.17 mm yr^{-1} (Table 6.3) for the same time period. By subtracting an oceanographic signal from the individual data sets before differencing, the time period of analysis was reduced to 44 years (1957 to 2001) from 51 (1950 to 2001). The revised trend –1.97±0.15 mm yr^{-1} then reflects greater differential uplift at a rate of 1.97±0.15 mm yr^{-1} (Table 6.4).

Figure 6.5b illustrates the differential sea level trends between Neah Bay and Victoria for using raw monthly mean sea levels as well as those corrected for oceanographic signals (see Section 6.4.2). A differential sea level trend –2.57±0.08 mm yr^{-1} was calculated from the raw data for the time period between 1934 and 2001, where data over common months was available. This reflects differential uplift at a rate of 2.57±0.08 mm yr^{-1} (Table 6.3) for the same time period. By subtracting an oceanographic signal from the individual data sets before differencing, the time period of analysis was reduced to 44 years (1957 to 2001) from 67 (1937 to 2001). The revised trend –2.13±0.1 mm yr^{-1} then reflects greater differential uplift at a rate of 2.13±0.11 mm yr^{-1} (Table 6.4).

6.4.4 Summary and Discussion of Tide Gauge Results

Single Tidal Station Summary

Based on the analysis of long-term (>20 year) MMSL data, uplift rates were calculated for 13 tidal stations in the southern and central Vancouver Island region. Stations were grouped into "inner" and "outer" coastal sites based in part on location (see Figure 3.6). For sites in both groups, common-signal oceanographic corrections were calculated and applied to all station data sets (with the exception of CAM and LIT) on a month-by-month basis. Trends at the Campbell River and Little River tidal stations, farther north on Vancouver Island, were calculated with respect to the sea level recorded at Point Atkinson.

Single Tidal Station Discussion

Two main assumptions were made during the analyses of the MMSL data: (1) the structural and tectonic regimes are 2-D along the margin in the study area (Figure 3.6) and (2) atmospheric and oceanic signals are common between stations located in close proximity to each other. Under these assumptions, the results from 13 tidal stations in the

study region generally indicate crustal uplift across and along the Cascadia margin (see Tables 6.1 and 6.2). As well, applying an oceanographic-signal correction has greatly reduced the variance in individual time series (cf. Tables 6.1 and 6.2), suggesting that most signals were common between stations.

Based on the corrected data, vertical crustal movements at these stations are described in two groups (with the exception of NEA): those to the north (TOF, ALB, CAM and LIT) and those to the south (BAM, REN, VIC, FUL, FRI, PAT, VAN, and ATK) of Barkley Sound, where the former group has relatively higher uplift rates. This observation is also noted in Figure 6.6, which is a comparison of uplift rates with previous studies. The sea level trends and calculated uplift rates from these studies are given in Tables 6.5 and 6.6. The vertical uplift rates were calculated by applying the PGR and ESL rise corrections to the trends of each station given in Table 6.1. There is general agreement between rates determined from the different studies. An exception is the large uplift rate for LIT from the *Wigen and Stephenson [1980]* study when annual mean sea levels were used (Table 6.6).

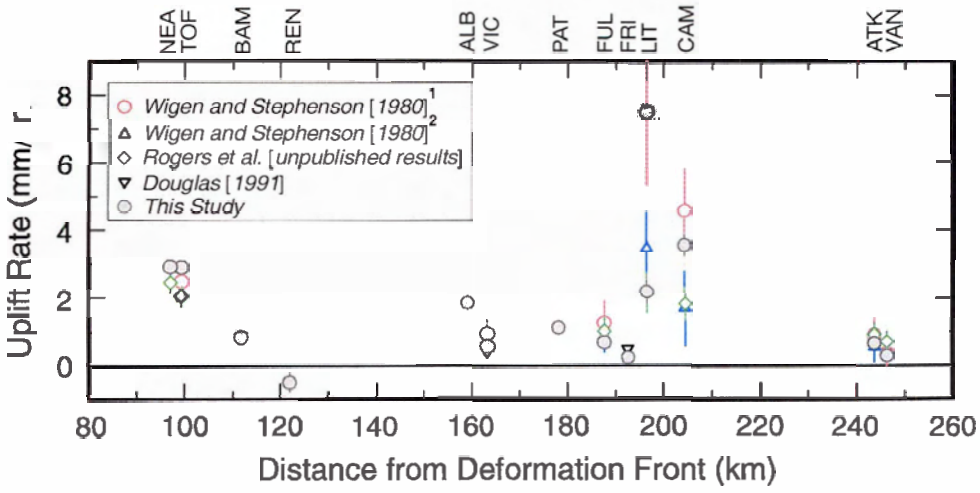

Figure 6.6. Uplift rates calculated for sea level trends, summarized in Table 6.6 (with references), for 13 tidal stations around south to central Vancouver Island. Uplift rates for each station were calculated using PGR and eustatic sea level rise corrections, as indicated in the text (see also Tables 6.1 and 6.2). Values are plotted as a function of distance from the deformation front along the profile shown in Figure 2.1.

Table 6.5. Sea Level Trends with Standard Errors from Previous Studies for West Coast Stations.

Station	*Wigen and Stephenson [1980]*[1]	*Wigen and Stephenson [1980]*[2]	*Rogers et al. [unpublished data]*	*Douglas [1991]*	This Study[3]
VIC	0.27±0.40		0.70±0.10	0.80	0.63±0.03
ATK	0.12±0.48	0.46±0.44	0.10±0.30		0.34±0.05
CAM	-3.57±1.22	-0.65±1.10	-0.80±0.50		-2.52±0.29
LIT	-6.46±2.15	-2.42±1.08	-1.10±0.60		-1.24±0.34
VAN	0.64±0.42		0.30±0.30		0.71±0.04
TOF	-1.25±0.47		-0.80±0.30		-1.67±0.10
ALB					-0.76±0.19
FUL	-0.15±0.65	0.25±0.44	0.10±0.40		0.40±0.05
BAM					0.39±0.09
REN					1.72±0.26
PAT					0.05±0.10
FRI				0.60	0.85±0.03
NEA			-1.50±0.30	-1.60	-1.64±0.09

Positive values indicate sea level up relative to land. Values are in mm yr^{-1}.

[1]Trends calculated from annual means.

[2]Trends calculated from differenced pairs using annual means. The standard errors have been corrected from published data as in *Riddihough [1982 and references therein]*.

[3]Trends are taken from Table 6.2 for MMSL corrected for common ocean signals. Uncertainties are described by the formal regression errors.

Table 6.6. Uplift Rates with Standard Errors from Previous Studies for West Coast Stations.

Station	*Wigen and Stephenson [1980]**	*Wigen and Stephenson [1980]**	*Rogers et al. [unpublished data]*	*Douglas [1991]*	This Study*
VIC	0.93±0.41		0.50±0.14	0.40	0.57±0.10
ATK	0.88±0.49	0.54±0.45	0.90±0.32		0.66±0.11
CAM	4.57±1.22	1.65±1.10	1.80±0.51		3.52±0.31
LIT	7.48±2.15	3.44±1.08	2.12±0.61		2.26±0.35
VAN	0.36±0.43		0.70±0.32		0.29±0.11
TOF	2.50±0.48		2.05±0.32		2.92±0.14
ALB					1.87±0.21
FUL	1.25±0.66	0.85±0.45	1.00±0.41		0.70±0.11
BAM					0.86±0.13
REN					-0.47±0.28
PAT					1.12±0.14
FRI				0.50	0.25±0.10
NEA			2.45±0.32	2.90	2.94±0.13

Positive values indicate crustal uplift (vertical velocity of the stations). Values are in mm yr^{-1}.
*Comments as in Table 6.5.

Paired Tidal Station Summary

Based on the analyses of long-term (>20 year) raw MMSL data, the west-to-east differential uplift rate across south central Vancouver Island is 1.58±0.17 mm yr^{-1} (Table 6.3). Across the northern Olympic Peninsula and southern tip of the island it is 2.57±0.08 mm yr^{-1} (Table 6.3). When the MMSL data at individual stations are corrected for oceanographic signals before differencing, the differential uplift rates become 1.97±0.15 mm yr^{-1} (Table 6.4) across south central Vancouver Island and 2.13±0.11 mm yr^{-1} (Table 6.4) across the northern Olympic Peninsula and southern tip of the island.

Paired Tidal Station Discussion

As with the differential uplift rates determined from the vertical component of GPS stations (within the large 2σ uncertainties associated with GPS time series trends; see Chapter 3), the paired tidal station results indicate greater differential uplift across the southern transect at NEA. However, the difference in rates across the margin along the two transects is much smaller than that observed using GPS (cf. Chapter 3). This may be a function of (1) a longer baseline between the tide gauge stations or (2) a significantly shorter time period of observation at the GPS stations. Uplift rates for the same time period as the GPS data were not calculated from tide gauge data due to the increased signal to noise ratio with shorter time series.

As with the repeat leveling and gravity data (Chapters 4 and 5), sea level trends for 11 of the stations used in this study were compared to those used in the *Dragert et al.* [*1994*] study, where sea level trends and the calculated uplift rates from the *G.C. Rogers et al.* (*unpublished data*) and *Savage et al.* [*1991*] studies are reported. As with the gravity data, they applied a PGR correction based on the *Tushingham and Peltier* [*1991*] study. The results of *Dragert et al.* [*1994*] indicate uplift of the outer coast relative to the inner coast of 2-3 mm yr^{-1}, which is similar to this study. They caution, however, that because of the broad along-margin zone that the tidal stations cover, northern Washington stations may be affected by a wider locked zone along the subduction thrust.

CHAPTER 7

Discussion

7.1 Introduction

This study presents the first detailed look at vertical deformation in the northern Cascadia region which includes an across margin profile covering the region of the forearc through to the backarc. The focus of this chapter is the reconciliation of uplift rates determined from four current geodetic data sets across this region (Chapters 3 to 6) and interpretation of these observations. Comparison between results from this study with predicted vertical interseismic deformation patterns from three models for the Cascadia margin allows testing of the hypothesis that the current locked zone, i.e. the seismogenic zone, is restricted to offshore Vancouver Island. Previously, *Dragert et al.* [*1994*] tested this hypothesis by using different downdip widths of locked and transition zones along the thrust plane. Comparisons between geodetic data and elastic dislocation models for this region have been given by *Savage et al.* [*1991*] and *Hyndman and Wang* [*1993*; *1995*].

Three models are used in this comparison: two [*Flück et al., 1997* (Model 1); *Wang et al., 2003* (Model 2)] are 3-D dislocation models of an elastic half-space and the third (Model 3) is a 2-D finite element viscoelastic model, which uses the same fault geometry as Model 1. Model 3 also includes a weaker crustal zone coincident with the Cascade volcanic belt that is possibly associated with high heat flow in the region [e.g. *Lewis et al., 1988; Hyndman and Lewis, 1995*]. The predicted vertical deformation patterns for all three models were calculated [*S. Mazzotti and J. He, PGC-GSC*] along the across-margin transect shown in Figure 2.1.

7.2 Summary of Results

The uplift rates determined from three independent methods are summarized in Table 7.1. Estimates from GPS, tide gauge and repeat leveling are illustrated as across-margin profiles in Figures 7.1 and 7.2 and summarized in map view in Figure 7.3. The figures illustrate the long-term (Figure 7.1) and short-term (Figure 7.2) nature of the repeat leveling data. The longer-term data of the Williams Lake line are included in both figures to provide continuity of vertical velocity estimates across the profile into the backarc.

Criteria for including data in this summary are: (1) GPS vertical position estimates are derived from >3 years of continuous data, (2) tide gauge trends are derived from ≥10 years of MMSL data, and (3) repeat leveling data are corrected for most systematic errors. Based on these criteria, the 1958 to 1983 time period of repeat leveling along the Williams Lake leveling line has been excluded from further discussions.

All GPS results have been corrected for vertical motion at DRAO (1.20±0.50 mm yr^{-1}) [*Altamimi et al., 2002*] and tide gauge velocity estimates have been corrected for eustatic sea level rise (1.80±0.10 mm yr^{-1} [*Douglas 1990*; *1997*]) and PGR [*Clague and James, 2002*]. Absolute and relative gravity equivalent uplift rates are based on all available data; for the summarized results it is assumed that no mass changes are occurring between the times of measurements.

The main results from analyses of repeat leveling and continuous vertical GPS positioning indicate little tilt across southern Vancouver Island at Tofino and a broad zone of uplift in the backarc centered near Pemberton (e.g. Figure 7.1). Differential uplift from MMSL trends between TOF and ATK indicates slightly higher landward tilting (1.97±0.15 mm yr^{-1}) than for the shorter baseline difference between UCLU and NANO (-0.18±0.90 mm yr^{-1}). As individual markers, with the exception of NEA, these tidal stations can qualitatively be separated into two groups (Section 6.4.4): those with lower (south of Barkley Sound) and those with higher (north of Barkley Sound) uplift rates. Neah Bay may have a relatively larger uplift rate resulting from the station being located closer to the wider locked portion of the subduction thrust [*Dragert et al., 1994*].

Table 7.1. Uplift rates for the northern Cascadia subduction zone.

Station	Uplift Rate (mm yr^{-1})		
	GPS[1]	Absolute Gravity[2]	Tide Gauge[2]
Ucluelet	3.20±1.03	2.56±1.08	
Nanoose Bay	3.37±1.00	3.17±1.10	
Neah Bay	4.18±1.20		2.94±0.13
Albert Head/Victoria	1.42±1.01	0.21±0.93**	0.57±0.10
Tofino			2.92±0.14
Bamfield	3.51±3.13*		0.86±0.13
Port Alberni	1.67±2.47*		1.87±0.21
Port Renfrew			-0.47±0.28
Friday Harbour			0.25±0.11
Fulford Harbour			0.70±0.11
Patricia Bay			1.12±0.14
Vancouver			0.29±0.11
Point Atkinson			0.66±0.11
Campbell River			3.52±0.31
Little River			2.26±0.35

[1]Errors are combined flicker noise, random walk, and white noise [*Mao et al., 1999*; *Mazzotti et al., 2003*].
[2]Errors are given as standard errors of the trend.
*Estimates are based on only 2 years of vertical data (courtesy of *H. Dragert, PGC-GSC*).
**Estimate courtesy of *A. Lambert* (*PGC-GSC*).

The observed tilt for the 1984 to 1990 time period along the Bamfield leveling line (~4 mm yr^{-1}) is distinctly different from the longer-term results (cf. Figures 7.1 and 7.2), suggesting either an unresolved problem with the data set or a transient in the data set (see Section 7.4.4). Results of refraction and rod scale sensitivity tests (Chapter 4) support the latter by indicating that an unreasonable large factor of 5-10 increase in the calculated systematic error corrections would be necessary to reduce the across-island tilt. Therefore, it is interpreted that the observed tilt between 1984 and 1990 is real and so leveling results from this time period will be treated as transient in further discussions. One implication of a transient is that an absolute datum for these elevation changes is no longer well defined and these data cannot establish absolute uplift rates but only relative elevation changes.

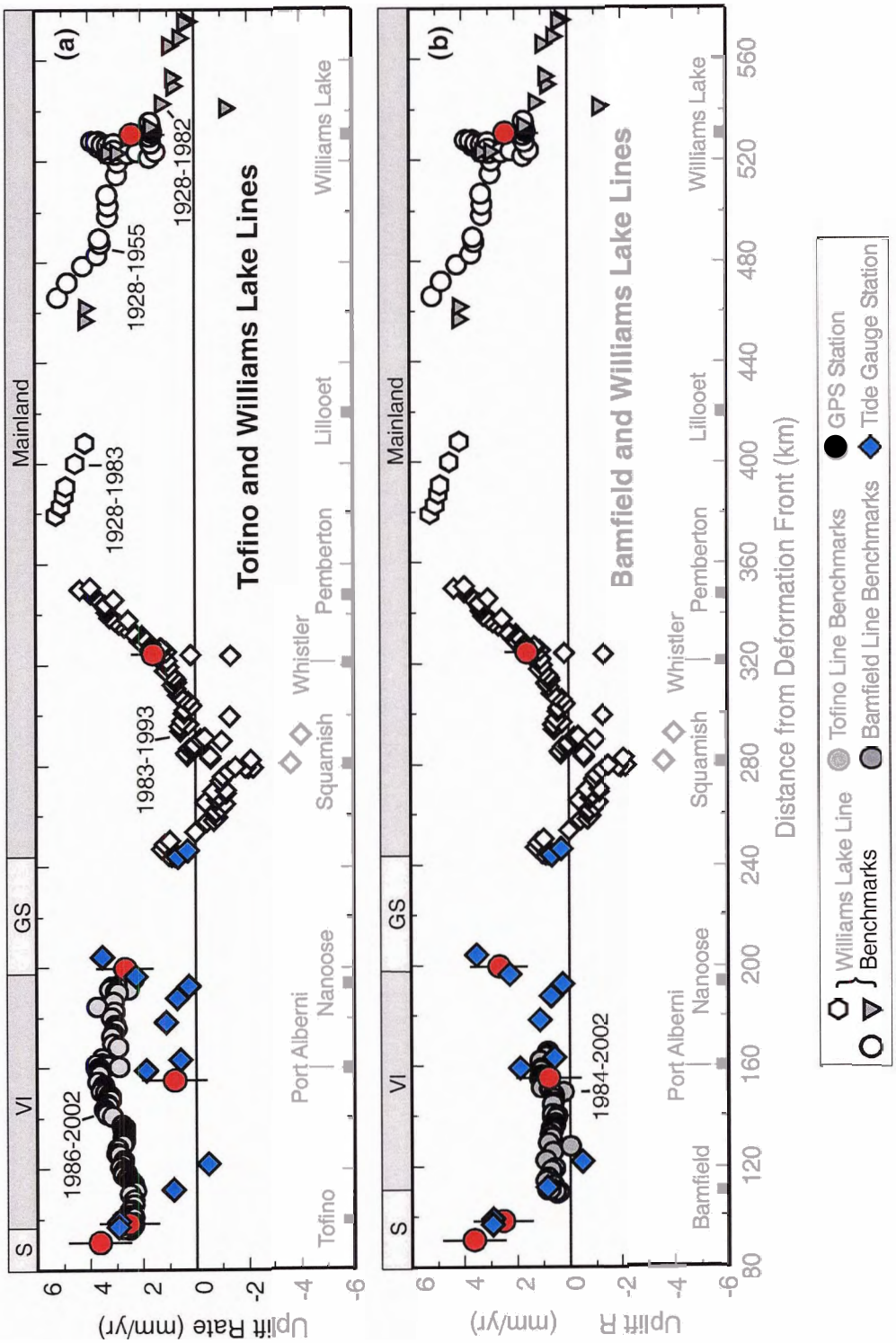

Figure 7.1. Long-term (decadal) uplift across the northern CSZ. (a) Tofino and (b) Bamfield leveling lines. Both figures show uplift rates derived for the Williams Lake leveling line, continuous GPS stations (corrected for NA plate- and DRAO-motion) and tidal stations (locations in Figure 3.6). Time periods for the repeat leveling are shown on the plots. Approximate projected locations of the coastlines of Vancouver Island and the adjacent mainland are shown along the top of each figure. S = shelf; VI = Vancouver Island; GS = Strait of Georgia

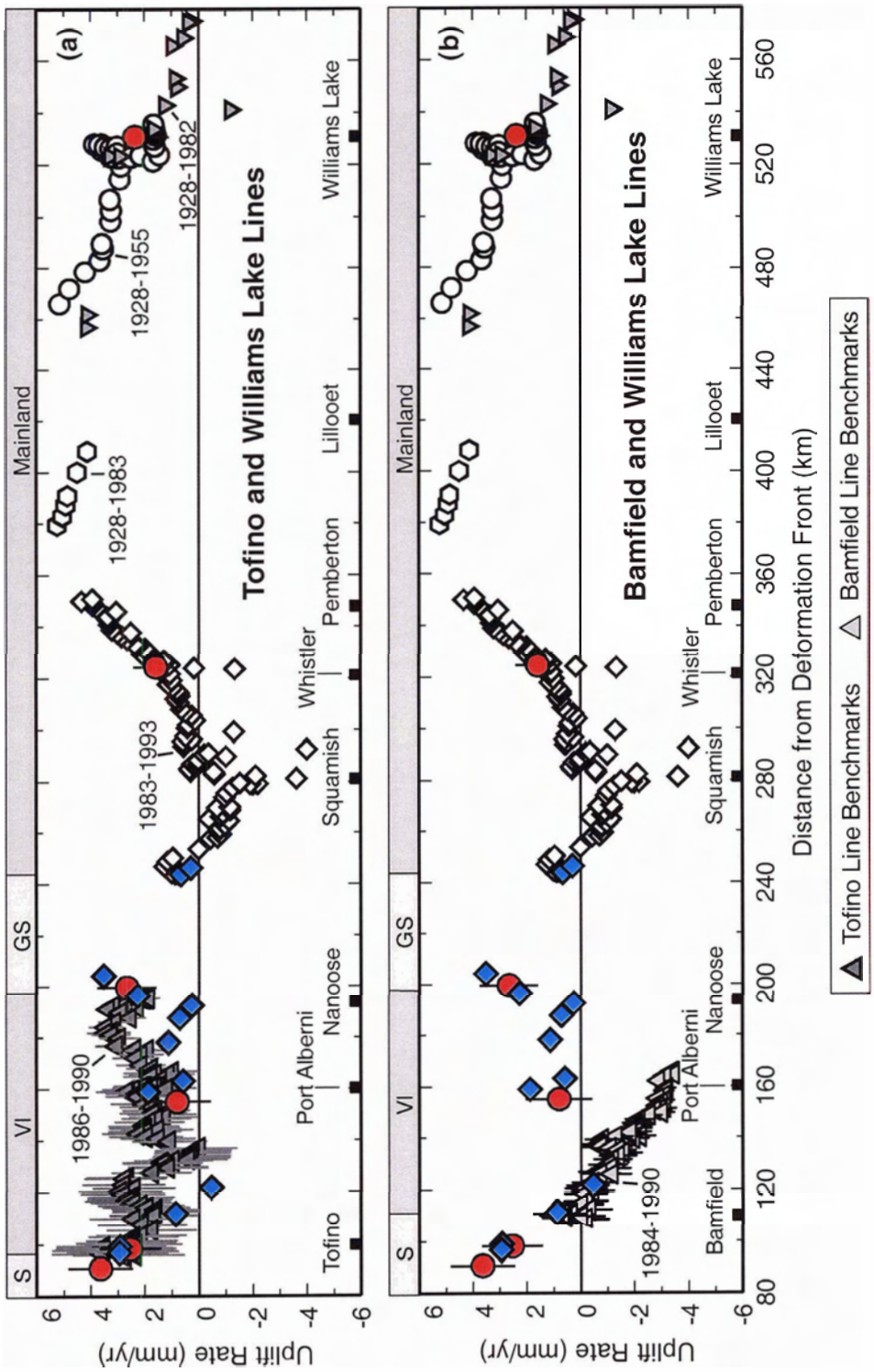

Figure 7.2. Short-term uplift rates across the northern CSZ. (a) Tofino and (b) Bamfield leveling lines. Results from tide gauge and continuous GPS stations are as shown in Figure 7.1. Both figures show uplift rates derived for the Williams Lake leveling line, continuous GPS stations (corrected for NA plate- and DRAO-motion) and tidal stations (locations in Figure 3.6; symbols as in Figure 7.1). Time periods for the repeat leveling are shown on the plots. Approximate projected locations of the coastlines of Vancouver Island and the adjacent mainland are shown along the top of each figure. S = shelf; VI = Vancouver Island; GS = Strait of Georgia

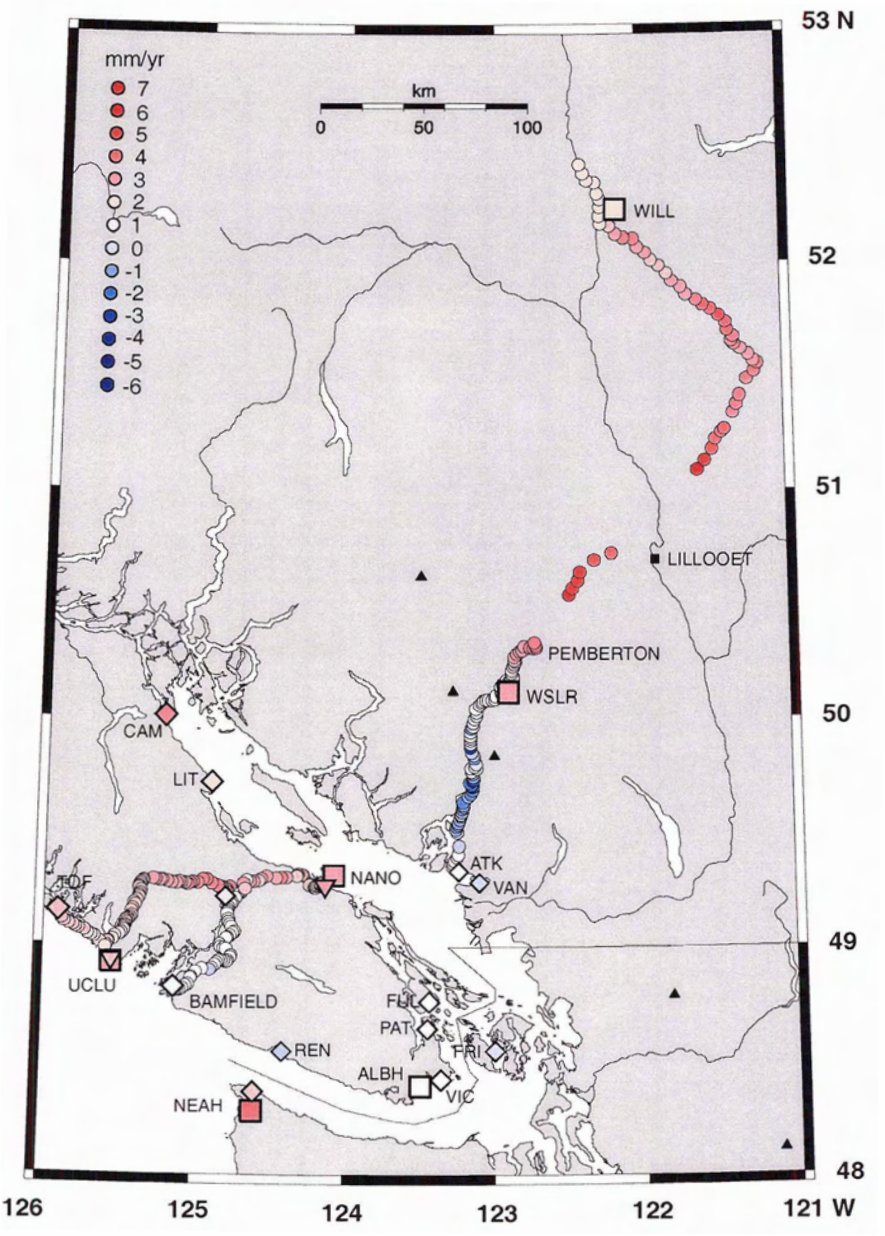

Figure 7.3. Map view of long-term uplift rate estimates across the northern Cascadia margin for repeat leveling (dots), continuous GPS (large squares), tidal (diamonds) stations, and absolute gravity stations (inverted triangles). Rates were plotted as 0.5 mm yr^{-1} increments, and 1 mm yr^{-1} increments are shown in the legend. Repeat leveling measurements are shown as the deformation rates referenced to long-term tide gauge or GPS stations (see Chapter 4). GPS and tide gauge station rates are those in Table 7.1.

Figure 7.4 illustrates equivalent uplift rates from repeat relative gravity measurements and those determined from linear trends of repeat absolute gravity measurements at Ucluelet and Nanoose. Rates determined from absolute gravity trends

are consistent within standard errors to those from GPS time series at both stations (Table 7.1). However, the across-island trends of the repeat relative gravity results indicate seaward tilting at rates of 3.3±2.6 mm yr^{-1} (1986 to 2002) and 7.3±3.5 mm yr^{-1} (1990 to 2002), which are distinctly different from those of the leveling transects (Figures 7.1, 7.2).

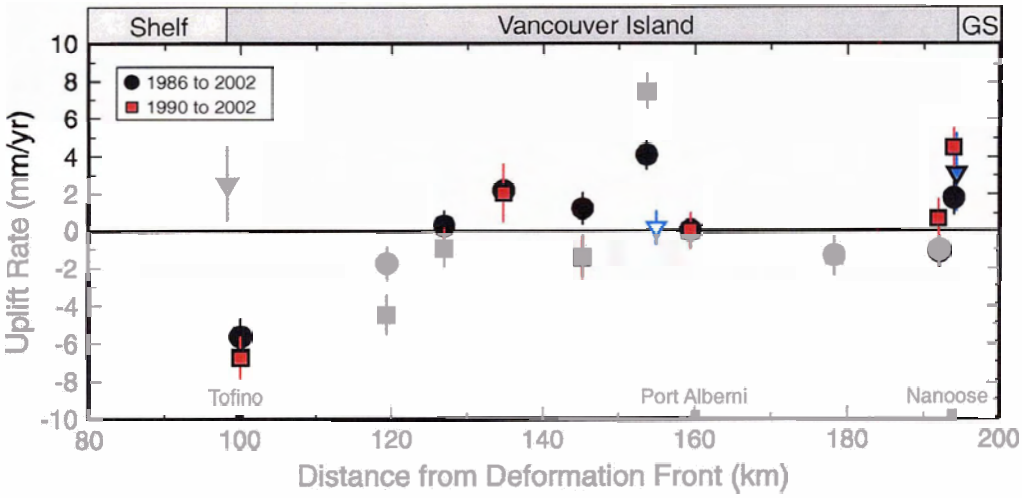

Figure 7.4. Equivalent uplift rates derived from repeat gravity measurements (time periods shown in the legend) and from the time series of repeat absolute gravity measurements (blue inverted triangles) between 1995 and 2002. Equivalent uplift rates were calculated using a deformation gradient of –0.19 μGal mm^{-1} [*Rundle, 1978*]. For comparison, the equivalent uplift rate for the absolute gravity station at Albert Head (Table 7.1) is shown as and open symbol. Note the vertical scale difference from Figure 7.1. GS = Strait of Georgia.

Closer examination of the long-term repeat gravity results indicates offsets between the two time periods, in opposing directions, for the western versus eastern stations (Figure 7.4). This suggests regional differences (e.g. changes in groundwater conditions). As detailed in Chapter 5, the eastern stations may be located on higher porosity sediments (Quadra sediments [*Halstead and Treichel, 1966*]), where changes in the seasonal groundwater level can be as much as 1 m. It is important then to stress that, while ground moisture corrections are taken for the absolute gravity time series, no such measurements are made at the relative gravity stations. However, the western stations are located mainly on rock outcrops, suggesting that any regional changes are occurring

relatively deeper than the penetration of moisture in any overlying soil or sediments. Deep, regional changes beneath western Vancouver Island are supported by comparison of absolute gravity results and continuous GPS height measurements at Ucluelet during an ETS [*Dragert et al., 2001*; *Rogers and Dragert, 2003*] event (see Section 5.4.4). By allowing for offsets at the times of the events, variance in the time series can be reduced. Assuming that offsets are due to elevation changes, uplift on the order of 1 cm would be required. As no such offsets are observed in the GPS data, it then suggests local bulk mass changes during the event (see Chapter 5).

Detailed modelling of both possible groundwater effects on the eastern coast (see Section 5.3.3; [*Halstead and Treichel, 1966*]) and potential mass redistribution occurring beneath the western coast of Vancouver Island coincident with the time of ETS [*Dragert et al., 2001*; *Rogers and Dragert, 2003*] events might provide a better fit between data sets. However, if mass redistribution is occurring, then changes in elevation calculated from gravity variations are not uniquely determined. For example, a –2 μGal change in gravity can be caused by a 1 cm uplift or by a 15 cm drop in the watertable of a 30% porosity soil (e.g. Quadra sediments [*Halstead and Treichel, 1966*]), assuming an infinite sheet approximation. While changes in elevation based on gravity may not be uniquely determined, it is interesting that the longer- versus shorter-time periods of gravity results (cf. Figures 5.2b and 5.3b) do not have similar trends. While there is a greater amount of scatter in the 1986 to 1990 observations as well as larger errors associated with the short time period, the similarity between repeat relative gravity and repeat leveling is noted, in that different length epochs provide different estimates of tilt.

The above results reflect a more complex system than suggested by the simple dislocation models for the region [e.g. *Flück et al., 1997*; *Wang et al., 2003*] (further discussion is given in Section 7.3). This was also noted in the discussion of *Holdahl et al.* [*1989*], who used least squares adjustment of repeat leveling and annual mean sea level data to determine a contour map of vertical crustal motion for coastal Washington and southwestern British Columbia. Some of the observed crustal deformation could be better explained using a time-dependent deformation model, with transient time scales of a few

years, and/or a model that allows differential deformation to occur along the margin. Results of repeat leveling across Vancouver Island suggest time dependent deformation (cf. Figures 7.1 and 7.2) and in conjunction with long-term tidal data, suggest differential deformation across Barkley Sound. This concept is explored further in Section 7.4.3.

Unlike Vancouver Island, vertical crustal motion across the Garibaldi Volcanic Arc has not been studied in great detail. A previous study [*Holdahl et al., 1989*] analyzed a portion of the repeat leveling data along the Williams Lake line and observed crustal uplift centered near Pemberton, as in this study. Although some correlation between uplift rates and topography exists over smaller scales, indicating possible refraction error, the large-scale deformation feature along the Williams Lake line is likely real.

However, the origin of this high degree of uplift (~3 mm yr^{-1} [*Holdahl et al., 1989*]; ~5 mm yr^{-1} [*this study*]) is still unknown. Possible explanations could include a combination of thermal expansion of the crust [*Holdahl et al., 1989*] and a weaker crustal zone focusing strain from the subduction zone, the location of which is coincident with high heat flow near the volcanic arc. Clearly such high uplift rates cannot be maintained over geological time scales since surface elevations of 3 to 5 km would result over 1 m.y.

7.3 Elastic Dislocation Models of the Cascadia Subduction Zone

The approach of *Savage* [*1983*] introduced the application of dislocation models to locked fault zones using the concept of 'back-slip' to predict the pattern of interseismic elastic strain accumulation across subduction zones [e.g. *Flück et al., 1997*; *Wang et al., 2003*]. Dislocation models developed for Cascadia include four main zones along the interplate surface. The geometry of the thrust has been determined from active seismic experiments [e.g. *Green et al., 1990*; *Hyndman et al., 1990*; *Hyndman, 1995b*] and earthquake data [e.g. *Crosson and Owens, 1987*; *Rogers, 1994*]. The downdip extents of the four main zones are generally defined by thermal constraints [*Hyndman and Wang, 1993*; *Oleskevich et al., 1999*].

From the updip to downdip portions of the plate interface, the four main zones along the subduction interface are [cf. *Hyndman and Wang, 1993*]: (1) a shallow, narrow zone of free-slip; (2) a zone that remains fully locked during the interseismic period; (3) a "transition" zone that is fully locked at the updip end and freely slipping at the downdip end; and (4) a zone of free-slip downdip of the transition zone (Figure 7.5). The shallow free-slip zone, located at the frontal thrusts, is likely controlled by the presence of stable-sliding clays that dehydrate at a temperature of 100-150°C. The exact position of the locked portion of the Cascadia subduction thrust cannot be resolved by land geodetic data if it is far offshore, and therefore it is defined by temperature limits [*Flück et al., 1997*; *Wang et al., 2003*]. This zone is located between the limit of clay dehydration and the location of the 350°C isotherm, which is the limiting temperature for seismicity in most continental areas and corresponds to the maximum depth of crustal earthquakes beneath Vancouver Island [*Hyndman and Wang, 1993*]. The transition zone is a region where the rate of motion during the interseismic period is assumed to increase downdip from zero to the full plate rate. This zone is a convenience allowed by the approach of *Savage* [*1983*] to avoid a physically unrealistic point at the downdip end of the locked zone, where relative plate motion would change abruptly from zero to the full plate rate. Although small thrust earthquakes do not occur in this zone, megathrust rupture is thought to extend some distance downdip into it [*Hyndman and Wang, 1993*]. At the downdip end of the transition zone, stable sliding then resumes at an average of full plate rates.

Recently, *Dragert et al.* [*2004*] have suggested a modification of this model for motions and coupling across the plate interface. The new model includes the ETS zone (Section 2.2) on the deeper portion of the interface (Figure 7.5), where displacement occurs in a stepwise fashion as stress periodically (period of ~14.5 months [*Dragert et al., 2001*; *Rogers and Dragert,* 2003]) accumulates and releases over a period of a few weeks. Through this process of episodic deep slip, *Dragert et al.* [*2004*] suggest that the locked zone updip is brought closer to failure during and immediately after an ETS event (see also *Mazzotti and Adams* [*2004*]).

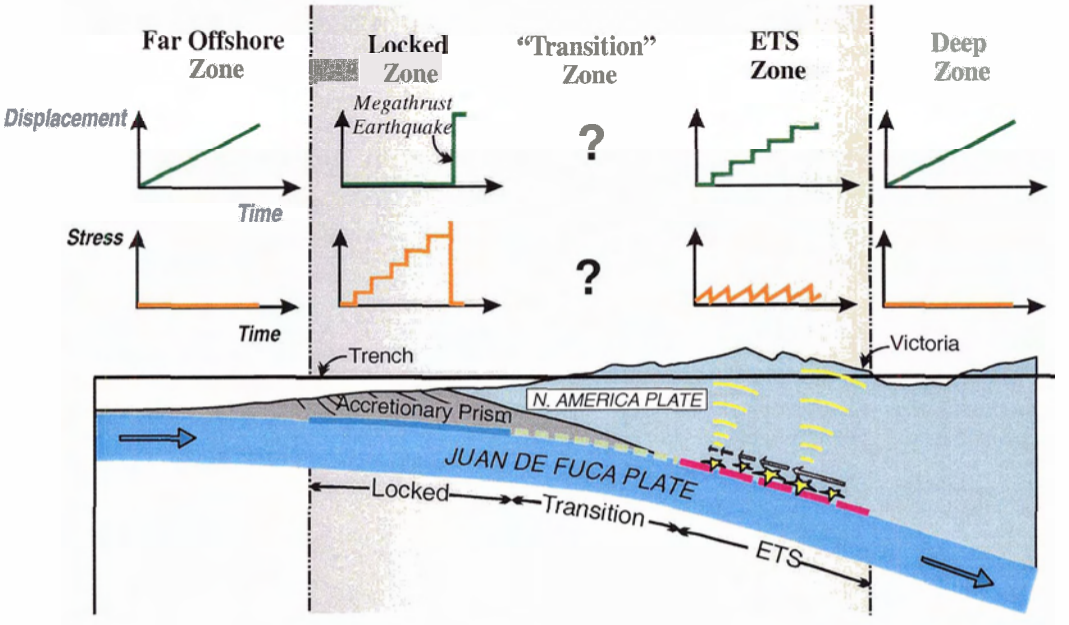

Figure 7.5. Schematic representation of a subduction zone profile indicating the characteristics of four zones during the coseismic and interseismic periods as well as a "stick-slip" or ETS zone, where episodic slip is thought to occur [*Dragert et al., 2004*].

7.3.1 Linear Transition Zone Model

Geometrical limits of 2-D dislocation models prompted *Flück* [*1996*] to develop a 3-D model (Model 1) based on point source solutions of *Okada* [*1985*]. By dividing the fault plane into a series of triangular elements, the fault geometry and non-uniform slip distributions can be approximated. This allows for varying width and dips of the transition and locked zones along the Cascadia margin, which could not be accommodated by previous models. To produce a smoother fault surface, a modification of the original 3-D model was made [*Flück et al., 1997*], where circular arcs were introduced that more accurately describe the geometry of the fault plane. Depth contours for the fault used in these models are well defined by Benioff-Wadati seismicity, offshore multichannel seismic reflection surveys, seismic refraction surveys, seismic tomography, and teleseismic waveform analysis [*Flück et al., 1997 and references therein*]. The depth of the locked and transition zones are defined by thermal and geodetic constraints [*Hyndman and Wang, 1993; 1995*]. In this model, the locked and transition zones are

approximately the same width for the northern CSZ region (Figure 7.6a) where the locked zone extends to the T1 isotherm (depth ~15 km) and the transition zone is located between the T1 and T2 isotherms (maximum depth ~25 km) (Figure 7.6b). The transition zone is defined by a linear, downdip decrease of the slip deficit (Figure 7.6b).

Dislocation rates at each of the model elements are defined by the kinematic constraints (plate convergence rate and direction). For this model, convergence occurs at 42 mm yr^{-1} in a direction of N69°E [*DeMets et al., 1990; 1994*]. Variations in either parameter along the margin were not incorporated by *Flück et al.* [*1997*], based on results from unpublished test models [*Flück, 1996*].

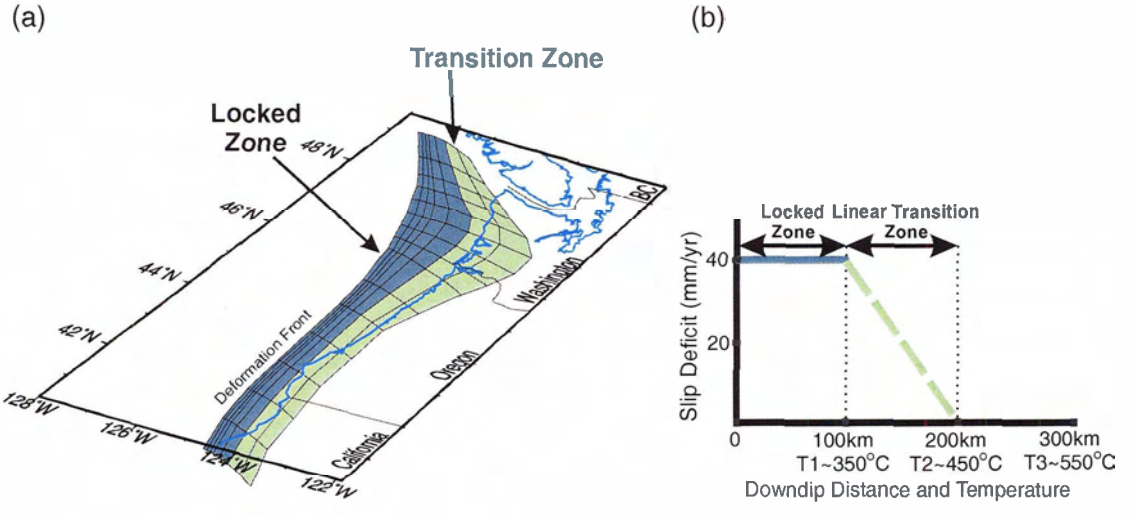

Figure 7.6. Elastic dislocation model of *Flück et al.* [*1997*] for the northern Cascadia subduction zone. (a) Geometry of locked and transition zones and (b) slip deficit and thermal ranges of the locked and linearly tapering transition zones [modified from *Flück et al., 1997*].

7.3.2 Exponential Transition Zone Model

A revision of the "linear transition zone" model by *Wang et al.* [*2003*] (Model 2) was driven by four reasons: (1) better horizontal constraints from recent GPS observations; (2) improved understanding of the secular northward motion and clockwise rotation of the forearc sliver of the Cascadia margin from geological studies [cf. *Wells et al., 1998*] and geodetic observations in Oregon [*Savage et al., 2000*; *McCaffrey et al.*.

2000] and northern California; (3) revised postglacial rebound analyses [cf. *Clague and James, 2002*]; and (4) an improved understanding of the time dependence of interseismic deformation and the nature of the transition zone.

As with the previous 3-D dislocation model, the updip and downdip limits of the locked zone are provided by thermal data as well as tide gauge and leveling data. However, these are in a "validating" role rather than primary constraints, which now come from horizontal deformation data. The revised model defines an "effective transition zone" (Figure 7.7a) in which the change from "fully-locked" to "free-slip" is described by an exponential rather than linear decrease with downdip distance (Figure 7.7b). This "effective" transition zone is extended downdip to the T3 isotherm at ~45 km depth (Figure 7.7b). This zone emulates viscoelastic relaxation of the mantle wedge and was necessary to provide in a better fit to observed GPS velocities of coastal and inland sites [*Henton, 2000*] that were previously over- and under-predicted, respectively [e.g. *Flück et al., 1997*].

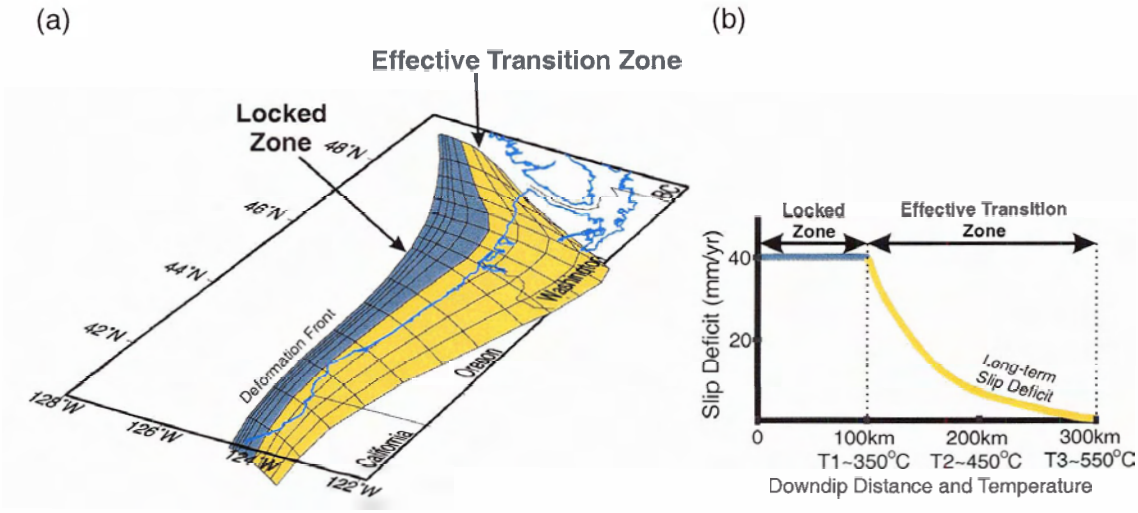

Figure 7.7. Elastic dislocation model of *Wang et al.* [*2003*] for the northern Cascadia subduction zone. (a) Geometry of locked and transition zones and (b) slip deficit and thermal ranges of the locked and exponentially tapering (effective) transition zones [modified from *Wang et al., 2003*].

Unlike the *Flück et al.* [*1997*] model, kinematic constraints used in Model 2 have accounted for continuous secular motion of the Cascadia forearc. The southern Cascadia

forearc is both moving in a northerly direction and rotating clockwise relative to North America around the Euler pole refined by *Wells and Simpson* [*2001*] (Table 7.2). Previous models [e.g. *Riddihough, 1984; DeMets et al., 1990, 1994; DeMets and Dixon, 1999*] feature a southward decrease in convergence rate and increase in obliquity, but have not included the observed forearc motion [*Wells et al., 1998*; *Savage et al., 2000*; *McCaffrey et al., 2000*]. With improved resolution of the Cascadia forearc motion, *Wang et al.* [*2003*] suggest that it may be more appropriate to use JdF-forearc rather than JdF-NA convergence to model interseismic deformation. Euler poles used by *Wang et al.* [*2003*] to derive the needed kinematic relationships are shown in Table 7.2. The JdF-forearc pole is applied to central and southern Cascadia in this model; however, it is assumed that forearc motion does not affect British Columbia. Therefore, the convergence rate predicted by the JdF-NA pole (Table 7.2) determined using JdF-PA [*DeMets et al., 1994*] and PA-NA [*DeMets and Dixon, 1999*] poles (Table 7.2), where PA is the Pacific plate, is applied to the northern Cascadia subduction zone.

Table 7.2. Euler Poles Involved in This Study's Discussions [adapted from *Wang et al., 2003*].

Pole	Latitude (°N)	Longitude (°E)	Rotation Rate (°/Ma)	References
JdF-NA1	29.40	-111.70	-1.090	*Riddihough* [*1984*]
JdF-NA2	20.70	-112.20	-0.800	*DeMets et al.* [*1990*]
JdF-NA3	26.63	-110.45	-0.804	(from PA-NA and JDF-PA in this table)
PA-NA	51.50	-73.70	-0.765	*DeMets and Dixon* [*1999*]
JdF-PA	28.30	29.30	0.501[a]	*DeMets et al.* [*1994*]
forearc-NA	45.54	-119.60	1.316	*Wells and Simpson* [*2001*]
JdF-forearc	67.40	-147.94	0.627	(from JDF-NA and forearc-NA)

[a]The rate was mistyped as 0.520 in the original reference.

It should be noted that while this model did not include forearc motion in northern Cascadia, results (combined permanent-campaign GPS velocities) from *Mazzotti et al. [2003]*, who use the *Wang et al. [2003]* model to re-evaluate interseismic coupling, suggest the presence of an independent northern Cascadia forearc (with a very small motion with respect to North America). They propose that southern Vancouver Island and northern-most Washington may experience northward (NW to NE) motion on the order of a few mm yr^{-1}. The authors provide arguments for both this small rate of motion (based in part on observed background seismicity [cf. *Hyndman and Weichert, 1983*; *Hyndman et al., 2003*] and heatflow data [*Hyndman and Wang, 1993*; *Oleskevich et al., 1999*]) and for motion to occur in a non-rigid block fashion (based on large residuals at robust permanent GPS stations).

7.3.3 "Soft Zone" Model

High heat flow, which characterizes the Garibaldi Volcanic Arc [e.g. *Lewis et al., 1988; Hyndman and Lewis, 1995*], is thought to create a zone where the only significant lithosphere strength would be in the uppermost part of the crust and where the overall lithospheric strength would be low. To investigate the possible effects of a rheologically "weak" or "soft" zone coincident with the broad region of high heat flow, a 2-D finite element model was employed [*J. He, PGC-GSC*] (Model 3). The main objective of this exercise was to determine whether a weaker zone near the volcanic arc could focus strain from subduction processes occurring to the west, thereby producing a zone of resolvable vertical crustal deformation to the east of the Strait of Georgia. This concept is supported by observed elevation changes along the Williams Lake leveling line (Figure 4.6). One implication of such a model might be that observed deformation rates could be modeled without the need for an extension of the seismogenic zone further downdip along the thrust plane.

The "soft zone" model uses the geometry of the 3-D elastic dislocation model of *Flück et al. [1997]*, with the addition of a 100 km-wide weaker crustal zone (Young's

modulus: $1.2x10^{11}$ kPa (upper crust) and $1.6x10^{11}$ kPa (mantle); viscosity: 10^{17} Pa s) underlying the volcanic arc (Figure 7.8) between the projected distances of 265 km and 365 km from the deformation front along the profile in Figure 2.1. The kinematic constraints (plate convergence rate and direction) are the same as those for Model 1 (see Section 7.3.1).

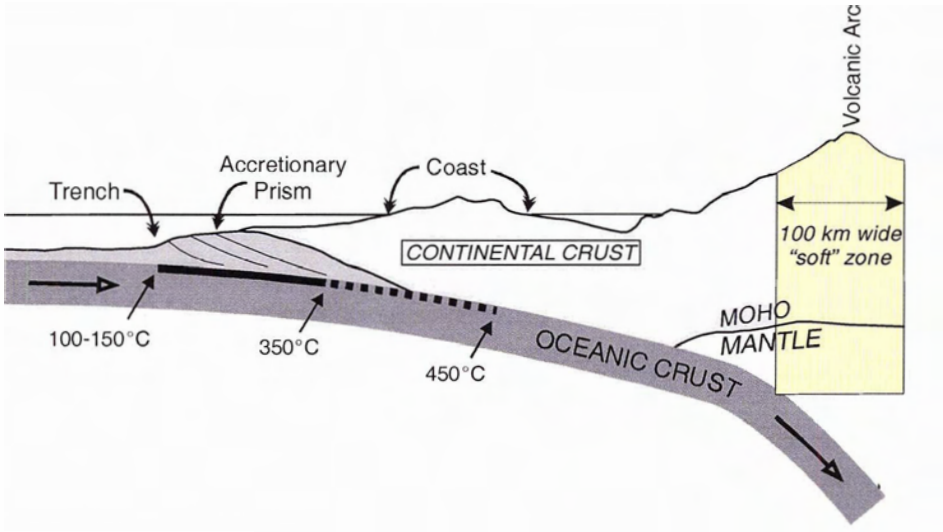

Figure 7.8. Cartoon cross-section of the northern Cascadia subduction zone showing the approximate location of a 100 km wide "soft" zone through the crust and mantle centered on the Garibaldi volcanic arc [modified from *Henton, 2000*]. The figure is not to scale.

7.3.4 Geodetic Data Comparisons to Dislocation Models

Comparisons with Linear and Exponential Transition Zone Models

Figures 7.9 and 7.10 illustrate the comparison of uplift rates determined from repeat leveling measurements (Chapter 4) (as longer- and shorter-term time periods), as well as from the time series of continuous GPS (Chapter 3) and tidal (Chapter 6) stations, to the predicted pattern of interseismic vertical deformation from Models 1-to-3 across the margin. This section will focus on comparing observed uplift rates with Models 1 and 2.

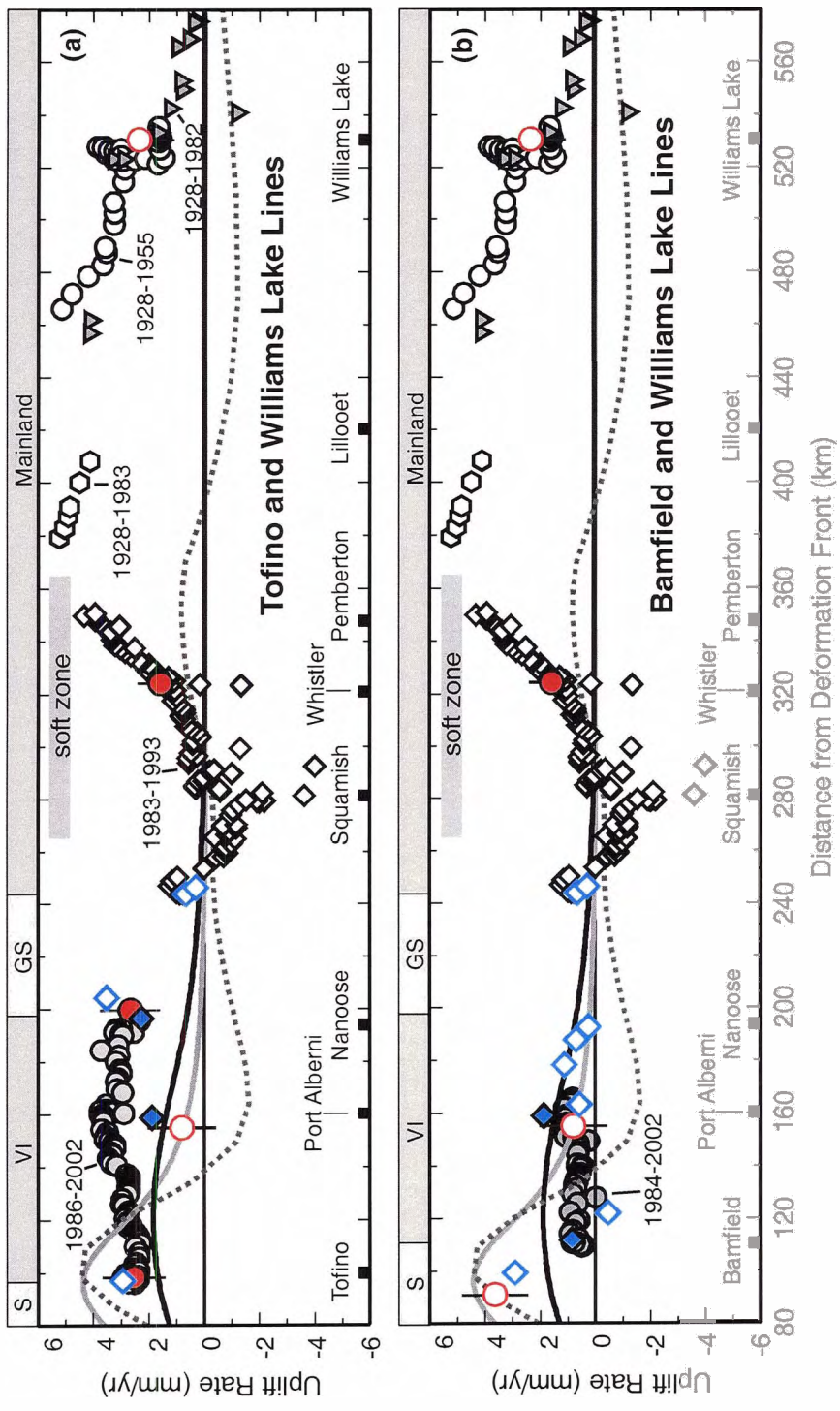

Figure 7.9. Predicted pattern of interseismic vertical deformation from elastic dislocation models with linear (thick grey line), exponentially (thick black line) decreasing slip deficit in the transition zone as well as a 2D finite element model (dashed grey line) replicating the geometry of the linear transition zone model, compared to long-term uplift rates derived from repeat leveling, tide gauge and continuous GPS stations across the northern CSZ. (a) Tofino and (b) Bamfield leveling lines. Both figures show uplift rates derived for the Williams Lake leveling line, continuous GPS stations (corrected for NA plate- and DRAO-motion) and tidal stations (locations in Figure 3.6; symbols as in Figure 7.1). Repeat leveling time periods are shown on the plots. Approximate projected locations of the coastlines of Vancouver Island and the adjacent mainland are shown along the top of each figure. S = shelf; VI = Vancouver Island; GS = Strait of Georgia.

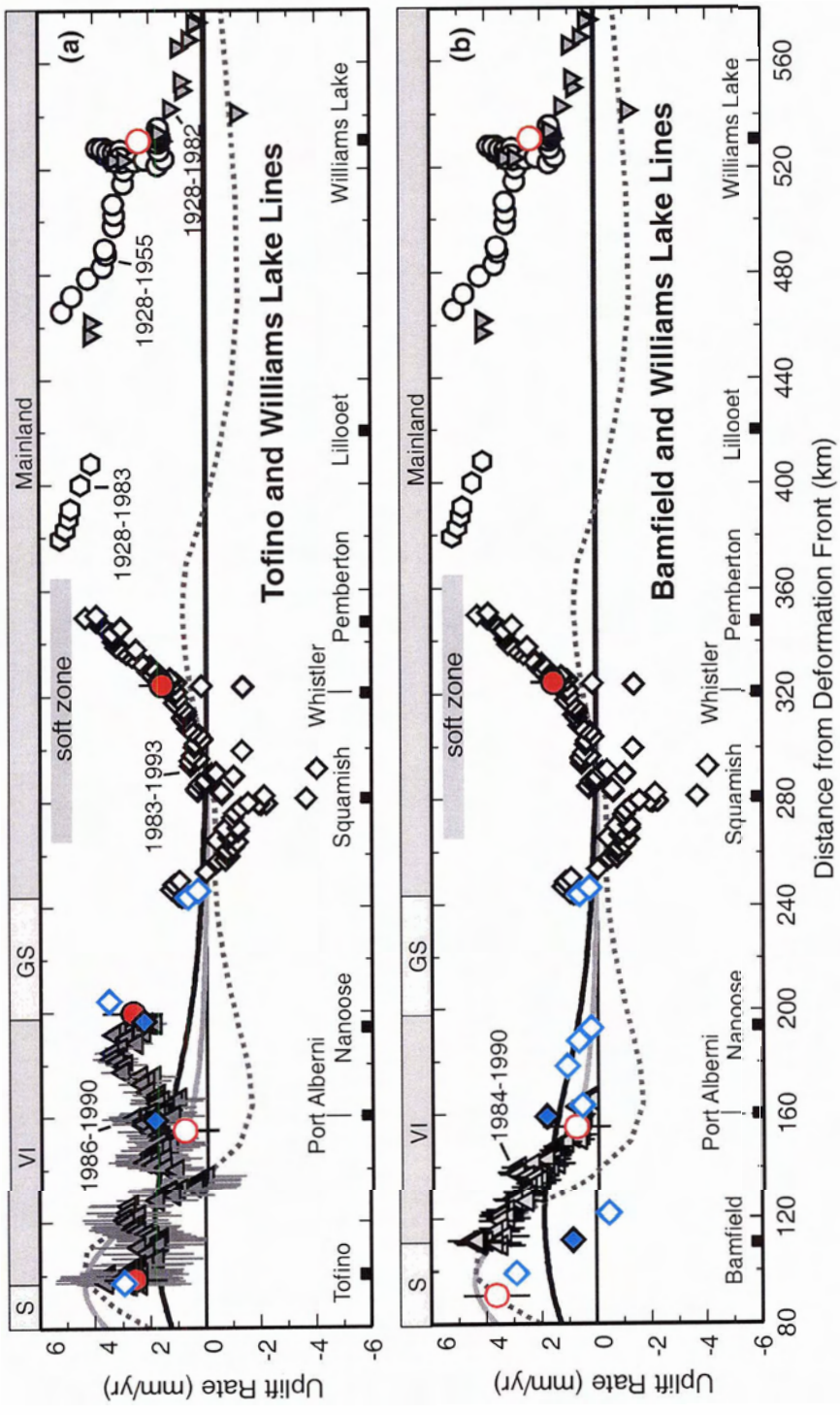

Figure 7.10. Predicted pattern of interseismic vertical deformation from elastic dislocation models with linear (thick grey line), exponentially (thick black line) decreasing slip deficit in the transition zone as well as a 2D finite element model (dashed grey line) replicating the geometry of the linear transition zone model compared to short-term uplift rates derived from repeat leveling, as well as rates from tide gauge and continuous GPS stations across the northern CSZ. (a) Tofino and (b) Bamfield leveling lines. Both figures show uplift rates derived for the Williams Lake leveling line, continuous GPS stations (corrected for NA plate- and DRAO-motion) and tidal stations (locations in Figure 3.6; symbols as in Figures 7.1 and 7.2). Repeat leveling time periods are shown on the plots. Approximate projected locations of the coastlines of Vancouver Island and the adjacent mainland are shown along the top of each figure. S = shelf; VI = Vancouver Island; GS = Strait of Georgia.

Leveling results have been referenced to tidal and continuous GPS stations on Vancouver Island and the mainland (Chapter 4). However, the 1984 to 1990 time period shown in Figure 7.10b represents relative elevation changes, and as such, has been shifted along the y-axis for better comparison with the models. As well, because of the more complex system that these results may reflect, continuous GPS and tidal stations not located within 50 km either side of the across-margin profile (Figure 2.1) are shown as open symbols (cf. Figures 7.1 and 7.9 and Figures 7.2 and 7.10).

The obvious difference in uplift rates to the north and south of Barkley Sound from repeat leveling and tide gauge results (cf. Figures 7.9a and 7.9b or 7.10a and 7.10b) is the basis for including results from Vancouver Island stations only in the appropriate figure, based on station location. For example, the Tofino tide gauge station is only shown in Figures 7.9a and 7.10a, which illustrate the uplift rates for repeat leveling along the Tofino line.

Repeat leveling from the Tofino line (Figure 7.9a) appears generally consistent with the predicted uplift rate pattern across the margin of Model 2. However, the magnitude of uplift along the eastern half of the leveling line for the longer time period (Figure 7.9a) indicates a slight (<1 mm yr^{-1}) bulge, where Model 2 predicts decreasing uplift rates east of central Vancouver Island. While there is greater scatter of the crustal uplift pattern and larger uncertainties for the 1986 to 1990 time period (Figure 7.10a), these data generally show a better fit to the predicted deformation rates of Model 2 than the longer time frame.

For the Bamfield leveling line, the longer time period (Figure 7.9b) does not correlate well with the magnitude of vertical deformation predicted by either Model 1 or 2. However, the general pattern of uplift along the transect is consistent with the latter. The shorter time period (Figure 7.10b) indicates a pattern more consistent with Model 1, which is expected as these data were used as a constraint for the model.

Figures 7.9 and 7.10 also illustrate the uplift rates determined from the time series of continuous GPS (red dots) and tidal stations (blue diamonds). As with the repeat leveling data, these results were projected to the profile shown in Figure 2.1. With the

exception of NANO, "absolute" uplift rates observed at continuous GPS stations are consistent within 1σ (standard error on trend including random and flicker noise; Chapter 3) to the predicted vertical deformation rates of Model 1. In most cases, the rates are also consistent with predictions of Model 2 within 2σ. As well, differential GPS results illustrate the lower amount of tilt across the margin at TOF predicted by Model 2.

Uplift rates determined for tidal stations suggest a generally better fit to the predicted across-margin deformation pattern of Model 2, with the low magnitude and broad peak (Figures 7.9 and 7.10). However, the magnitude of uplift determined for tidal stations to the north and south of Barkley Sound are distinctly different. In the southern region, with the exception of a couple of tide gauge results (e.g. ALB), Model 2 slightly over-predicts vertical crustal motion. To the north of Barkley Sound, Model 2 consistently under-predicts vertical crustal motion. While TOF indicates an uplift rate somewhere between those predicted by Models 1 and 2, LIT and CAM indicate rates 2-3 times higher than Model 2 and ~4 times higher than Model 1. As well, both models predict a smooth landward decrease in deformation rates towards zero near the eastern coast of Vancouver Island, which does not replicate the observed uplift on the mainland.

The releveling observations illustrated in Figures 7.9 and 7.10 suggest either (1) the tide gauge results do not reflect the true uplift rates across Barkley Sound or (2) the model is truly under-predicting uplift rates north, and over-predicting uplift rates south of Barkley Sound. The latter is supported by vertical crustal motions determined at 13 individual tidal stations, which clearly show a consistent pattern of higher uplift rates to the north of Barkley Sound relative to southern stations (Figure 7.3). Although there are fewer stations, this pattern is also observed in the vertical component GPS results if NEAH is excluded. In this second case, it is suggested that a better fit to the current data might be found by allowing for some form of differential vertical deformation across Barkley Sound in current deformation models. Differential deformation across Barkley Sound is explored further in Section 7.4.3.

Figure 7.11 illustrates the predicted pattern of vertical deformation from Cascadia models compared to equivalent uplift rates determined from repeat gravity measurements

across Vancouver Island and from the time series of repeat absolute gravity measurements (Chapter 5). Model 3 (dashed line in Figure 7.11) will be discussed in detail in the following section.

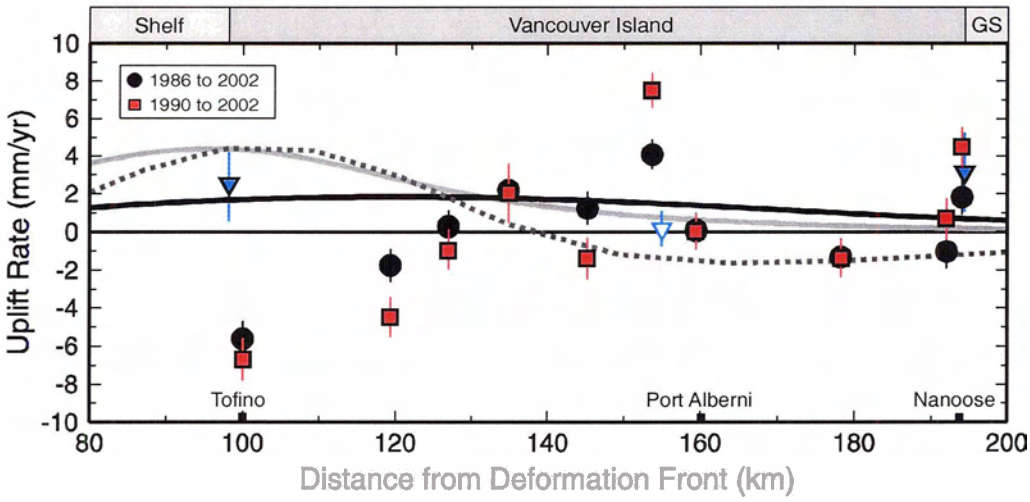

Figure 7.11. Predicted pattern of interseismic vertical deformation from elastic dislocation models with linear (thick grey line), exponentially (thick black line) decreasing slip deficit in the transition zone as well as a 2D finite element model (dashed grey line) replicating the geometry of the linear transition zone model compared to equivalent uplift rates derived from repeat relative gravity measurements (time periods in legend) and from the time series of repeat absolute gravity measurements (blue inverted triangles) between 1995 and 2002. Equivalent uplift rates were calculated using a deformation gradient of –0.19 μGal mm^{-1} [*Rundle, 1978*]. For comparison, the equivalent uplift rate for the absolute gravity station at Albert Head (Table 7.1) is shown as an open symbol. Note the vertical scale difference from Figure 7.1. GS = Strait of Georgia.

If an average trend were taken for the eastern relative gravity stations, the observed uplift pattern is comparable to that predicted by either Model 1 or 2. Within 2σ, uplift at the Nanoose absolute gravity site is consistent with this observation. This is in contrast to the western end of the transect. Here, the Ucluelet absolute gravity trend suggests that either model could be correct (within 1σ), whereas the repeat relative gravity results suggest ~6 mm yr^{-1} of subsidence. However, the gravity transects reflect relative values, and a DC shift of ~10 mm yr^{-1} upwards could rectify the western data to the predicted rates. This would then shift the eastern station rates, making them inconsistent with predicted rates. The inconsistencies between observed and predicted

rates (Figure 7.11) suggest, again, that the gravity results are a function of not only crustal uplift or subsidence, but also of mass redistribution.

Comparison with "Soft Zone" Model

Figures 7.9 and 7.10 show the initial comparison of net uplift rates along the (a) Tofino, (b) Bamfield, and Williams Lake leveling lines, as well as those determined for continuous GPS and tidal stations, to the predicted pattern of interseismic vertical deformation for the "soft zone" model (Model 3).

Model 3 is the product of a first effort to introduce potential effects of high heat flow in the region [e.g. *Lewis et al., 1988; Hyndman and Lewis, 1995*] on the present-day vertical deformation pattern. The resulting pattern is more complex than previous models (1 or 2) predict. Where the uplift peak on western Vancouver Island is generally consistent with Model 1 (as expected), rates decrease far more rapidly than the previous model, to a region of subsidence around Port Alberni. This pattern then repeats on the mainland at a smaller magnitude. Uplift rates determined from the Vancouver Island leveling data, as with Model 1, do not reflect this predicted deformation pattern. Only small-scale correlations are evident (e.g. ~120 km from the deformation front; Figure 7.10a). As well, uplift rates observed at GPS and tide gauge stations indicate little correlation with predicted vertical deformation rates of Model 3. However, NEAH and UCLU are consistent with model predictions within 2σ.

It is also clear that uplift rates observed along the Williams Lake leveling line are not entirely accounted for by Model 3, particularly from the central to eastern portion of the transect, where the model predicts subsidence and the observations indicate uplift. There is also no correlation between results from tide gauge stations (ATK and VAN) or continuous GPS stations (WSLR and WILL).

A similar misfit between observed uplift and predicted deformation rates is found for the repeat gravity observations (Figure 7.11). While the equivalent uplift rate observed at the absolute gravity station UCLU is consistent with the "soft zone" model, NANO indicates ~3 mm yr^{-1} of uplift, whereas Model 3 predicts ~1 mm yr^{-1} of

subsidence. In general, Model 3 does not adequately replicate observed uplift across the northern Cascadia margin determined from repeat leveling measurements, the vertical component of continuous GPS stations, long-term monthly mean sea level trends, or repeat relative and absolute gravity measurements.

7.3.5 Summary Discussion of Geodetic Data and Model Comparisons

The large-scale pattern of uplift rates across the northern Cascadia margin determined in this study (see Chapters 3-6) is roughly consistent with the predicted vertical deformation pattern from Model 2 [*Wang et al., 2003*], which indicates lower magnitudes and a broader peak of uplift rates across Vancouver Island. However, this model does not allow for vertical deformation of the mainland area that is observed along the Williams Lake leveling line. By using a geometrically more complex 2-D model (Model 3), it is evident that, while the observed uplift pattern on the mainland can partially be reproduced, it is at the expense of fitting what would be regarded here as the more robust data on Vancouver Island. It then follows that while further refinement of the geometry and elastic parameters of the weaker zone is needed to accurately replicate the observed uplift pattern, the structure and elastic properties of the northern Cascadia subduction zone are probably more complex than current models reflect. If the structure is not 2-D or there are different tectonic processes occurring along the margin, then two points are raised: (1) one must be careful when projecting data to an across-margin profile, such that data are within some small distance from the transect (e.g. 50 km) and (2) profiles of predicted deformation patterns from models must be generated for specific across-margin transects, as the observations along transects of different azimuths or different locations along the margin may indicate different tilt rates.

It is also clear that while the longer-term data (Figure 7.9) fit the predicted across-margin vertical deformation pattern reasonably well, the shorter-term data along the Bamfield leveling line (Figure 7.10b) illustrate that the geometry of Model 1, including the nature of the transition zone with a linear decrease in slip deficit downdip, is perhaps

more appropriate on that time scale. While current data are too limited to provide a unique answer for comparisons between observed uplift and predicted vertical deformation rates, perhaps the nature of the subduction zone changes slightly on a smaller time scale than used in current models, such that it transforms between something similar to the geometry used in Model 1 [*Flück et al., 1997*] and that used in Model 2 [*Wang et al., 2003*].

7.4 Interpretation of Current Geodetic Deformation in Northern CSZ

Results determined from four independent vertical measurement methods (Chapters 3-6) in this study have given an improved representation of the current subduction-related crustal deformation occurring across the northern Cascadia margin, which illustrates a more complex pattern of deformation than predicted by current models. As such, this may indicate a more 3-dimensional setting than these models utilize. There is also a distinct difference between transects taken to the north and south of Barkley Sound (see Figure 3.6), which may result from different processes affecting these regions.

7.4.1 Comparison with Existing Geophysical Results and Structural Features for the Study Region

Vancouver Island

The northern Cascadia margin has been extensively studied with a variety of geophysical techniques (see Chapter 2). In particular, the tectonic history and structure of southern Vancouver Island has been explored in great detail using seismic techniques, magnetic, gravity, heat flow, and seismicity data [as summarized by *Hyndman, 1995b*]. Crustal deformation studies [e.g. *Dragert et al., 1994*; *Henton, 2000*] compliment these results using a combination of GPS, tide gauge, gravity and releveling techniques across the margin to resolve the present day tectonic regime.

No obvious correlations can be made between the observed vertical deformation and spatial patterns of gravity or magnetic anomalies. The only set of observations from existing data that show a linear across-margin trend in this area is that of a decrease in heat flow from the outer to inner coast of Vancouver Island (Figure 2.13). However, the difference in heat flow across the island (~10 mW m^{-2}) is unlikely to cause an observable difference in crustal deformation, particularly over the short time periods observed.

Crustal seismicity beneath this region of Vancouver Island is limited (Figure 2.3), and only a handful of shallow (<10 km depth) events occur. Most of the recorded earthquakes in the last 18 years are located in the subducting Juan de Fuca plate. It is therefore unlikely that present-day seismicity has resulted in observable displacements that could effect the observed deformation rates along the Tofino and Bamfield leveling transects (Figure 3.6). However, stress orientations of intraslab earthquakes in the region [*Bolton, 2003*] support a complex stress regime on both a local and regional scale.

Mainland British Columbia

Over the volcanic arc, heat flow measurements have been reported as high and scattered, the source of which could be hydrothermal activity [*Hyndman and Lewis, 1995*]. In the backarc, heat flow measurements remain high and may reflect a regional thinning of the lithosphere [e.g. *Keen and Hyndman, 1979*]. To provide a mechanism for the crustal uplift observed in this study, both over the volcanic centers and into the backarc (e.g. Figure 4.6 or 7.1), a change in the heat flux, resulting in thermal expansion of the crust, would need to be ongoing. Associated with thermal expansion of the crust, spatially concentrated background seismicity might be expected where the highest deformation rate gradient is observed. A comparison between the observed deformation rates derived from repeat leveling and the location of crustal seismicity (between 1985 and 2003) is illustrated in Figure 7.12. One concentration of seismicity occurs in the upper crust beneath the projected location of the leveling line, however, the depths of some events are not well constrained due to the relatively sparse seismic network in that

region. As well, high temperatures associated with volcanism may limit seismicity immediately near the volcanic arc, thereby complicating comparisons to releveling data.

Focal mechanisms can provide another key piece of information about the source mechanisms of crustal earthquakes. However, for this region the mechanism for only one event is currently available, in part due to the low magnitude of events [*John Ristau, personal communication, 2004*]. Ongoing, low magnitude seismicity is observed to the immediate west in the Strait of Georgia. However, only recently has there been evidence to support active faulting there (approximately where the profile used in this study is located; Figure 2.3) [*Cassidy et al., 2000*].

The observed change in heat flow near the Garibaldi Volcanic Arc (see Figure 2.13) is also coincident with the change from high to low Bouguer gravity (near the mainland coast) as well as to the general location of a major seismic discontinuity [*Berry and Forsyth, 1975*]. Similar patterns in the across-margin heat flow trend (abrupt increase just west of the volcanic arc) have been reported to the south in Washington [*Blackwell et al., 1990a*] and Oregon [*Blackwell et al., 1982*; *Blackwell et al., 1990b*] States. A similar finding for comparison between the across margin heat flow and gravity gradient is also reported by *Blackwell et al.* [*1982*] and *Blackwell et al.* [*1990b*] for Oregon. However, in the scope of this project, there does not appear to be any correlation with the gravity results and ongoing crustal deformation. If the gravity anomaly arises from the contrast in lithosphere temperatures and therefore the associated crustal thicknesses on either side of this boundary [*Hyndman and Lewis, 1995*], then perhaps it could be considered a second order feature reflecting the subsurface conditions that are motivating current crustal deformation. In this case, it could then, for example, potentially identify the westernmost extent of a crustal "soft" zone centered near the volcanic arc.

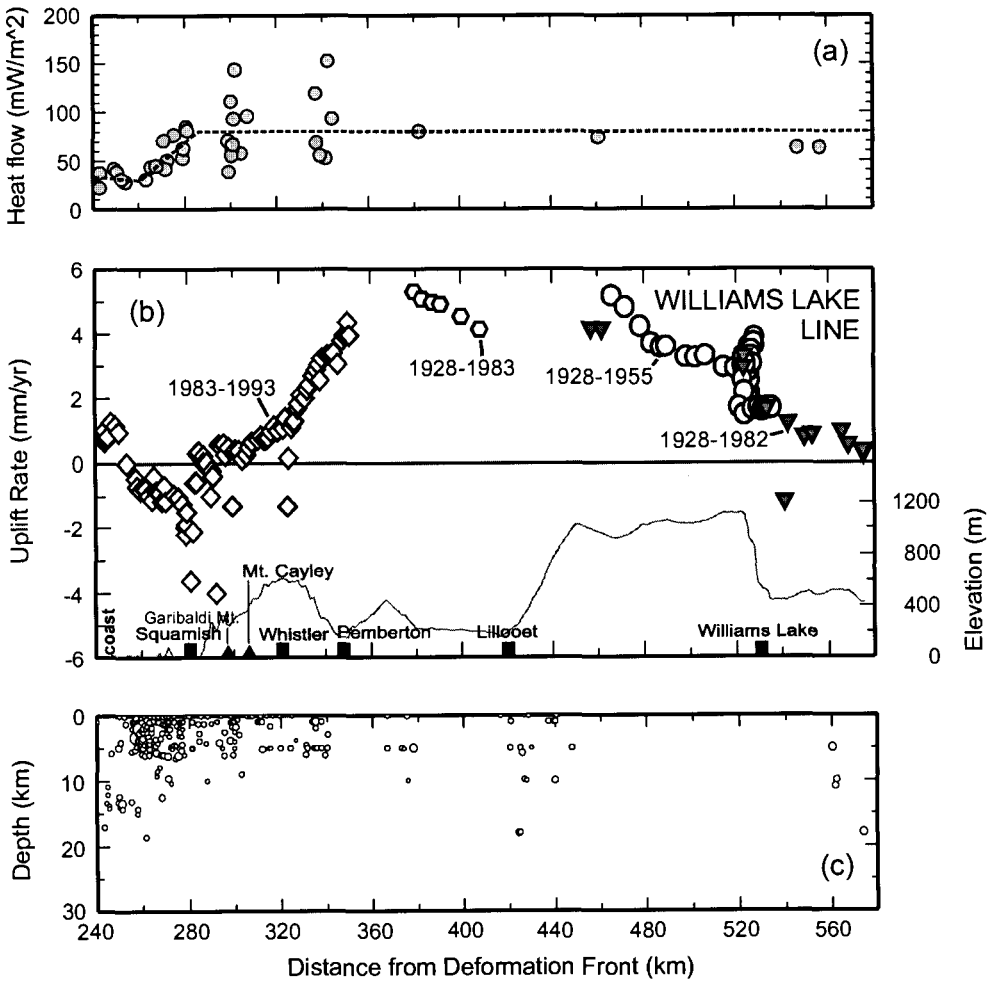

Figure 7.12. (a) Heat flow data [*Lewis et al., 1988; Hyndman and Lewis, 1995*] with approximate average shown as dashed line (see Figure 2.13 for details), (b) repeat leveling data, and (c) crustal seismicity (1985 to 2003) projected to the profile in Figure 2.1 along the Williams Lake leveling line. Time periods for repeat leveling are shown in (b).

7.4.2 The Role of Crustal Faults on Vertical Deformation Patterns

On a smaller scale, variations in deformation patterns across the margin could be related to active faulting or block-type movements. As changes in elevation can be a function of strain accumulation in the crust (as in this study), measurable vertical motions might be detectable across active crustal faults using the leveling technique. The main interest in crustal faults for this study is to describe abrupt, local changes in the

deformation pattern described by the releveling data (Chapter 4). However, while there may be indications of active faulting in the Strait of Georgia from seismic studies [*Cassidy et al., 2000*] there is no evidence for similar findings on land along any of the leveling lines in this study (Figure 3.6). While both Vancouver Island and the adjacent mainland (Coast Belt) have multiple along-margin faults (e.g. Figures 2.7 or 2.8), only the Beaufort fault zone (BFZ) on the island is thought to have a possible correlation with seismicity [*Rogers and Hasegawa, 1978*]. Most of the crustal faults in this region are thought to be Eocene in age [*Yorath et al., 1999*] and are no longer active.

While the Tofino leveling line crosses at least three known major Tertiary-recent crustal faults, including the BFZ, the location of only one of the faults can be correlated with an abrupt change in the leveling profile. However, there is no evidence (e.g. current seismicity) to suggest that the fault is active. Unfortunately, no data were collected across the BFZ in 2002 due to the destruction of 10 km of benchmarks during road construction. Similarly, the Bamfield leveling line to the south (Figure 3.6) crosses at least one known major Tertiary-recent fault zone (Cowichan Lake fault zone (CLFZ); Figure 2.7). However, no abrupt change in deformation rates along the leveling profile is observed at this location.

Nevertheless, strain accumulation along some crustal faults is evidenced by the M~7 1946 [*Rogers and Hasegawa, 1978*] and 1918 [*Cassidy et al., 1988*] crustal earthquakes beneath Vancouver Island. If it is assumed that the interseismic vertical deformation resulting from strain accumulation along those geological structures is similar to that observed along the repeat leveling lines in this study (on the order of a few mm yr^{-1}; Chapter 4), the return periods of such events would be greater than that suggested by the earthquake parameters [e.g. *Rogers and Hasegawa, 1978*]. However, further investigation is needed to quantify this.

7.4.3 Differential Vertical Deformation Across Barkley Sound

One possible interpretation of the complex vertical deformation results could be that differential deformation is occurring in the regions to the north and south of Barkley Sound. Comparison between long-term relative Tofino and Bamfield leveling line results (e.g. Figure 7.1) indicate no significant difference in the tilt pattern of deformation across southern Vancouver Island. However, the difference in magnitude arises when the leveling lines are referenced to the respective tide gauge stations, which indicate a differential uplift rate of ~ 2 mm yr^{-1} (Tables 6.1 and 6.2). This then raises the matter of a bias affecting one or both of the tidal stations. Alternatively, if the uplift rates determined at the two tidal stations are reflective of the true tectonic signal, then the combined results from the tide gauge stations and repeat leveling lines might suggest differential deformation occurring across Barkley Sound.

While present day differential deformation across this area has not been investigated previously, *Johnston and Acton* [*2003*] summarize three lines of evidence that suggest extension has occurred in the past (Eocene) in and west of the Port Alberni Inlet-Barkley Sound area. They use this as the basis to their argument that a change in the strike of Vancouver Island, observed at Barkley Sound, results from the accretion of the Crescent terrane during the Eocene. Their study focused on this collision resulting in a 'rotation' of southern Vancouver Island. They present two possible models for the rotation of southern Vancouver Island: (1) block rotation and (2) a "bending" episode. Both models would result in extension of the Barkley Sound region and compression of the southeastern part of the island, where an orogeny (Southern Vancouver Island Orogeny) is observed. They concluded through examination of structural features across the island that the orogeny formed mainly as a bending of the crust with a later component of block rotation. In the scope of this study, their findings provide the basis for discussion on potential contemporary differential deformation occurring across Barkley Sound. While there is no evidence to suggest continued present-day rotation of southern Vancouver Island resulting from collision of the Crescent terrane, if there were indeed an earlier episode of rotation, a weak zone in the crust above the subducting Juan

de Fuca plate could have been established. This could then provide a region where strain from ongoing subduction might be accumulating differently on either side of the structure. However, the magnitude of deformation may be below the measurable accuracy of the vertical component using the methods in this study. Ultimately, a full suite of data in both the vertical and horizontal components will be necessary to address this issue adequately. In the scope of the results presented in this study (see Chapters 3-6), measurements from continuous methods (GPS and tide gauge) may be more revealing than those that are repeated at different time intervals over a period of 4 or 10 years (leveling, gravity). While deformation rates from the stations at Ucluelet and Bamfield would be ideal, the continuous GPS and absolute gravity stations at the latter have not been in operation for a long enough period to provide a satisfactory resolution of displacement. However, repeat leveling conducted between Tofino and Ucluelet as part of the Tofino leveling line (Figure 3.6) indicate that there is little to no differential vertical deformation (<0.5 mm yr^{-1}) along this section of the survey line. Therefore, the observed (vertical) deformation rate at the Tofino tidal station may be applicable to Ucluelet.

Further support for this type of interpretation could come from the general pattern of vertical deformation around southern Vancouver Island (Figure 7.3; Table 7.1). In general terms, stations to the south of Barkley Sound indicate a lower magnitude of crustal motion than those to the north (e.g. CAM). This is with the exception of results from Neah Bay, which may be affected by the wider locked portion of the subduction thrust [*Dragert et al., 1994*].

7.4.4 Temporal Dependence of Deformation Rates Across Northern Cascadia Margin

Another interpretation of vertical deformation results in this study points to a temporal dependence of vertical deformation rates in the northern Cascadia region. Viscoelastic models [*Wang et al., 2001*] describe this over the course of the megathrust earthquake cycle; however, these predictions are on the order of centuries. As discussed

in Chapter 4, results of repeat leveling along the Bamfield line (Figure 4.5) illustrate a distinct difference in tilt rates of the 1984 to 1990 time period to those of the 1984 to 1994 and 1984 to 2002 time periods. These repeat leveling results raise two lines of discussion for the cause of any differences observed both along the same survey line (between different time periods) as well as results observed along the other leveling lines. The results could suggest either a temporal change in vertical deformation rates over the observed time period or, alternatively, an unresolved problem with the data (e.g. improperly calculated refraction corrections). It was previously determined that systematic errors affecting elevation determinations are most likely correctly modeled, leaving the possibility of transients to be explored. Deformation patterns obtained from using each survey along the Bamfield line as the reference survey support a transient interpretation. Theoretically, if vertical deformation rates were constant over the full time period observed by the releveling surveys, assuming no systematic errors remain, then any time period taken (i.e. any survey could be used as the reference) should result in the same deformation pattern within the described errors. However, this test resulted in significantly different uplift patterns for different time periods.

Also, if it is argued that the uplift observed along the Williams Lake leveling line is real, then because there is no conclusive evidence to suggest otherwise (e.g. improper refraction corrections), the 1984 to 1990 time period of the Bamfield leveling line may be real and reflect a short-term time dependent deformation rate across the margin. However, there is good agreement between the two time periods on the eastern end of the Williams Lake leveling line, which would suggest that deformation rates have remained constant over those time periods. Alternatively, the process causing the transient signal may only affect crustal rates at the outboard end of the transect. Nonetheless, estimates for 2 years of continuous vertical GPS positioning between Bamfield and Port Alberni indicate 1.84±3.99 mm yr^{-1} of landward tilt, which is directionally consistent with increased tilting over short time intervals.

Although there are some indications that the 1984 to 1990 time period represents a transient (which is assumed for discussions at the beginning of this chapter), results

from the Tofino leveling line do not support this interpretation. The similarity in long- and short-term tilt rates north of Barkley Sound is supported by long-term repeat relative gravity results (Figure 5.2b). However, a direct comparison between the leveling and gravity results are tenuous due to the possibility that the gravity data are observing processes other than those causing elevation changes.

As well, if there were a change in the vertical deformation rate within the time frame of observations used in this study, then there should also be some indicator in the time series from the tidal stations (e.g. change in slope). However, the time series of tide gauges used in this study may still contain residual oceanographic signals (Figures 6.1 and 6.3) and it may therefore be difficult to resolve the tectonic signal from shorter time series. Likewise, the short time series of continuous GPS stations in the region do not allow for discrimination of slope changes caused by a tectonic origin; the errors of the vertical components would simply be too large. Additionally, the time periods of the GPS measurements do not overlap the leveling results for the 1984 to 1990 time period.

While all of the data sets analyzed here do not point to a common interpretation and at this stage no suggestions are given for the source of transients (if real), these discrepancies may be partially explained if it is assumed that differential deformation across Barkley Sound is ongoing. That is, perhaps transients exist to the south of Barkley Sound and not to the north, or there is a difference in the change of rates for transients in the two different regions. Again, there are clearly not enough vertical deformation data at this point to provide a regional interpretation regarding transients and it can only be reiterated that the current data (Chapters 3-6) point to a complex system. However, with no evidence to support that there is something inherently wrong with the 1990 releveling survey or corrections applied to that data, the tilt rate determined for the 1984 to 1990 time period is then interpreted as being real (i.e. a transient).

7.4.5 Northern Cascadia Forearc Motion

A possible complication for interpreting the observed deformation pattern in the southern portion of the study region (see Figure 3.6) could result from northward motion of a northern Cascadia forearc. Vertical motions from this source were not factored into the crustal motion estimate in this study based on the constraints of current dislocation models [*Flück et al., 1997*; *Wang et al., 2003*], which assumed that British Columbia was not affected by forearc motion. Other studies [e.g. *Wells and Simpson, 2001*; *Mazzotti et al., 2002*; *Wang et al., 2003*] have suggested that the southernmost tip of Vancouver Island and northwestern Washington State have some component of shortening resulting from forearc migration. *Mazzotti et al.* [*2002*] calculate long-term shortening rates in this region of 5-6 mm yr^{-1}. Their rates are based on the observed 3-3.5 mm yr^{-1} shortening from GPS estimates, with the addition of 1-4 mm yr^{-1} of north-south extension related to the interseismic loading of the margin. They concluded that these shortening estimates are in agreement with rates determined from seismicity in the region [*Hyndman et al., 2003*]. In the scope of this study, the shortening estimates of *Mazzotti et al.* [*2002*] could indicate a component of uplift at GPS and tidal stations around southern Vancouver Island.

In their study, the forearc has been divided into "inner" and "outer" components, with greater shortening occurring in the latter. If greater shortening due to forearc motion is an indicator of an associated greater uplift component, then potentially, the observed difference in differential deformation rates across the margin from the continuous GPS and tide gauge data for the northern and southern transects (cf. Figures 3.9 and 6.4) could be partially resolved. In the *Dragert et al.* [*1994*] study, two possible explanations were suggested for the observed difference in deformation magnitude between along-margin stations: (1) the real statistical uncertainties for individual stations were larger than those calculated or (2) a component of deformation from a source other than the subduction thrust exists. While there are differences between uplift rates derived from tidal stations in the two studies (Section 6.4.4), similar, general across margin, trends are observed.

7.5 Implications for Seismic Hazard in the Northern Cascadia Subduction Zone

The landward limit of the seismogenic zone can be described by the observed deformation pattern across the subduction zone as presented in this thesis. It was shown in Section 7.3 that the most current geodetic results for vertical deformation in the northern Cascadia region are more consistent with the *Wang et al.* [*2003*] model than that of *Flück et al.* [*1997*]. As such, it is then inferred that the geometry defined in this model is more appropriate for this region. This landward limit also impacts the expected coseismic ground motion at major urban centers located 100-200 km inland as well as the expected magnitude of megathrust events [*Hyndman, 1995b*]. This geometry [*Wang et al., 2003*] implies the potential for slightly greater shaking at locations along the northern Cascadia margin (e.g. Victoria). While ground motion on the coast is expected to be somewhat greater than previously thought, the risk for tsunami location and damage should not be significantly different than what the *Flück et al.* [*1997*] model could predict; the updip limit of the seismogenic zone (the major factor in tsunami generation) has not changed between models.

Preliminary results from a recent study, which modeled the slip deficit rates along the subduction thrust based on GPS velocities [*McCaffrey et al., 2004*] has the potential to impact seismic hazard for this region as well. Results from their unconstrained model [cf. *McCaffrey et al., 2004*] indicate that south-to-central Vancouver Island could be anomalous with respect to coupling compared to the rest of the Cascadia margin. Along the remainder of the margin, the fully locked zone is located offshore and the free-slipping portion landward of the coast. However, from the Alberni Inlet in the south to somewhere north of Tofino, perhaps the Nootka Fault Zone, stronger coupling of the plates appears to extend ~30 km further inland underneath Vancouver Island. Such a change in coupling along strike would affect cross-island tilting by reducing the uplift rate at Ucluelet and Tofino while augmenting the uplift rate at Nanoose.

Caution is given to any interpretation of this preliminary study at this stage, as these results come from only one GPS network and only over one time period. However, if these results are real, a reassessment of both previous interpretations for this as well as

the seismic hazard associated with the subduction thrust will need to be undertaken. Additional to the increased shaking landward during a megathrust event, questions could be raised regarding the crustal stress regime landward of the "new" locked zone location. This would then support one suggestion from data in this study, that the region north of Barkley Sound is behaving differently than the region to the south, with respect to accumulating strain from ongoing subduction. Additional support for a more complex along-margin tectonic regime may come from coseismic subsidence estimates for the 1700 Cascadia megathrust event [*Leonard et al., 2004*]. These estimates illustrate a distinct along margin variation, where the Tofino region has undergone less subsidence than the central portion of the Cascadia margin.

CHAPTER 8

Conclusions

In this thesis, contemporary vertical crustal deformation across the northern Cascadia subduction zone has been investigated using a combination of geodetic techniques, including the height component of continuous GPS data, repeat leveling surveys, repeat relative and absolute gravity surveys, and long-term (>40 years) monthly mean sea level data. Based on the analyses of nearly 8 years of continuous GPS data, it is evident that the differential uplift rate across south-central Vancouver Island between UCLU and NANO (-0.18±0.90 mm yr^{-1}) is distinctly different than across the southern tip of Vancouver Island between NEAH and ALBH (2.86±0.94 mm yr^{-1}). This is consistent with differential rates determined from MMSL data (if PGR tilt estimates [*Clague and James, 2002*] are subtracted), which indicate landward tilting between TOF and ATK of 1.97±0.15 mm yr^{-1} and between NEA and VIC of 2.13±0.11 mm yr^{-1}.

Long-term (decadal) repeat leveling surveys also indicate little tilt (<0.5 mm yr^{-1} landward) across Vancouver Island at Barkley Sound, as well as a broad zone of uplift, centered near Pemberton, on the mainland (see also *Holdahl et al.* [*1989*]). While the results suggest a maximum uplift of up to ~5 mm yr^{-1}, it is not well constrained (Figures 3.6 and 4.6). The source of such a broad-scale feature is unknown. However, possible explanations could be a combination of thermal expansion of the crust [*Holdahl et al., 1989*] and a weaker crustal zone, coincident with high heat flow near the Garibaldi Volcanic Arc, focusing strain from the subduction zone. Nevertheless, clearly such high uplift rates cannot be maintained over geological time scales.

Decadal tilt rates on Vancouver Island are inconsistent with those of shorter-term tilt estimates, which have been used to constrain dislocation models for the region. It is concluded that the 1984 to 1990 epoch along the Bamfield leveling line is a transient,

illustrating ~4 mm yr^{-1} of landward tilt. However, a reasonable explanation for the source of such a transient has not been found.

Repeat absolute gravity measurements at UCLU and NANO are consistent with rates determined using GPS and monthly mean sea level data, whereas repeat relative gravity results (seaward tilt on the order of 3-7 mm yr^{-1}) are at odds with the combined low-tilt estimates from other techniques. However, comparison between the time series of absolute gravity and GPS stations at Ucluelet suggests that local bulk mass changes could be contributing to the observed equivalent crustal deformation signal [*A. Lambert, personal communication, 2004*]. If episodic mass redistribution were taking place, two implications could then be: (1) time-dependant rates for trends in gravity readings at stations across the island could be introduced and (2) gravity results may not be directly comparable to other geodetic techniques, unless these changes can be accurately quantified.

Comparison between results from this study with predicted vertical interseismic deformation patterns from three models for the Cascadia margin allows testing of the hypothesis that the current locked zone, i.e. the seismogenic zone, is restricted to offshore Vancouver Island. The large-scale pattern of vertical deformation across the northern Cascadia margin determined in this study is roughly consistent with predicted vertical deformation described by the dislocation model of *Wang et al. [2003]*. However, this model does not replicate observed vertical deformation on the mainland. Therefore, a 2D finite element viscoelastic model including a 100-km wide "soft" crustal zone, centered on the Garibaldi Volcanic Arc, was attempted [*J. He, PGC-GSC*]. However, the resulting fit to data on the mainland was poor and at the expense of fitting the more robust data on Vancouver Island. Therefore, it is concluded that the first-order across-margin deformation pattern resulting from this study is most consistent with the model of *Wang et al., [2003]*, and consequently, the current location of the seismogenic zone might best be depicted by that used in this model.

Nonetheless, details of the vertical deformation results presented here reflect a more complex system than suggested by the simple dislocation models, and might be

better explained using a time-dependent deformation model, with transient time scales of a few years, or a model that allows differential deformation to occur along the margin. This concept is supported by preliminary results of a recent study [*McCaffrey et al., 2004*], which indicates that south-to-central Vancouver Island could be anomalous with respect to coupling, compared to the rest of the Cascadia margin, where stronger coupling could extend ~30 km further inland beneath Vancouver Island than current dislocation models suggest.

Some implications of a more complex system than suggested by the simple dislocation models is that caution should be taken in choosing or comparing across-margin profiles along the margin (e.g. profiles of different azimuths) and that the width of these profile should be limited to some small distance (e.g. 50 km) from the transect. This would ensure that any observed differences in tilt are not simply artifacts of where profiles are chosen.

REFERENCES

Altamimi, Z., Sillard, P., and Boucher, C. 2002. ITRF2000: A new release of the International Terrestrial Reference Frame for earth science applications. Journal of Geophysical Research. **107**. 2214, doi: 10.1029/2001JB000561.

Balazs, E. I. and Young, G. M. 1982: Corrections applied by the National Geodetic Survey to precise leveling observations. *NOAA Technical Memorandum NOS NGS 34*. 1982. 12 pp.

Barnes, D.F. 1966. Gravity changes during the Alaska earthquake. Journal of Geophysical Research. **71**, p. 451-456.

Berry, M.J. and Forsyth, D.A. 1975. Structure of the Canadian Cordillera from seismic refraction and other data. Canadian Journal of Earth Sciences. **21**, p. 182-208.

Beutler, G., Bock, H., Brockmann, E., Dach, R., Fridez, P., Gurtner, W., Hugentobler, U., Ineichen, D., Johnson, J., Meindl, M., Mervart, L., Rothacher, M. Schaer, S., Springer, T., and Weber, R. 2002. Bernese GPS Software Version 4.2. Edited by U. Hugentobler, S. Schaer, and P. Fridez. Astronomical Institute, University of Berne, Berne, Switzerland. 557 pp.

Blackwell, D.D., Steele, J.L., Kelley, S.A., and Korosec, M. 1990a. Heat flow in the state of Washington and thermal conditions in the Cascade Range. Journal of Geophysical Research. **95**, p. 19495-19516.

Blackwell, D.D., Bowen, R.G., Hull, D.A., Riccio, J., and Steele, J.L. 1982. Heat flow, arc volcanism, and subduction in northern Oregon. Journal of Geophysical Research. **87**, p. 8735-8754.

Blackwell, D.D., Steele, J.L., Frohme, M.K., Murphey, C.F., Priest, G.R., and Black, G.L. 1990b. Heat flow in the Oregon Cascade Range and its correlation with regional gravity, Curie point depths, and geology. Journal of Geophysical Research. **95**, p. 19475-19493.

Bolton, M.K. 2003. Juan de Fuca plate seismicity at the northern end of the Cascadia Subduction Zone. M.Sc. Thesis. University of Victoria, Victoria, British Columbia, Canada. 238 pp.

Brandon, M.T. 1989. Deformational styles in a sequence of olistostromal mélanges, Pacific Rim Complex, western Vancouver Island, Canada. Geological Society of America Bulletin. **101**, p. 1520-1542.

Bustin, A., Hyndman, R.D., Lambert, A., Ristau, J., He, J., Dragert, H., and Van der Kooij, M. Fault parameters of Nisqually earthquake determined from moment tensor solutions and the surface deformation from GPS and InSAR. Bulletin of the Seismological Society of America. **94**, p. 363-376.

Calvert, A.J. 1996. Seismic reflection constraints on imbrication and underplating of the northern Cascadia convergent margin. Canadian Journal of Earth Sciences. **33**, p. 1294-1307.

Calvert, A.J. and Clowes, R.M. 1990. Deep, high-amplitude reflections from a major shear zone above the subducting Juan de Fuca plate. Geology. **18**, p. 1091-1094.

Cassidy, J.F., Ellis, R.M., and Rogers, G.C. 1988. The 1918 and 1957 Vancouver Island earthquakes. Bulletin of the Seismological Society of America. **78**, p. 617-635.

Cassidy, J.F., Rogers, G.C., and Waldhauser, F. 2000. Characterization of active faulting beneath the Strait of Georgia, British Columbia. Bulletin of the Seismological Society of America. **90**, p. 1188-1199.

Chelton, D.B. and Enfield, D.B. 1986. Ocean signals in tide gauge records. Journal of Geophysical Research. **91**, p. 9081-9098.

Clague, J.J. and James, T.S. 2002. History and isostatic effects of the last ice sheet in southern British Columbia. Quaternary Science Reviews. **21**, p. 71-87.

Clowes, R.M., Brandon, M.T., Green, A.G., Yorath, C.J., Sutherland Brown, A., Kanasewich, E.R., and Spencer, C. 1987. LITHOPROBE – southern Vancouver Island: Cenozoic subduction complex imaged by deep seismic reflections. Canadian Journal of Earth Sciences. **24**, p. 31-51.

Coles, R.L. and Currie, R.G. 1977. Magnetic anomalies and rock magnetizations in the southern Coast Mountains, British Columbia: possible relation to subduction. Canadian Journal of Earth Sciences. **14**, p. 1753-1770.

Crosson, R.S. and Owens, T.J. 1987. Slab geometry of the Cascadia subduction zone beneath Washington from earthquake hypocenters and teleseismic converted waves. Geophysical Research Letters. **14**, p. 824-827.

Davis, R.E., Foote, F.S., Anderson, J.M., and Mikhail, E.M. 1981. Surveying Theory and Practice, Sixth Edition. McGraw-Hill Inc. United States of America. 929 pp.

Dehler, S.A. and Clowes, R.M. 1992. Integrated geophysical modeling of terranes and other structural features along the western Canadian margin. Canadian Journal of Earth Sciences. **29**, p. 1492-1508.

DeMets, C., Gordon, R.G., Argus, D.F., and Stein, S. 1990. Current plate motions. Geophysical Journal International. **101**, p. 425-478.

DeMets, C., Gordon, R.G., Argus, D.F., and Stein, S. 1994. Effect of recent revisions to the geomagnetic reversal time scale on estimates of current plate motions. Geophysical Research Letters. **21**, p. 2191-2194.

DeMets, C., and Dixon, T.H. 1999. New kinematic models for the Pacific-North America motion from 3 Ma to present, I: Evidence for steady motion and biases in the NUVEL-1A model. Geophysical Research Letters. **26**, p. 1921-1924.

Douglas, B.C. 1991. Global sea level rise. Journal of Geophysical Research. **96**, p. 6981-6992.

Douglas, B.C. 1997. Global sea level rise: A redetermination. Surveys in Geophysics. **18**, p. 279-292.

Dragert, H., Chen, X., and Kouba, J. 1995. GPS monitoring of crustal strain in Southwest British Columbia with the WCDA. Geomatica. **49**, p. 301-313.

Dragert, H., James, T., and Lambert, A. 2000. Ocean loading corrections for continuous GPS: A case study at the Canadian coastal site Holberg. Geophysical Research Letters. **27**, p. 2045-2048.

Dragert, H., Lambert, A., and Liard, J. 1981. Repeated Precise Gravity Measurements on Vancouver Island, British Columbia. Journal of Geophysical Research. **86**, p. 6097-6106.

Dragert, H., Wang, K., and James, T.S. 2001. A silent slip event on the deeper Cascadia subduction interface. Science. **292**, p. 1525-1528.

Dragert, H., Wang, K., and Rogers, G., Geodetic and seismic signatures of episodic tremor and slip in the Cascadia subduction zone. *In* Proceedings of the Second International Symposium on Slip and Flow Processes in and below the Seismogenic Region. Mar. 10-14, 2004. Sanjo Kaikan, Univ. of Tokyo, Tokyo, Japan.

Dragert, H., Hyndman, R.D., Rogers, G.C., and Wang, K. 1994. Current deformation and the width of the seismogenic zone of the northern Cascadia subduction thrust. Journal of Geophysical Research. **99**, p. 653-668.

England, T.D.J. 1989. Lithostratigraphy of the Nanaimo Group, Georgia Basin, southwestern British Columbia. *In* Current Research, Part E. Geological Survey of Canada. Paper 89-1E. p. 197-206.

England, T.D.J. and Calon, T.J. 1991. The Cowichan fold and thrust system, Vancouver Island, southwestern British Columbia. Geological Society of America Bulletin. **103**, p. 336-362.

Flück, P. 1996. 3-D dislocation model for great earthquakes of the Cascadia subduction zone, Diploma Thesis, Swiss Federal Institute of Technology (ETH), Zurich, Switzerland. 106 pp.

Flück, P., Hyndman, R.D., and Wang, K. 1997. Three-dimensional dislocation model for great earthquakes of the Cascadia subduction zone. Journal of Geophysical Research. **102**, p. 20539-20550.

Friedman, R.M., Mahoney, J.B. and Cui, Y. 1995. Magmatic evolution of the southern Coast Belt: Constraints from Nd-Sr isotopic systematics and geochronology of the southern Coast Plutonic Complex. Canadian Journal of Earth Sciences. **32**, p. 1681-1698.

Gabrielse, H., Monger, J.W.H., Wheeler, J.O. and Yorath, C.J. 1991. Part A. Morphological belts, tectonic assemblages, and terranes. *In* Chapter 2 of Geology of the Cordilleran Orogen in Canada. Edited by H. Gabrielse and C.J. Yorath. Geological Society of Canada, Geology of Canada, No. 4, p. 15-28.

Gareau, R.M. 1986. History of precise leveling in Canada and the North American vertical datum readjustment. M.Sc. Thesis, University of Calgary, Calgary, Alberta, Canada. 216pp.

GPS Analysis of Olympia quake at RPI. 2004 (March 6). Retrieved from http://ees2.geo.rpi.edu/rob/wa/olympia.html

Green, A., Clowes, R.M., and Ellis, R.M. 1990. Crustal studies across Vancouver Island and adjacent margin, *In* Studies of Laterally Heterogeneous Structures Using Seismic Refraction and Reflection Data, edited by A.G. Green, Geological Survey of Canada, Paper 89-13. p. 3-25.

Green, A.G., Clowes, R.M. Yorath, C.J., Spencer, C., Kanasewich, E.R., Brandon, M.T., and Sutherland Brown, A. 1986. Seismic reflection imaging of the subducting Juan de Fuca plate. Nature. **319**, p. 210-213.

Halstead, E.C. and Treichel, A. 1966. Groundwater resources of the coastal lowland and adjacent islands, Nanoose Bay to Campbell River, east coast, Vancouver Island. Geological Survey of Canada Bulletin. **144**, 42 pp.

Henton, J.A. 2000. GPS studies of crustal deformation in the northern Cascadia Subduction Zone. Ph.D. Dissertation. University of Victoria, Victoria, British Columbia, Canada.

Hofmann-Wellenhof, B., Lichtenegger, H., and Collins, J. 2001. GPS Theory and Practice. Fifth, Revised Edition. Springer-Verlag Wien. New York. 382 pp.

Holdahl, S.R. A model of temperature stratification for correction of leveling refraction. NOAA Technical Memorandum, NOS. NGS 31. 1981.

Holdahl, S.R., Faucher, R., and Dragert, H. 1989. Contemporary vertical crustal motion in the Pacific Northwest. *In* Slow Deformation and Transmission of Stress in the Earth. Geophysical Monograph Series. 49. Edited by S.C. Cohen and P. Vanicek. American Geophysical Union. Washington, D.C. pp. 17-29.

Hyndman, R.D. 1988. Dipping seismic reflectors, electrically conductive zones, and trapped water in the crust over a subducting plate. Journal of Geophysical Research. **93**, p. 13391-13405.

Hyndman, R.D. 1995a. Giant earthquakes along the west coast of North America. Scientific American. **273**, p. 68-75.

Hyndman, R.D. 1995b. The Lithoprobe corridor across the Vancouver Island continental margin: the structural and tectonic consequences of subduction. Canadian Journal of Earth Sciences. **32**, p. 1777-1802.

Hyndman, R.D. and Lewis, T.J. 1995. Review: The thermal regime along the southern Canadian Cordillera Lithoprobe corridor. Canadian Journal of Earth Sciences. **32**, p. 1611-1617.

Hyndman, R.D. and Wang, K. 1993. Thermal constraints on the zone of major thrust earthquake failure: The Cascadia subduction zone. Journal of Geophysical Research. **98**, p. 2039-2060.

Hyndman, R.D. and Wang, K. 1995. Constraints on the rupture zone of great earthquakes on the Cascadia subduction thrust from current deformation and thermal regime. Journal of Geophysical Research. **100**, p. 22133-22154.

Hyndman, R.D. and Weichert, D.H. 1983. Seismicity and rates of relative motion on the plate boundaries of western North America. Geophysical Journal of the Royal Astronomic Society. **72**, p. 59-82.

Hyndman, R.D., Mazzotti, S., Weichert, D., and Rogers, G.C. 2003. Large earthquake rate of occurrence in Puget Sound-S. Georgia Strait predicted from geodetic and geological deformation rates. Journal of Geophysical Research. **108**, 2033, doi:10.1029/2001JB001710.

Hyndman, R.D., Yorath, C.J., Clowes, R.M., and Davis, E.E. 1990. The northern Cascadia subduction zone at Vancouver Island: Seismic structure and tectonic history. Canadian Journal of Earth Sciences. **27**, p. 313-329.

Hyndman, R.D., Rogers, G.C., Dragert, H., Wang, K., Clague, J.J., Adams, J., and Bobrowsky, P.T. 1996. Giant earthquakes beneath Canada's west coast. Geoscience Canada. **23**, p. 63-72.

James, T.S., Clague, J.J., Wang, K., and Hutchinson, I. 2000. Postglacial rebound at the northern Cascadia subduction zone. Quaternary Science Reviews. **19**, p. 1527-1541.

Johnston, S.T. and Acton, S. 2003. The Eocene southern Vancouver Island orocline – a response to seamount accretion and the cause of fold-and-thrust belt and extensional basin formation. Tectonophysics. **365**, p. 165-183.

Journeay, J.M. 1990. Structural and tectonic framework of the southern Coast Belt, British Columbia. Geological Survey of Canada, Paper 90-1E. p. 183-197.

Journeay, J.M. and Csontos, L. 1989. Preliminary report on the structural setting along the southeast flank of the Coast Belt, British Columbia. *In* Current research, Part E. Geological Survey of Canada, Paper 89-1E. p. 177-187.

Journeay, J.M. and Friedman, R.M. 1993. The Coast Belt thrust system: evidence of shortening in the Coast Belt of southwestern British Columbia. Tectonics. **12**, p. 756-775.

Journeay, J.M. and Mahoney, J.B. 1994. Cayoosh assemblage: regional correlations and implications for terrane linkages, southern Coast Belt. *In* Current research, Part A. Geological Survey of Canada, Paper 94-1A. p. 165-175.

Keen, C.E. and Hyndman, R.D. 1979. Geophysical review of the continental margins of eastern and western Canada. Canadian Journal of Earth Sciences. **16**, p. 712-747.

Kurtz, R.D., DeLaurier, J.M., and Gupta, J.C. 1990. The electrical conductivity distribution beneath Vancouver Island: A region of active plate subduction. Journal of Geophysical Research. **95**, p. 10929-10946.

Lambert, A. and Beaumont, C. 1977. Nano variations in gravity due to seasonal groundwater movements: Implications for the gravitational detection of tectonic movements. Journal of Geophysical Research. **82**, p. 297-306.

Lambert, A. and Courtier, N. Absolute gravity measurements of vertical deformation in the Cascadia subduction zone: Dealing with the seasonal soil moisture signal. Proceedings, Canadian Geophysical Union. Banff, May, 2000 (abstract).

Lambert, A., Liard, J., and Dragert, H. 1979. Canadian precise gravity networks for crustal movement studies: an instrument evaluation. Tectonophysics. **52**, p. 87-96.

Lambert, A., Pagiatakis, S.D., Billyard, A.P. and Dragert, H. 1998. Improved ocean tide loading corrections for gravity and displacement: Canada and northern United States. Journal of Geophysical Research. **103**, p. 30231-30244.

Lambert, A., Courtier, N., Dragert, H., James, T.S., Schmidt, M., Wang, K., and He, J. Absolute Gravity Measurements in the Cascadia Subduction Zone. EOS Transactions, American Geophysical Union, Abstract supplement, 2001 Fall Meeting, F285, December 10-14, 2001 (abstract).

Larsen, C.F., Echelmeyer, K.A., Freymueller, J.T., and Motyka, R.J. 2003. Tide gauge records of uplift along the northern Pacific-North American plate boundary, 1937 to 2001. Journal of Geophysical Research. **108**, doi:10.1029/2001JB001685.

Leonard, L.J., Hyndman, R.D., and Mazzotti, S. 2004. Coseismic subsidence in the 1700 great Cascadia earthquake: Coastal estimates versus elastic dislocation models. Geological Society of America Bulletin. **116**, p. 655-670.

Lewis, T.J., Bentkowski, W.H., Davis, E.E., Hyndman, R.D., Souther, J.G., and Wright, J.A. 1988. Subduction of the Juan de Fuca plate: Thermal consequences. Journal of Geophysical Research. **93**, p. 15207-15225.

Malone, S.D. and Bor, S.S. 1979. Attenuation patterns in the Pacific Northwest based on intensity data and location of the 1872 North Cascades earthquake. Bulletin of the Seismological Society of America. **69**, p. 531-546.

Mao, A., Harrison, C.G.A., and Dixon, T.H. 1999. Noise in GPS coordinate time series. Journal of Geophysical Research. **104**, p. 2797-2816.

Massey, N.W.D. 1986. Metchosin Igneous Complex, southern Vancouver Island: ophiolite stratigraphy developed in an emergent island setting. Geology. **14**, p. 602-605.

Mazzotti, S. and Adams, J. 2004. Near-Term Probabilities of the Next Great Earthquake on the Cascadia Subduction Zone. Seismological Research Letters. **75**, p. 243.

Mazzotti, S., Dragert, H., Hyndman, R.D., Miller, M.M., and Henton, J.A. 2002. GPS deformation in a region of high crustal seismicity: N. Cascadia forearc. Earth and Planetary Science Letters. **198**, p. 41-48.

Mazzotti, S., Dragert, H., Henton, J., Schmidt, M., Hyndman, R.D., James, T., Lu, Y., and Craymer, M. 2003. Current tectonics of northern Cascadia from a decade of GPS measurements. Journal of Geophysical Research. **108**, No. B12, 2554. doi:10.1029/2003JB002653.

McCaffrey, R., Qamar, A., King, R., and Dragert, H. 2004. Pacific Northwest velocity field: constraints on fault coupling and block motions in Cascadia. Poster presented at the UNAVCO board of directors meeting. Colorado, U.S.A.

McCaffrey, R., Long, M.D., Goldfinger, C., Zwick, P.C., Nabelek, J.L., Johnson, C.K., and Smith, C. 2000. Rotation and plate coupling along the southern Cascadia subduction zone. Geophysical Research Letters. **27**, p. 3117-3120.

Miller, M.M., Melbourne, T., Johnson, D., and Sumner, W.Q. 2002. Periodic slow earthquakes from the Cascadia subduction zone. Science. **295**, p. 2423.

Miller, M.M., Johnson, D.J., Rubin, C.M., Dragert, H., Wang, K., Qamar, A., and Goldfinger, C. 2001. GPS-determination of along-strike variation in Cascadia margin kinematics: Implications for relative plate motion, subduction zone coupling, and permanent deformation. Tectonics. **20**, p. 161-176.

Monger, J.W.H. 1990. Georgia Basin: Regional setting and adjacent Coast Mountains geology, British Columbia. Geological Survey of Canada, Paper 90-1F. p. 95-107.

Monger, J.W.H. 1991. Georgia Basin Project: Structural evolution of parts of southern Insular and southwestern Coast Belts, Geological Survey of Canada, Paper 91-1A. p. 219-229.

Monger, J.W.H. and Price, R.A. 1979. Geodynamic evolution of the Canadian Cordillera – progress and problems. Canadian Journal of Earth Sciences. **16**, p. 770-791.

Morken, D.M., Haines, B.J., and Nerem, R.S. 2003. Utilizing site-specific antenna phase center calibration maps for reducing the noise in the GPS vertical. EOS, Transactions, American Geophysical Union. **84**, Fall Meeting Supplement, Abstract G51A-07.

Muller, J.E. 1977. Evolution of the Pacific Margin, Vancouver Island, and adjacent regions. Canadian Journal of Earth Sciences. **14**, p. 2062-2085.

Muller, J.E. and Jeletzky, J.A. 1970. Geology of the Upper Cretaceous Nanaimo Group, Vancouver Island and Gulf Islands, British Columbia. Geological Survey of Canada Paper, 69-25. Natural Resources Canada, Ottawa, Ontario. 77 pp.

Nedimović, M.R., Hyndman, R.D., Ramachandran, K., and Spence, G.D. 2003. Reflection signature of seismic and aseismic slip on the northern Cascadia subduction interface. Nature. **424**, p. 416-420.

Okada, Y. 1985. Surface deformation due to shear and tensile faults in a half space. Bulletin of the Seismological Society of America. **75**, p. 1135-1154.

Oleskevich, D.A., Hyndman, R.D., and Wang, K. 1999. The updip and downdip limits to great subduction earthquakes: Thermal and structural models of Cascadia, south Alaska, SW Japan, and Chile. Journal of Geophysical Research. **104**, p. 14965-14991.

Pacific Northwest Seismograph Network. 2004 (March 6). Retrieved from www.ess.washington.edu/SEIS/EQ_Special/WEBDIR_01022818543p/welcome.html

Pagiatakis, S.D. 1990. The response of a realistic earth to ocean tide loading. Geophysical Journal International. **103**, p. 541-560.

PSMSL. 2003 (September 22) Permanent Service for Mean Sea Level. Retrieved from http://www.nbi.ac.uk/psmsl/psmsl_individual_stations.html

Ramachandran, K. 2001. Velocity structure of S.W. British Columbia, and N.W. Washington, from 3-D non-linear seismic tomography. Ph.D. Dissertation, University of Victoria, Victoria, British Columbia, Canada.

Ramachandran, K., Dosso, S.E., Zelt, C.A., Spence, G.D., Hyndman, R.D., and Brocher, T.M. Upper crustal structure of southwestern British Columbia from the 1998 seismic hazards investigation in Puget Sound. Journal of Geophysical Research (in press).

Ramachandran, K., Dosso, S.E., Zelt, C.A., Spence, G.D., Hyndman, R.D., and Brocher, T.M. Forearc structure beneath southwestern British Columbia: A 3-D tomographic velocity model. Journal of Geophysical Research (submitted).

Riddihough, R.P. 1979. Gravity and structure of an active margin – British Columbia and Washington. Canadian Journal of Earth Sciences. **16**, p. 350-363.

Riddihough, R.P. 1982. Contemporary movements and tectonics on Canada's west coast: A discussion. Tectonophysics. **86**, p. 319-341.

Riddihough, R.P. 1984. Recent movements of the Juan de Fuca plate system. Journal of Geophysical Research. **89**, p. 6980-6994.

Rogers, G.C. 1988a. An assessment of the megathrust earthquake potential of the Cascadia subduction zone. Canadian Journal of Earth Sciences. **25**, p. 844-852.

Rogers, G.C. 1988b. Seismic potential of the Cascadia subduction zone. Nature. **332**, p. 17.

Rogers, G.C. 1994. Earthquakes in the Vancouver area. *In* Geology and Geological Hazards of the Vancouver Region, Southwestern British Columbia. Edited by J.W.H. Monger. Geological Survey of Canada Bulletin. **481**, p. 221-2290.

Rogers, G.C. and Crosson, R.S. Intraslab earthquakes beneath Georgia Strait/Puget Sound. Kirby, Stephen, Wang, Kelin, and Dunlop, Susan, eds. 2002. The Cascadia Subduction Zone and Related Subduction Systems-Seismic Structure, Intraslab Earthquakes and Processes, and Earthquake Hazards: U.S. Geological Survey Open-File Report 02-328, 169 p. on 1 CD-ROM, and Geological Survey of Canada Open File 4350.

Rogers, G.C. and Dragert, H. 2003. Episodic tremor and slip on the Cascadia Subduction Zone: The chatter of silent slip. Science. **300**, p. 1942-1943.

Rogers, G.C. and Hasegawa, H.S. 1978. A second look at the British Columbia earthquake of 23 June, 1946. Bulletin of the Seismological Society of America. **68**, p. 653-676.

Rohr, K.M.M. and Furlong, K.P. Ephemeral plate tectonics at the Queen Charlotte triple Junction. Geology. **23**, p. 1035-1038.

Rundle, J.B. 1978. Gravity changes and the Palmdale uplift. Geophysical Research Letters. **5**, p. 41-44.

Satake, K., Wang, K., and Atwater, B. 2003. Fault slip and seismic moment of the 1700 Cascadia earthquake inferred from Japanese tsunami descriptions. Journal of Geophysical Research. **108**. No.B11, 2535, doi:10.1029/2003JB002521.

Satake, K., Shimazaki, K. Tsuji, Y., and Ueda, K. 1996. Time and size of a giant earthquake in Cascadia inferred from Japanese tsunami records of January 1700. Nature. **379**, p. 246-249.

Savage, J.C. 1983. A dislocation model of strain accumulation and release at a subduction zone. Journal of Geophysical Research. **88**, p. 4984-4996.

Savage, J.C. and Plafker, G. 1991. Tide gauge measurements of uplift along the south coast of Alaska. Journal of Geophysical Research. **96**, p. 4325-4335.

Savage, J.C., Lisowski, M., and Prescott, W.H. 1991. Strain accumulation in Western Washington. Journal of Geophysical Research. **96**, p. 14493-14507.

Savage, J.C., Svarc, J.L., Prescott, W.H., and Murray, M.H. 2000. Deformation across the forearc of the Cascadia subduction zone at Cape Blanco, Oregon. Journal of Geophysical Research. **105**, p. 3095-3120.

Sella, G., Dixon, T.H., and Mao, A. 2002. REVEL: A model for recent plate velocities from space geodesy. Journal of Geophysical Research. **107**. No.B4, doi:10.1029/2000JB000033.

SOPAC. 2003 (October 30). Scripps Orbit and Permanent Array Center. Retrieved from http://sopac.ucsd.edu/cgi-bin/refinedModelTerms.cgi

Spence, G.D., Clowes, R.M., and Ellis, R.M. 1985. Seismic structure across the active subduction zone of western Canada. Journal of Geophysical Research. **90**, p. 6754-6772.

Staff of the Pacific Northwest Seismograph Network. 2001. Preliminary report on the Mw=6.8 Nisqually, Washington earthquake of 28 February 2001. Seismological Research Letters. **72**, p352-361.

Thatcher, W. 1984. The earthquake deformation cycle at the Nankai Trough, southwest Japan. Journal of Geophysical Research. **89**, p. 3087-3101.

Tushingham, A.M. and Peltier, W.R. 1991. ICE-3G: A new global model of Late Pleistocene deglaciation based upon geophysical predictions of post-glacial relative sea level change. Journal of Geophysical Research. **96**, p. 4497-4523.

Vanicek, P. 1978. To the problem of noise reduction in sea-level records used in vertical crustal movement detection. Physics of the Earth and Planetary Interiors. **17**, p. 265-280.

Vanicek, P. and Krakiwsky, H. 1986. Geodesy: The Concepts, Second Edition. Elsevier Science Publishers. Netherlands. 697 pp.

Vanicek, P., Castle, R.O., and Balazs, E.I. 1980. Geodetic leveling and its applications. Reviews of Geophysics and Space Physics. **18**, p. 505-524.

Wang, K., He, J., Dragert, H., and James, T.S. 2001. Three-dimensional viscoelastic interseismic deformation model for the Cascadia subduction zone. Earth Planets and Space. **53**, p. 295-306.

Wang, K., Wells, R., Mazzotti, S., Hyndman, R.D., and Sagiya, T. 2003. A revised dislocation model of interseismic deformation of the Cascadia subduction zone. Journal of Geophysical Research. **108**, No.B1. 2026, doi:10.1029/2001JB001227.

Wells, R.E. and Simpson, R.W. 2001. Northward migration of the Cascadia forearc in the northwestern U.S. and implications for subduction deformation. Earth Planets and Space. **53**, p. 275-283.

Wells, R.E., Weaver, C.S., and Blakely, R.J. 1998. Forearc migration in Cascadia and its neotectonic significance. Geology. **26**, p. 759-762.

Wessel, P. and Smith, W.H.F. 1998. New improved version of Generic Mapping Tools released. EOS Transactions. American Geophysical Union. **79**. F579.

Wigens, S.O. and Stephenson, F.E. 1980. Mean sea level on the Canadian West Coast. *In* Proceedings of 2nd International Symposium on Problems Related to the Redefinition of North American Vertical Geodetic Networks (NAD). Canadian Institute of Surveying and Mapping, Ottawa. pp. 105-124,

Wilson, D.S. 1986. A kinematic model for the Gorda deformation zone as a diffuse southern boundary of the Juan de Fuca plate. Journal of Geophysical Research. **91**, p. 10259-10269.

Yorath, C.J., Sutherland Brown, A. and Massey, N.W.D. 1999. Lithoprobe, southern Vancouver Island, British Columbia: geology. Geological Survey of Canada Bulletin, **498**. Natural Resources Canada, Ottawa, Ontario. 145 pp.

Yorath, C.J., Green, A.G., Clowes, R.M., Sutherland Brown, A., Brandon, M.T., Kanasewich, E.R., Hyndman, R.D., and Spencer, C. 1985. Lithoprobe, southern Vancouver Island: Seismic reflection sees through Wrangellia to the Juan de Fuca plate. Geology. **13**, p. 759-762.

Zhao, D., Wang, K., Rogers, G.C. and Peacock, S.M. 2001. Tomographic image of low P velocity anomalies above slab in northern Cascadia subduction zone. Earth Planets and Space. **53**, p. 285-293.

Zschau, J. 1976. Tidal sea load tilt of the crust, and its application to the study of crustal and upper mantle structure. Geophysical Journal of the Royal Astronomic Society. **44,** p. 577-593.

APPENDIX A

Geodetic Station Locations

Table A.1 shows the geographic locations of the continuous GPS, tide gauge, and absolute gravity stations used in this study. Station abbreviations are as in the main body of text.

Table A.1. Geodetic station locations.

Station	Latitude (N) (degree/minute/second)	Longitude (W) (degree/minute/second)
	GPS	
UCLU	48° 55' 32"	125° 32' 29"
NANO	49° 17' 41"	124° 5' 11"
ALBH	48° 23' 23"	123° 29' 15"
NEAH	48° 17' 52"	124° 37' 30"
WSLR	50° 7' 36"	122° 55' 16"
WILL	52° 14' 13"	122° 10' 4"
	TIDE GAUGE	
ATK	49° 20' 24"	125° 15' 0"
VAN	49° 17' 24"	123° 6' 36"
FUL	48° 46' 12"	123° 27' 0"
PAT	48° 39' 0"	123° 27' 0"
FRI	48° 32' 48"	123° 0' 36"
VIC	48° 25' 12"	123° 22' 12"
CAM	50° 1' 12"	125° 13' 48"
LIT	49° 43' 48"	124° 54' 0"
TOF	49° 9' 0"	125° 54' 36"
ALB	49° 13' 48"	124° 48' 36"
BAM	48° 49' 48"	125° 7' 48"
REN	48° 33' 0"	124° 25' 12"
NEA	48° 22' 6"	124° 37' 0"
	ABSOLUTE GRAVITY	
UCLU	48° 55' 18"	125° 32' 22"
NANO	49° 16' 6"	124° 8' 48"